MINERALOGICAL AND GEOCHEMICAL PROPERTIES OF MESSINIAN GYPSUM OCCURRENCE IN POLATLI SAZILAR REGION, ANKARA

A THESIS SUBMITTED TO
THE GRADUATE SCHOOL OF NATURAL AND APPLIED SCIENCES
OF
MIDDLE EAST TECHNICAL UNIVERSITY

BY

HAYRİYE ÇAKMAK

IN PARTIAL FULFILLMENT OF THE REQUIREMENTS
FOR
THE DEGREE OF MASTER OF SCIENCE
IN
GEOLOGICAL ENGINEERING

DECEMBER 2008

Approval of the thesis:

MINERALOGICAL AND GEOCHEMICAL PROPERTIES OF MESSINIAN GYPSUM OCCURRENCE IN POLATLI SAZILAR REGION, ANKARA

submitted by **HAYRİYE ÇAKMAK** in partial fulfillment of the requirements for the degree of **Master of Science in Geological Engineering Department, Middle East Technical University** by,

Prof. Dr. Canan Özgen _____
Dean. Graduate School of **Natural and Applied Sciences**

Prof. Dr. Zeki Çamur _____
Head of Department, **Geological Engineering**

Assist. Prof. Dr. Fatma Toksoy Köksal _____
Supervisor, **Geological Engineering Dept., METU**

Assist. Prof. Dr. Peter Redecke _____
Co-Supervisor, **Knauf A.Ş.**

Examining Committee Members:

Prof. Dr. Cemal Göncüoğlu _____
Geological Engineering Dept., METU

Assist. Prof. Dr. Fatma Toksoy Köksal _____
Geological Engineering Dept., METU

Prof. Dr. Zeki Çamur _____
Geological Engineering Dept., METU

Prof. Dr. Asuman Günal Türkmenoğlu _____
Geological Engineering Dept., METU

Prof. Dr. Ergüzer Bingöl _____
Geological Engineer, KNAUF A.Ş.

Date: 02.12.2008

I hereby declare that all information in this document has been obtained and presented in accordance with academic rules and ethical conduct. I also declare that, as required by these rules and conduct, I have fully cited and referenced all material and results that are not original to this work.

Name, Last Name: Hayriye Çakmak

Signature:

ABSTRACT

MINERALOGICAL AND GEOCHEMICAL PROPERTIES OF MESSINIAN GYPSUM OCCURRENCE IN POLATLI SAZILAR REGION, ANKARA

Çakmak, Hayriye

M. Sc., Department of Geological Engineering

Supervisor: Assist. Prof. Dr. Fatma Toksoy Köksal

Co-Supervisor: Assist. Prof. Dr. Peter Redecke

December 2008, 105 pages

The objective of this study is to understand the petrographical, mineralogical and geochemical characteristics of Messinian (Upper Miocene) gypsum occurrence in Polatlı Sazılar region, Ankara and to determine the impurities associated with gypsum. Moreover, it is aimed to interpret the usability of this raw material with impurities in plaster and plasterboard production based on industrial standards.

Based on petrographical study, the first variety of gypsum which have different physical properties is white massive, micro crystalline and translucent gypsum. Prismatic, transparent, idiomorphic and cleavage dominated selenite is the second variety. The gypsum rock is also identified that it is composed of sand sized selenite crystals and gypsum grains in a calcite and clay rich matrix. These impurity minerals also observed in thin beds alternating with gypsum.

Scanning electron microscopic (SEM) studies are conducted to determine the relationship between the impurity mineral, gypsum and the selenite. X-ray diffractometry (XRD) studies were used to identify the type of clay minerals. In

the samples, Ca-smectite is the essential impurity clay mineral. Rarely, mixed layer of illite-smectite is also identified.

Geochemical studies also shows that as the amount of clay impurity increases, MgO, Al_2O_3, Fe_2O_3, Na_2O, K_2O (wt%) increases with decreasing SO_3 (wt%). On the other hand, impurity of calcite controls the CaO (wt%) content in varying amounts. Five different groups of samples indicating different abundance of clay and calcite impurities are interpreted. The clay rich samples are enriched, in general, in vanadium, nickel, copper and chromium.

Keywords: Gypsum, Selenite, Impurity, Ca-Smectite, Polatlı-Ankara

ÖZ

ANKARA, POLATLI SAZILAR YÖRESİNDEKİ MESSİNİYEN YAŞLI JİPS OLUŞUMUNUN MİNERALOJİK VE JEOKİMYASAL ÖZELLİKLERİ

Çakmak, Hayriye

Yüksek Lisans, Jeoloji Mühendisliği Bölümü

Tez Yöneticisi: Yard. Doç. Dr. Fatma Toksoy Köksal

Ortak Tez Yöneticisi: Yard. Doç. Dr. Peter Redecke

December 2008, 105 sayfa

Bu çalışmanın amacı Ankara, Polatlı Sazılar bölgesindeki Messiniyen (Üst Miyosen) yaşlı jips oluşumunun petrografik, mineralojik ve jeokimyasal özelliklerini ortaya koymak, içerisindeki safsızlıkları incelemektir. Bunların yanısıra, safsızlıklarla birlikte bu ham maddenin alçı ve alçı plaka üretiminde kullanılabilirliğini endüstriyel standartlara bağlı olarak açıklamak hedeflenmiştir.

Petrografik çalışmalara göre, farklı fiziksel özelliklere sahip jips türlerinden ilki, beyaz, masif, çok küçük kristalli, yarı transparan olan türdür. İkinci tür ise prizmatik, transparan, öz şekilli ve dilinimli selenittir. Jips kayacı ise kalsit ve kilce zengin bir matrikste yer alan kum tanesi boyutunda selenit kristalleri ve jips tanelerinden oluşmaktadır. Bu safsızlık mineralleri ince tabakalar halinde jips ile ardalanmalı olarak da gözlemlenmektedir.

Taramalı electron mikroskobu çalışmaları safsızlık mineralleri, jips ve selenite arasındaki ilişkiyi belirlemek üzere gerçekleştirilmiştir. X-ışını difraktometresi çalışmaları ise kil tipini belirlemek amacıyla gerçekleştirilmiştir. Bu örneklerde,

Ca-smektit başlıca safsızlık kil mineralidir. Nadir olarak, karışık tabakalı illit-smektit tipi de tanımlanmaktadır.

Jeokimyasal analizlere göre kil safsızlık miktarı arttıkça, MgO, Al_2O_3, Fe_2O_3, Na_2O, K_2O (%ağ) değerleri de artmakta, SO_3 (%ağ) değeri ise azalmaktadır. Öte yandan, kalsit safsızlığı değişen oranlarda CaO (%ağ) değerini control eder. Farklı kil ve kalsit zenginleşmesi gösteren beş farklı örnek grubu tanımlanmıştır. Kilce zengin örnekler, genel olarak vanadiyum, nikel, bakır ve kromca zenginleşmişlerdir.

Anahtar Kelimeler: Jips, Selenit, Safsızlık, Ca-Simektit, Polatlı-Ankara

To my dearest family

ACKNOWLEDGEMENTS

I am greatly indebted to my supervisor Assist. Prof. Dr. Fatma Toksoy KÖKSAL for her invaluable guidance, comments, encouragement and helpful criticism at every stage of this thesis.

I would like to express my gratitude to my co-supervisor Assist. Prof. Dr. Peter REDECKE for his precious contributions, recommendations and guidance in preparation of this thesis.

I would like to express my special thanks to Chairman of Knauf A.Ş. Ms. Isabel KNAUF, General Manager Mr. Mehmet ÖZAYDIN and General Manager Mr. Orhan DÜZGÜN for providing me the study area of this thesis and enabling me to prepare such a thesis. I am highly indebted to their support and valuable understandings.

I would like to thank to Prof. Dr. Asuman GÜNAL TÜRKMENOĞLU for her valuable helps and contributions while utilizing the XRD device and the interpretation of the data.

I would like to express my special thanks to Prof. Dr. Ergüzer BİNGÖL for his kind help, valuable contributions and understanding during various times of this thesis.

I would like to thank also to technical personnel of Geological Engineering Department of METU, especially to Mr. Orhan KARAMAN for preparing the thin sections and to Mr. Zafer KAPLAN for performing X-ray scanning.

I also want to thank to my friend Ms. Selen ESMERAY for her great motivation and endless encouragements and would like to thank my friend Mr. Turgay SENLET for his kind behavior and help while preparing the format of this thesis. I am also grateful to my colleague Mr. Cumhur ALTUN for his kind help and nice manner.

This thesis study is supported by METU Graduate School of Natural and Applied Science, Project of Research Foundation Grant (BAP-2004-07-02-01) and Scientific and Technological Research Council of Turkey (TÜBİTAK).

I would like to finally express my thanks to my mother Mrs. Fatma ÇAKMAK who especially helped me in performing some analysis with great care and my brother Mr. Seyhun ÇAKMAK for their support, motivation and endless help.

Finally, I would like to thank my brother Mr. Serkan ÇAKMAK and Ms. Belgin BELENLİ ÇAKMAK for their support and kind help.

TABLE OF CONTENTS

LIST OF TABLES

TABLES

LIST OF FIGURES

FIGURES

CHAPTER 1

INTRODUCTION

1.1 Purpose and Scope

Gypsum is one of the important industrial raw materials, used mainly in plaster, plasterboard production and in cement production as a retarder. The production cycle initiates with processing of the raw gypsum. Hence, gypsum characteristics play a significant role in the quality of products. In this sense, the identification and evaluation of raw gypsum nature is a fundamental and crucial practice for further applications.

The main objective of this study is to establish mineralogy, petrography and geochemistry of Messinian (Upper Miocene) gypsum occurrence in Polatlı Sazılar region, Ankara (containing impurities e.g., clay, marl, siliceous material, etc.) in order to constitute a through investigation about the nature of the rock.

In order to perform such a study, two drillcores were acquired from an active gypsum quarry for petrographical studies. The length of the drillcore I is 19.50 m and of drillcore II is 21.50 m, and the distance between the drillings is 50 m. By studying the two drillcores, different varieties of gypsum crystals and their association with each other have been identified at different meters and the relationship between these minerals and the impurities have been determined petrographically. From the parts that are petrographically rich in clayey material, X-ray diffraction studies have been conducted to be able to determine compositional change of the of the clayey material through different parts of the drillcore. In addition, chips of certain rock samples illustrating mainly different

variety of gypsum and impurities have been analyzed by scanning electron microscopy and energy dispersive X-ray analysis method, as well as by geochemical studies.

1.2 Methods of Study

This study was mainly conducted in two major parts: the field study and the laboratory study.

1.2.1 Field Work

Two drillcores have been selected (on the field) that best represent the gypsum quarry. Initially, it is planned to gather more drillcores; however, it is observed that the most of the samples were weathered and decomposed. Hence, these two chosen drillcores depict the quarry features best.

The lithological determination on drillcore samples has been conducted in the field. 20 samples from drillcore I, and 7 samples from drillcore II have been selected (randomly) representing the lithologically significant parts for microscopic analysis.

1.2.2 Laboratory Work

Laboratory work is based on petrographical, mineralogical, geochemical studies which are conducted through various applications such as petrographic microscope studies, scanning electron microscope with energy dispersive x-ray analysis and X-ray diffraction analysis and geochemical analysis. The list of the samples used in the analysis is given in Table 1.

Petrographic studies were conducted by polarized microscope. Totally, randomly selected 27 samples from drillcore I and drillcore II were prepared in

Middle East Technical University at Department of Geological Engineering. Microscopic studies were performed by using Nikon E 200 (Japan) model polarizing microscope.

Mineralogical studies were carried out through Scanning Electron Microscope (SEM) and X-ray Diffraction Analysis (XRD). Scanning electron microscope studies were performed in order to show the three dimensional crystal relationship using the benefit of higher resolution and broad magnification range opportunity in determinations. For this purpose, 8 gypsum samples that were identified petrographically were selected. In addition to the SEM, energy dispersive X-ray analyzer (EDS) was used to examine the chemical composition semi-quantitatively. Specimens were mounted as chips on the aluminum stubs and coated with gold and palladium. The specimens were analyzed by Quanta 400F Field Emission with EDAX Genesis energy dispersive analysis system. The analyses of 8 specimens were carried out at Central Laboratory at the Middle East Technical University. The samples were examined at 30 kV accelerating voltage with a range of 130X to 6000X magnification. Since the device was broken down in central laboratory, next study was performed at Metallurgical Engineering Department at Middle East Technical University by 40 kV Jeol 6400 scanning electron microscope equipped with Digital Imaging and Noran Inst. Series II X-ray microanalyser.

7 samples that were petrographically rich in clayey material and 3 clay samples were examined using X-ray diffractometry (XRD) at the Department of Geological Engineering in Middle East Technical University. The analyses were conducted by a Rigaku X-ray diffractometry with Ni-filtered CuKα radiation at the voltage 30kV and current of 10 mA. The random samples were screened under 63μ and the specimens were put onto a glass sample holder (3x4 cm) with a 1.5 cm^2 area place for the specimen. Four oriented samples are prepared: air-dried, ethylene glycolated, 300°C oven and 550°C oven. Air-dried samples are left for drying for half a day. Ethylene glycolated samples are heated up to 60°C

in an ethylene glycolated desiccator. Two of the samples are heated up to 300 °C and 550°C. Oriented specimens are put on glass slides (2x7mm). Count data on both random and oriented samples were recorded at the steps of 2°2θ/min with a starting angle of 2°2θ. The scanning range of random samples was 2°2θ to 40°2θ, and of oriented samples, 2°2θ to 30°2θ, respectively.

Geochemical analysis of 10 gypsum samples and 8 clay samples were carried out in Research and Development Laboratory of Knauf Gips KG, in Germany to detect the major and trace elements. The elemental analyses were carried out by Varian 725 Inductively Coupled Plasma – Optic Emission Spectrometer (ICP-OES) and combined water and carbonates were determined by Q500 Thermo Gravimeter Analyzer (TGA). The determined oxides for gypsum samples are CaO, MgO, Al_2O_3, Fe_2O_3, Na_2O, K_2O and SrO and for clay samples, additional to these compounds the trace elements Ti, V, Cr, Ni, Mo, Cu are analyzed.

1.2.3 Geographic Setting

The study area is an active gypsum quarry located at approximately 95 km southwest of Ankara. The 1: 25 000 scaled topographic map of quadrangle I27-c2 within northing 4393000-4394000 and easting 240700-240800 covers the area (Figure 1)

The study area is accessible through Eskişehir-Ankara highway that takes nearly 75 km to reach to Polatlı district. The gypsum quarry can be reached by taking 20 km more from the stabilized road leading to Sazılar village.

The main geographic features in the region are Porsuk River along east-west direction and Sakarya River in the north-south direction. The typical continental climate is effective in the study area.

Table 1. List of the samples used in the analysis

Source	Sample No	Petrographic Study	SEM	XRD	Geochemical Study
Drillcore I	P1	x	x		
Drillcore I	P2	x			
Drillcore I	P3	x			
Drillcore I	P4	x	x		
Drillcore I	P5	x	x		
Drillcore I	P6	x			
Drillcore I	P7	x			
Drillcore I	P8	x			
Drillcore I	P9	x	x		
Drillcore I	P10	x			
Drillcore I	P11	x			
Drillcore I	P12	x			
Drillcore I	P13	x			
Drillcore I	P14	x			
Drillcore I	P15	x	x		
Drillcore I	P16	x			
Drillcore I	P17	x			
Drillcore I	P18	x			
Drillcore I	P19	x			
Drillcore I	P20	x			
Drillcore II	P21	x	x		
Drillcore II	P22	x			
Drillcore II	P23	x			
Drillcore II	P24	x	x		
Drillcore II	P25	x			
Drillcore II	P26	x	x		
Drillcore II	P27	x			
Drillcore I	P28			x	
Drillcore I	P29			x	
Drillcore I	P30			x	
Drillcore I	P31			x	
Drillcore II	P32			x	
Drillcore II	P33			x	
Drillcore II	P34			x	
Drillcore I	P35				x
Drillcore I	P36				x
Drillcore I	P37				x
Drillcore I	P38				x
Drillcore I	P39				x
Drillcore II	P40				x
Drillcore II	P41				x
Drillcore II	P42				x
Drillcore II	P43				x
Drillcore II	P44				x
Quarry	P45				x
Quarry	P46				x
Quarry	P47				x
Quarry	P48				x
Quarry	P49				x
Quarry	P50				x
Quarry	P51				x
Quarry	P52				x

1.3 Previous Work

Previous work can be reviewed in four parts as the geology and the stratigraphy of the region, gypsum and the impurities, occurrence and the origin of gypsum, and distribution of gypsum deposits in the world and Turkey.

1.3.1 Geology and Stratigraphy of the Region

Once the publications and researches about Polatlı region are taken into consideration, it is seen that a few studies have been performed in the region and its surroundings. These scientific researches and the publications could be categorized into two groups as and studies on the volcanism of the nearby region and stratigraphical and the paleontological studies.

Geological studies conducted in the region are mostly concentrated on the mapping of the area and its surroundings. The first known study was performed by Weingart (1954). He prepared the geological maps of 1: 100.000 scaled maps of Sivrihisar and Ankara and recognized Paleozoic, Jurassic, Late Cretaceous, Paleocene, Eocene, Oligocene, and Neogene aged rock units at the west of Polatlı.

Erol (1955) revised the geological map of Weingart (1954) and restudied the Neogene areas. In his study, he indicated that the volcanics of Temelli are somewhat different from the volcanics around Polatlı and Çiledağ.

Akarsu (1956), for the first time, mapped the area around Polatlı, at a scale of 1: 25.000. He pointed out the presence of Upper Cretaceous, Paleocene and Eocene flyschs that unconformably overlie each other.

Sirel (1975) conducted stratigraphical research in the southern part of Polatlı. He also determined that the rock units of Upper Jurassic, Paleocene, Eocene and

Neogene age crop out 10 km south of Polatlı. He identified that Çaldağ Formation is definitely composed of conglomerate, lacustrine limestone, sandstone and lignite, which are deposited in deltaic environment. In addition, the author identified the age of Kırkkavak Formation as Tanesian-Late Ilerdian and the age of Eski Polatlı Formation which unconformably overlies Kırkkavak Formation as Lower Cuisian.

Ünalan and et.al (1976) defined Early-Mid Eocene aged Beldede Formation that is composed of reddish to brownish conglomerate, sandstone, siltstone and clayey, sandy limestone. Yurteri (1989) define the Beldede Formation of Ünalan et al. (1976) as Duatepe Formation. The age of this formation is determined by the aid of its fossil content (*Nummilites laevigatus Bruguiere, Nummilites globus Leymerie, Assilina exponens Sowerby)* by Ünalan et al. (1976) and Yurteri (1989).

Gözler et al. (1996) carried out geological studies both around Sakarya region and south of the region. They defined the Mid-Late Miocene rock units as Porsuk Formation. Porsuk Formation is composed of conglomerate-sandstone unit, tuff unit, marl and clay unit, gypsum rich marl and clay unit, gypsum rich red mudstone unit and limestone unit. They proposed that the units are deposited in a lake environment with an age of Mid-Late Miocene. Yağmurlu and Helvacı (1994) named the units including evaporates as Kirmir Formation. Karakaş and Varol (1994) define the unit composed of gypsum, limestone and clayey dolomite as Sakarya Formation. Ece at al. (2003) defined the units consisting of gypsum, clay and clayey limestone as İlyaspaşa Formation and define the units of dolomitized limestone as Tatar Formation.

Temel et al. (2000) determined in their study in Polatlı that the basaltic volcanic activity started at Miocene. The authors indicated that the volcanism has been originated from basalt source in an island arc setting depending on the major and the trace element data. (Temel et al., 2001, 2005).

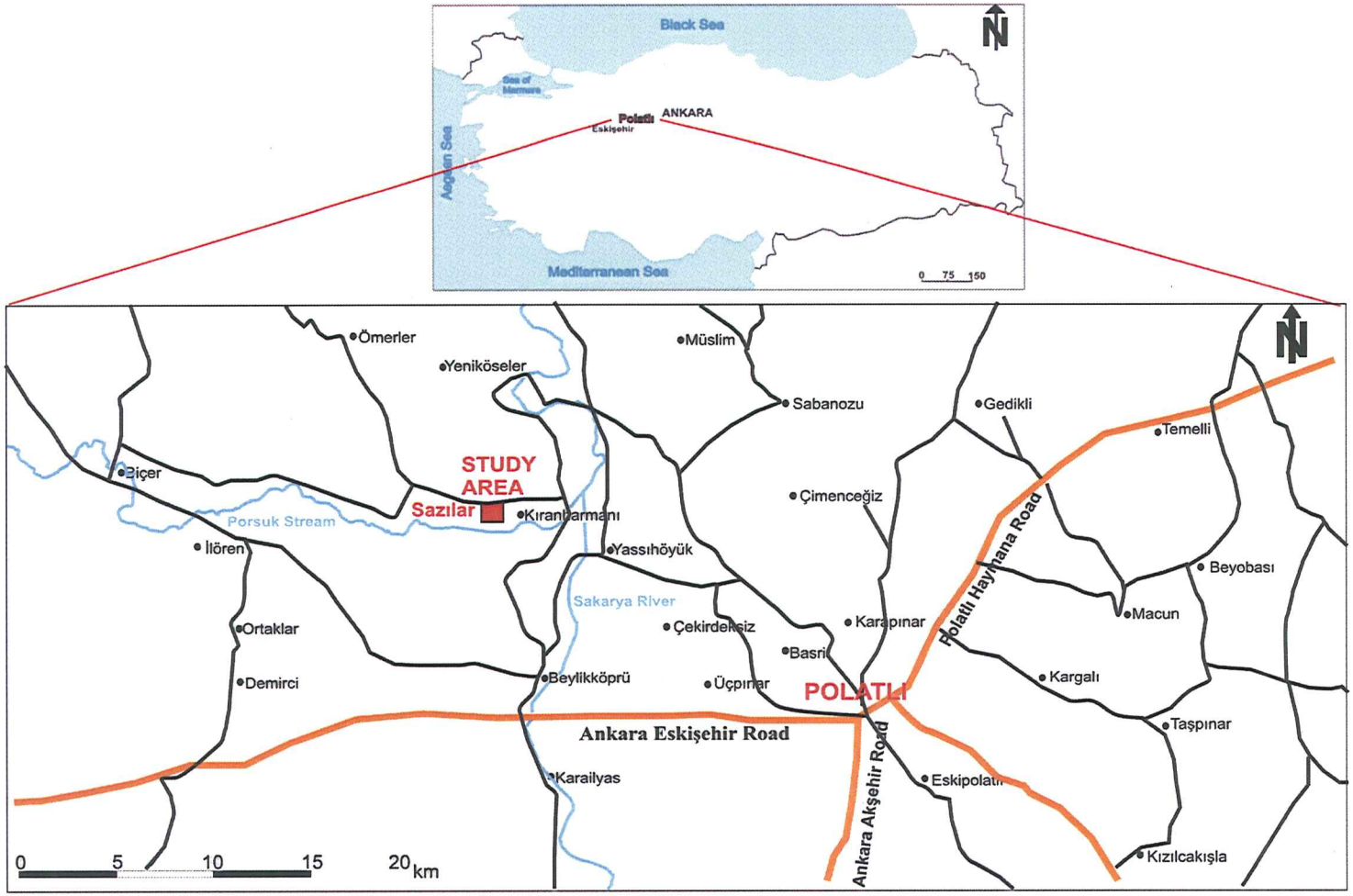

Figure 1. Location map of the study area

Bingöl (2004) described in his study the gypsum deposits of Turkey and he mentioned that the Messinian aged gypsum in Polatlı-Sivrihisar basin has granular selenitic texture and is intercalated with clay, limestone, dolomite and marl. He proposed that the layers are horizontal and the Syngenetically, the deposition of dolomite, magnesite, atapulgite, sepiolite, smectite and illite are common.

Altay et al (2006) studied the mineralogical and chemical properties of various types of gypsum occurrences at Sivrihisar region. According to the authors, Neogene lacustrine sediments, in ascending order, have been named as İlyaspaşa, Sakarya and Kepen formations. The Sakarya Formation consists of gypsum associated with dolomite, dolomite-bearing sepiolite and calcite and in places, palygorskite. In this formation, gypsum occurrences are classified according to their mineralogical features: namely (1) dolomite -bearing gypsum (clay to sand-sized, white, lenticular and discoidal crystals, whereas the gypsum crystal size is coarser in the lower levels); (2) displacively grown gypsum that developed as fracture fillings (lenticular, shallow tail and rosette shaped, honey brown and colorless gypsum crystals).The upper gypsum levels sparsely dolomitic, especially gypsum rich and become calcite rich in the uppermost layers.

1.3.2 Gypsum and the Impurities

Gypsum (hydrous calcium sulfate) is both a mineral name and a rock name. The chemical formula of gypsum is $CaSO_4.2H_2O$. In gypsum, the anionic $(SO_4)^{-2}$ groups, where S occurs in tetrahedral coordination with respect to O^{-2} with the covalent bonds, are the fundamental structure units of sulphates. The isolated $(SO_4)^{-2}$ tetrahedra is connected by eight-coordinated polyhedra that consist of Ca^{2+} bonded to six oxygens and two water molecules. The isolated $(SO_4)^{-2}$ tetrahedra and the neighboring Ca^{2+} cations that share oxygens define planar units within the structure. These units are separated from each other by H_2O

layers parallel to {010}, and this is the structural feature that accounts for the perfect {010} cleavage of gypsum (Zoltai and Stout, 1996), (Figure 2).

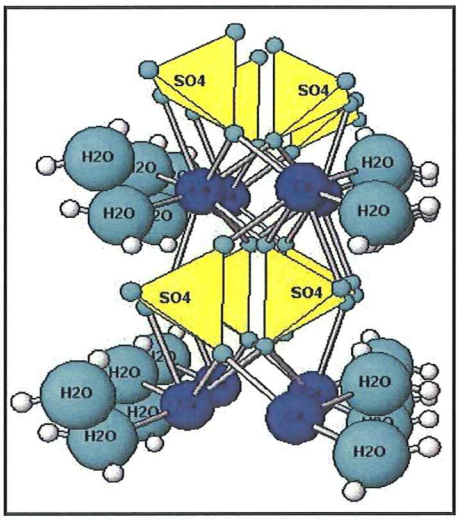

Figure 2. Crystal structure of gypsum (Nesse, 2000) (yellow: SO_4, blue: Ca, green: oxygen and white: hydrogen)

Concerning the crystallographic structure of the gypsum, it has a monoclinic structure with four cleavages in four directions. Indeed, perfect {010} cleavage determines the crystal shape. Two good cleavages parallel to the {110} prism intersect angles of 42° and 138°. Cleavage folia are flexible in certain directions, but not elastic, it is brittle (Nesse, 2000).

Gypsum has a low birefringence value of 0.009 and would normally show only weak interference colors of the 1st order similar to quartz in thin section and has low negative relief (Milovskii, 1985).

Once the physical properties of gypsum are considered, it is white to colorless. It has a luster of vitreous, pearly or sometimes silky. It is transparent to translucent and has a hardness of 1.5-2.0 and can be scratched by fingernail. Its specific gravity is 2.3-2.4 with a streak of white (Harben and Bates, 1990).

Gypsum is found in a number of forms such as massive rock gypsum, alabaster, selenite, satin spar and gypsite. Massive rock gypsum comprises most of the commercial gypsum and occurs as a sedimentary rock, interbedded in most places with shale, limestone or dolomite. This rock is a compact, massive, finely crystalline to granular rock. It is white when pure, but may be gray, bluish-gray, pink, or yellow, owing to such impurities as organic matter, clay and iron oxide. Alabaster is a pure, compact and fine grained variety suitable for use in sculpture or turning into artistic form; it may be white or selected for attractive coloration. Selenite is clear monoclinic gypsum crystallized in flat, transparent, flexible, foliated plates, found in clays or surface vugs in gypsum. It has pearl like luster. Satin spar is a fine silky fibrous variety with the axes of the crystalline fibers perpendicular to the vein or joint in which it has formed. Gypsite is weakly consolidated earthy mixture of gypsum with clay and sand. It is a surficial material that forms as an efflorescent crust in regions of little rain and rapid evaporation (Jorgensen, 1994).

Gypsum can be confused with anhydrite having the formula of $CaSO_4$. However, there are some criteria used to differentiate these two minerals. Initially, concerning optical properties, anhydrite has higher birefringence and cleavages intersecting at 90°. Secondly, in hand specimen, anhydrite has a higher specific gravity and has a little dark gray in colour when we compare with gypsum. In addition, anhydrite has a higher hardness than gypsum (Leeder, 1982).

Pure gypsum contains 20.9 % combined water, 46.6 % sulfur trioxide (SO_3) and 32.5 % lime (CaO). Standard specifications read the minimum purity for material to be called gypsum is 70 % $CaSO_4.2H_2O$. Most of the commercial gypsum is 85 to 95 % pure as produced (Ries, 1985).

Concerning the impurities, the number of minerals that can occur in evaporate deposits is quite large and many can be found as impurities in calcium sulfate

deposits. Their occurrence is often dependent upon the mode of formation of the deposit. In varying degrees, most gypsum and anhydrite deposits contain terrigeneous and calcareous clastic sediments, and commonly clay minerals, as well as chemical precipitates such as carbonates (Carr, 1994).

In sabkha type deposits, these preexisting sediments fill internodular spaces of the gypsum and anhydrite, or form crude layers. Relatively insoluble evaporite minerals such as celestite, certain borates, some carbonate minerals, and silica may occur in calcium sulfate deposits as discrete crystals, crystal aggregates or nodules, and probably are in many cases original depositional features. However, strontium or boron, which may be present in only trace amounts in anhydrite, may migrate during gypsification to result in strontium and boron mineral accumulations (Carr, 1994).

Soluble evaporite minerals, e.g., halite, sylvite, mirabilite, epsomite, and others also frequently found in calcium sulphate deposits. These minerals most commonly become associated with the clay minerals that may be present, probably being adsorbed on the clay mineral surfaces. They also are associated with the carbonate impurities where they may be adsorbed onto mineral surfaces, held as fluid inclusions, or included in a disordered lattice. In addition, these soluble minerals can occur as microfracture filling (Carr, 1994).

Briefly, impurities may be separated into three categories based on solubility and water content shown in Table 2.

1.3.3 Origin and Occurrence of Gypsum

Evaporite deposits are composed dominantly of varying proportions of halite (rock salt), anhydrite and gypsum. Although approximately 80 minerals have been reported from evaporite deposits (Stewart, 1963), only about a dozen of

these minerals are common enough to be considered important evaporite rock formers.

Table 2. Category of the impurities based on solubility and water content (Carr, 1994)

Insoluble Relatively Insoluble	**Hydrous but Insoluble**	**Soluble Minerals**
Calcite $CaCO_3$	Smectite Grp. (Montmorillenite)	Halite NaCl
Dolomite $CaMg(CO_3)_2$		Slyvite KCl
Anhydrite $CaSO_4$		Mirabilite $Na_2SO_4.10H_2O$
Anhydrous Clays e.g. Kaolinite, Brucite		Epsomite $MgSO_4.7H_2O$
Silica Minerals e.g. Quartz, Chalcedony		Glauberite $Na_2Ca(SO_4)_2$
		Syngenite $K_2Ca(SO_4)_4$
		Polyhalite $K_2Ca_2Mg(SO_4)_4.2H_2O$

Evaporite minerals are commonly classified into those of marine origin and those of non-marine origin, although Hardie (1991) suggests that identifying the marine or non-marine origin of evaporites on the basis of their mineralogy and chemistry may not be entirely justified. The most common minerals generally considered to characterize marine evaporites are the calcium sulfate minerals gypsum and anhydrite. Gypsum is more abundant than anhydrite in modern evaporite deposits but anhydrite is more abundant in ancient deposits (Boggs, 2001).

Considering an evaporation sequence, when ocean water is evaporated in the laboratory, evaporite minerals are precipitated in a definite sequence that was

first demonstrated by Usiglio (1848) (in Clarke, 1924). Minor quantities of carbonate minerals begin to form when the original volume of seawater is reduced by evaporation to about one-half. Gypsum appears when the original volume has been reduced to 20 percent, halite forms when the water volume reaches approximately 10 percent of the original volume. The precipitation of gypsum causes an increase in the Mg/Ca ratio in remaining water, which favors the process of dolomitization. Dolomite occurs in association in many ancient sedimentary successions, as well as in some modern environments. Magnesium and potassium salts are deposited when less than about 5 percent of the original volume of seawater remains. The same general sequence of evaporite minerals occurs in natural evaporite deposits, although many discrepancies exist between the theoretical sequences predicted on the basis of laboratory experiments and the sequences actually observed in the rock record. In general, the proportion of $CaSO_4$ (gypsum and anhydrite) is greater and the proportion of Na-Mg sulfates is less in natural deposits than predicted from theoretical considerations (Boggs, 2001)

Gypsum accumulates in basins or on supratidal salt flats under arid conditions. It is found in every geologic system from Cambrian through Quaternary. Its occurrence can be observed on every continent in the world. Gypsum deposits for the most part belong to the sedimentary class in which the mineral occurs in beds or layers intercalated between limestones, shales and sandstones, or more rarely with rock salt. In such association, they usually have been considered as precipitations from the evaporation of saline waters in basins in which the shales, limestones or rock salt were laid down. The saline waters may have existed as a salt lake, or they may have been a part of the sea shut off from the open ocean by a bar or enclosed as a gulf (Newland, 1929).

The older, well established concept of deposit formation idealized a brine-filled basin having restricted circulation (Branson, 1915, King, 1971) which permits limited replenishment of the brine as it evaporates. Increasing the brine

concentration leads to precipitation of the contained salts in the inverse order of their solubility, and substantial thickness of essentially monomineralic deposits (e.g., calcium sulfate) are visualized as being derived from this type regime. In addition, according to Branson (1915), gypsum may have been deposited in a series of lakes under the following conditions: some evaporation occurred in the first lake, from which the water flowed to the next; more concentration took place in the second lake; and the final deposition occurred in the last lake under sediment-free conditions. This theory would account for the pure beds of gypsum which occur and also for the thick beds (due to the concentrated solutions in the last lake of the chain).

A more recent concept of evaporate deposition has resulted from considerable work done in the Trucial Coast of Arabia (Butler, 1970; Kinsman, 1966) which describes the sabkha supratidal environment wherein calcium sulfate minerals are currently being deposited (sabkha, an Arabic word denoting salt-flat). These deposits are characterized by a distinctive sequence of sediments including lagoonal limestones, intertidal algal mat limestones, and precipitation of gypsum crystals and nodular anhydrite in the preexisting host sediments, which if originally calcium carbonate, become dolomitized. Clastic sediments, if present, are unaffected chemically, but are contorted and displaced as the gypsum crystals and nodular anhydrite grow in them. In the sabkha regime a basin is not required for deposition, although some concentration of the original seawater brine does take place in alongshore lagoons. Thick chloride accumulations would not be expected (Schroeder, 1970).

Another common environment for the accumulation of gypsum is in salt domes. A 'caprock' of anhydrite, often with gypsum and porous limestone in its upper part, rests with sharp contact on the top of the salt column. This caprock can be thin and irregular. It presumably accumulated as a residue leached from the salt as the column rose through water-saturated sediments and was dissolved.

Although salt domes are important as producers of salt and sulfur, they are only minor sources of commercial gypsum (Harben and Bates, 1990).

Gypsum may also precipitate along fractures, bedding planes or in other available spaces where ground water carrying sulfate ions from the oxidation of sulfates comes into contact with carbonate rocks. Gypsum also occurs in minor amounts in some igneous and hydrothermal deposits, i.e. eastern Indonesia (P. Redecke, oral communication). Such deposits have no influence on gypsum production economics (Carr, 1994).

Gypsum carries no fossils, and despite minor differences in texture and composition, gypsum from one deposit is much the same as that from another. The associated rocks are restricted in variety, consisting mainly of other evaporates, carbonate rocks, and shale. Gypsum is sufficiently widespread in occurrence so that only readily accessible deposits, mostly flat lying or nearly so and at or near the surface are utilized (Bates, 1969).

1.3.4 Distribution of Gypsum Deposits in the World and Turkey

Gypsum is mainly found in the Permian, Triassic and Tertiary formations in the world. The Permian includes the Upper Permian (Zechstein deposits, Germany). The Triassic consists of Lower (Bundsandstein), Middle (Muschelkalk), and Upper Triassic (Keuper).

The Tertiary deposits include the Eocene which is observed in Spain, Persia and, the Oligocene observed in Paris, and the Miocene occurred in Mediterranean area and Africa. The Jurassic and Cretaceous formations which lie between the Triassic and Tertiary are almost devoid of useful gypsum deposits, as are the older pre-Permian formations.

1.3.4.1 Significant Deposits in the World

France, Germany, Canada, United Kingdom, Australia and United States are the countries where important gypsum deposits are present. In the following paragraph, details about these gypsum occurrences are explained below.

France: The main areas of production are Paris and Rhone Basins. Lower Eocene beds are exploited in the Paris Basin by approximately a dozen open-pit mine and three underground mines. In the Rhone Basin, Upper Eocene and Oligocene gypsum beds are over 400 feet thick. (Harben and Bates, 1990).

Germany: Gypsum deposits have three different geological age: Zechstein, Muschelkalk, and Keuper. The most important is the Zechstein, of Permian age, especially in the borders of the Harz Mountains near Stadtoldendorf. Three minor occurrences are in the Keuper of Franconia, Bavaria, and Baden-Württemberg (Lüttig, 1980).

Canada: Maritime region of eastern Canada has become the largest gypsum mining district in the world. Of particular importance is the Windsor group of Mississippian age, which includes more than 3000 feet of red beds, limestone, anhydrite, gypsum and salt. The Windsor Group represents the only period of marine deposition during the Carboniferous of this region (Appleyard, 1983).

United Kingdom: Most of the gypsum produced in the UK comes from Nottinghamshire, Sussex and the Vale of Eden, with smaller amounts from Staffordshire and north Yorkshire. The most important commercial beds are Permo-Triassic in age, except for those in Sussex which are Jurassic (Harben and Bates, 1990).

Australia: The commercial deposits, all of Quaternary age, are located in the low-rainfall areas of South Australia, Western Australia, Victoria, and New

South Wales. The bulk of production comes from Holocene lake deposits, particularly those less than 6000 years old, either inland or along the coast (Harben and Bates, 1990).

United States of America: The principal gypsum producing areas in North America are Iowa, Michigan, New York-Ontario, Ohio, Indiana, Virginia and California. In western Imperial County and neighboring San Diego County, close to the Mexico border, gypsum deposits occur in the Split Mountain member of the Imperial Formation (Miocene). The beds range in thickness from 5 to 100 feet, the thickest beds occurring in the crests of folds (Prentice, 1990).

1.3.4.2 Significant Deposits in Turkey

Gypsum deposits are present at different parts of Turkey and these occurrences are mainly Tertiary in age. Below major gypsum occurrences is explained and figure 3 illustrates the major gypsum occurrences in Turkey.

Beypazarı basin is a large basin that extends to Beypazarı, Nallıhan, Mihalıççık, Sivrihisar, Emirdağ, Polatlı and Ayaş. Gypsum is the major occurrence, but anhydrite is also observed in minor amount (Önenç, 2004). Gypsum in Beypazarı-Çayırhan basin intercalates with marl and limestone, is related to the Messinian transgression, 8-21 m thick and white to ivory in colour and has selenitic and granular texture. Gypsum overlies glauberite mineralization over 1-2 m thick smectite. Chloride content increases as the gypsum comes closer to glauberite. Actually, the chloride content is 100 ppm at the surface and 4000 ppm in the deeper parts. The swelling clay content is 1,6-2,5 %.

In Polatlı Sivrihisar basin, gypsum beds are of Messinian age, 3-20m thick, ivory to white in colour gypsum is present with selenitic texture. Gypsum intercalates with claystone, limestone, dolomite and marl. The layers are

generally horizontal, the inclination does not exceed 7-8°. The chloride content is less than 10 ppm. The swelling clay content is 0,9 - 2,6 % (Bingöl, 2004).

Gypsum deposits in Düzce-Kaynaşlı basin crop out in the south of E5 highway. The gypsum is of Upper Eocene-Oligocene age, white coloured, has granular texture and overlies 20m thick anhydrite. The thickness of gypsum is 10-12 m.

Bala-Tuz Gölü basin and Ulukışla basin includes the most economical and high quality gypsum deposits. The thickness of the Upper Eocene-Miocene layers, generally white coloured gypsum ranges from 5 to 25 m. Below the gypsum, anhydrite is present with a thickness of 60 m. The chloride and swelling clay content is very low (Bingöl, 2004).

In Çankırı-Çorum basin, in two different stratigraphical zones, structurally and texturally different two gypsum levels are present. Upper Eocene-Oligocene, 2-6 m thick, layered and/or lenticular and nodular gypsum is present in the region. Gypsum is intercalated with sandstone, claystone, siltstone and conglomerate and isoclinal and/or convolute folding is observed. The swelling clay content is %3,6.

Kırıkkale-Yozgat basin is between the Çankırı-Çorum and Bala-Tuzgölü basins and the gypsum has the same properties as the gypsum in these basins. In the region, Upper Eocene-Oligocene age, light grayish, white and pinkish gypsum, 20-30 m thick and Messinian age, white to gray coloured gypsum are observed. It is intercalated with 5-15 m thick marl, limestone and sandstone.

In eastern Anatolia, Sivas basin includes prominent gypsum occurrences. This basin extends to west of Bünyan and to Ecemiş Fault in the west; to Munzur mountains in the northeast and covers an area with a length of 400 km and width of 50-100 km. The gypsum is intercalated with marl and claystones and has a thickness of 150 m. The white to yellowish white and grayish gypsum is of

Upper Eocene-Miocene age. In the southern part of Sivas, celestine deposits are present with massive, granular gypsum

The gypsum occurrences in Pasof, Norman and Aşkale in Northeast Anatolia are of Oligo-Miocene age. The gypsum is yellowish to white in colour and has a thickness of 12 m (in Aşkale 8-12m). It is lenticular and layered (in Aşkale, in some parts massive and granular) and intercalated with limestone, sandstone and mudstone. The thickness of the gypsum is 150 m (Bingöl, 2004).

In Kars-Kağızman, Tuzluca Basin, gypsum occurrences are observed along Aras River and deposited at the upper part of the Pliocene aged continental deposits. Apart from these deposits, Neogene aged gypsum deposits are situated from Tortum, Narman, Oltu to Kars-Şenkaya.

South East Anatolia Basin is an important basin where gypsum deposits are of Oligocene-Miocene age. Gypsum reserves are also present in Siirt-Baykan, Kurtulan, Batman-Merkez, Beşeri and Diyarbakır- Çınar, Bismil (Önenç, 2004).

In Denizli-Kaplık (Kızılyer) region, gypsum is still exploited and has a thickness of nearly 40 m. It is white to gray in colour and brecciated. The genesis and the age of the deposits are under discussion. The clay and chloride content is low.

In Mersin-Adana-İskenderun, there are six gypsum occurrences with thicknesses of 10-30 m. White and light gray gypsum is present in the middle of the selenitic, granular and massive gypsum. The chloride content is 10-33 ppm and swelling clay content is 0,3-0,7% (Bingöl, 2004).

Apart from these gypsum deposits, some other less significant gypsum occurrences are also present in Konya-Cihanbeyli, Nevşehir-Gülşehir and Hacıbektaş, Kayseri-Bünyan, Hatay-İskenderun, Malatya-Hekimhan, Tokat-Artova, Giresun-Şebinkarahisar, Tunceli-Merkez (Önenç, 2004).

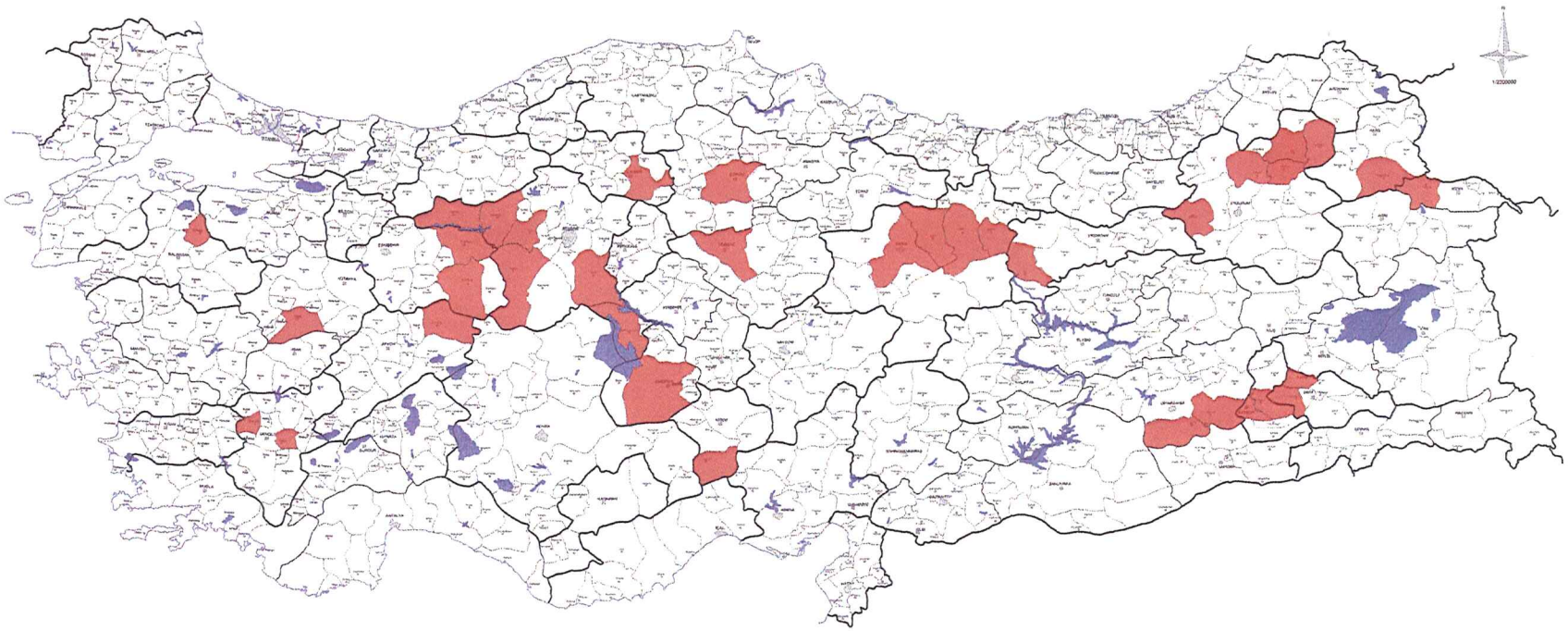

Figure 1. Major gypsum occurrences in Turkey (modified from Bingöl, 2004; gypsum occurrences are indicated by red colour)

CHAPTER 2

REGIONAL GEOLOGY

2.1 Geological Setting of Haymana-Polatlı Basin

Tuz Gölü basin complex consists of Haymana-Polatlı sub basin and Tuz Gölü sub basin. These two basins evolved coevally, but independently, during Late Cretaceous to Eocene (Görür et al. 1984; Çemen, 1999).

The Haymana-Polatlı Basin, 70 km SW of Ankara, was developed within a continental collision regime at the northern branch of the Neo-Tethys (İzmir-Ankara suture zone). The Sakarya Continent to the N-NW, the metamorphic block of Kırşehir to the east and Menderes-Taurid block to the south surround the basin (Görür et al., 1984; Göncüoğlu, 1992) (Figure 4).

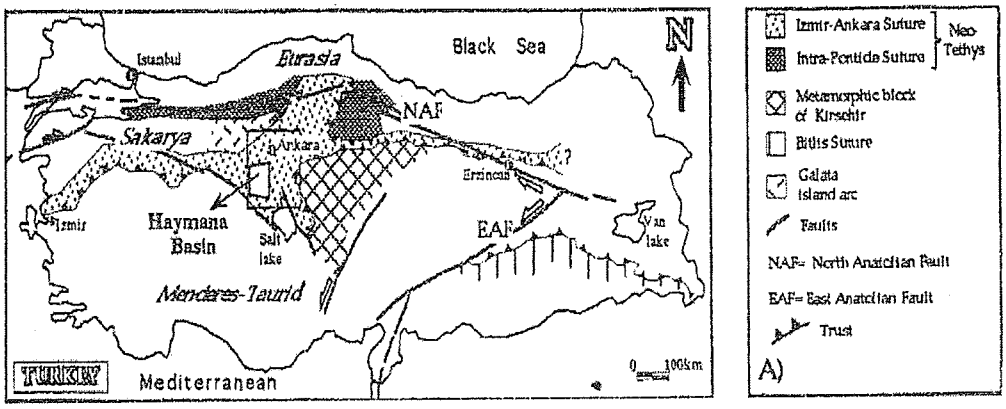

Figure 4. Main structural features of Turkey (modified after Koçyigit, 1991 in Çiner, 1993)

Due to the existence of calc-alkaline volcanism in the Pontides during Tertiary, with the frequent occurrence of volcanoclastic sediments and the presence of an ophiolitic basement in the basin, many authors (Şengör and Yılmaz, 1981; Görür et al. 1989; Koçyiğit, 1991; Çiner, 1992) suggested that the Haymana Basin was developed on a fore-arc accretionary wedge that was active from the Upper Cretaceous to the Lower Eocene. Arc activity in the Sakarya Continent during the Paleocene suggests a subduction towards the North (Fourquin, 1975)

Koçyiğit (1991) stated that in Haymana-Polatlı basin, the sediments of forearc basins and rocks of accretionary wedge were deformed, raised, and finally thrust on each other. In the Haymana-Polatlı basin, the sedimentary sequence is more than 5 km thick (Ünalan et al., 1976; Görür 1981; Görür et al., 1984; Koçyiğit, 1991). The Maastrichtian to Eocene sequence is dominated mostly by deep marine flysh (Koçyiğit, 1991) and it also contains local reefal buildups and volcanic intercalations (Görür, 1981, Koçyiğit and Lünel, 1987).

Basement of Haymana sub-basin, is composed of the Jurassic-Early Cretaceous carbonate cover of the Sakarya Continent (Şengör and Yılmaz, 1981), the Karakaya Complex forming a part of the pre Jurassic basement of the Sakarya Continent (Görür et al., 1984) and the Ankara mélange (Bailey and MacCallien, 1953; Norman, 1975; Ünalan et al., 1976; Görür and Derman, 1978; Norman et al., 1980; Koçyiğit, 1991)

Maastrichtian aged Haymana Formation (Rigo de Righi and Cortesini, 1959; Reckamp and Özbey, 1960; Schimidt, 1960; Reckamp and Özbey, 1960; Akarsu, 1971; Sirel, 1975; Ünalan et al., 1976; Görür, 1981; Görür et al., 1984) overlies this composite basin, mostly with an unconformity. The formation consists of turbidites that are composed of dominantly sandstone and shale intercalations with frequent conglomerates, olistostromes and debris-flow deposits. The clastics are derived most probably from Karakaya Complex and Ankara mélange and metamorphic rock fragments including composite quartz, and potassic and

sodic feldspars derived from the basement of the Sakarya Continent (Ünalan et al., 1976; Görür and Derman, 1978; Norman et al., 1980; Görür et al., 1984) (Figures 5 and 6)

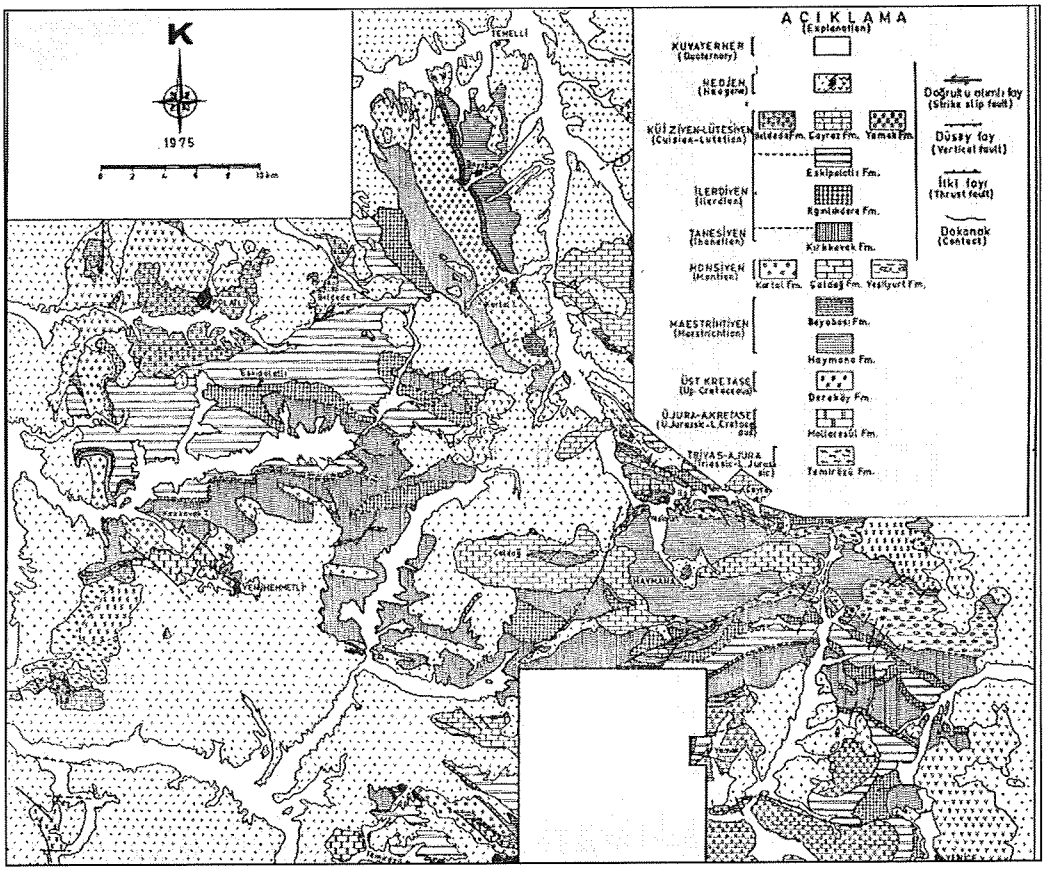

Figure 5. Geological Map of Haymana Polatlı Region (Ünalan et al., 1976)

Late Maastrichtian aged Asmaboğazı Formation (Görür, 1981) conformably overlies the Haymana formation and represented by rudist and coral rich sandstone, shale and limestone beds. This formation is a good key horizon for the Haymana basin. This formation is named as Beyobası Formation by Ünalan et al. (1976).

Asmaboğazı Formation is overlain by Kartal, Çaldağ and Kırkkavak Formations, respectively. During the Paleocene, deposition of terrestrial red conglomerate,

sandstone and siltstone sequence of the Kartal Formation (Rigo de Righi and Cortesini, 1959; Reckamp and Özbey, 1960; Sirel, 1975; Ünalan et al., 1976; Görür, 1981; Görür et al., 1984) and reefal limestones of the Çaldağ Formation (Rigo de Righi and Cortesini, 1959; Yüksel, 1970; Akarsu, 1971, Görür, 1981; Görür et al., 1984) characterized the basin edges, whereas relatively deeper water shale limestone intercalations of the Kırkkavak Formation were laid down in the interior of the basin (Görür et al., 1984). The age of Kartal Formation is suggested by Ünalan et al. (1976) as Montian; however, the main development of Kartal Formation within the Haymana-Polatlı basin is considered to be from Maastrichtian to Eocene (Görür, 1981; Görür et al., 1984). In addition, Rigo de Righi and Cortesini (1959), Sirel (1975), Ünalan et al. (1976) state the age of the Çaldağ Formation as Montian. However, Görür (1981) indicate the horizontal and vertical boundary relations between Çaldağ and the Kırkkavak Formations indicate Montian to Thanetian age for Çaldağ Formation (Figure 6).

Kırkkavak Formation is overlain by Ypresian-Lutetian aged Eski Polatlı Formation (Rigo de Righi and Cortesini, 1959; Reckamp and Özbey, 1960; Akarsu, 1971; Sirel, 1975; Ünalan et al., 1976; Görür, 1981; Görür et al., 1984). Eski Polatlı Formation contain clasts of serpentinite, dunite, peridotite, diabase, basalt, radiolarian cherts and glaucophane schists derived from the ophiolitic mélanges of the Karakaya Complex and the Ankara mélange, as well as micaschists and amphibolites from the ophiolitic mélange and Sakarya basement, and rhyolitic lava flows from the Sakarya magmatic arc (Görür et al., 1984) Ünalan et al. (1976) named the conglomeratic lower parts of the Eski Polatlı Formation as Ilgınlıkdere Formation. The upper parts of the Eski Polatlı Formation laterally and vertically pass into the shallow marine nummulitic limestones of the Çayraz Formation and terrestrial clastic sediments of Kartal Formation (Görür, 1981, Görür et al., 1984). These levels of the Eski Polatlı Formation have been named as Yamak Formation by Ünalan et al. (1976). The deposition of the Kartal and Çayraz formations was terminated by the arrival of a

slice of ophiolitic mélange (Ünalan et al., 1976; Görür, 1981, Görür, et al., 1984).

Both the mélange nappe and the underlying rocks were later covered unconformably by terrestrial conglomerates, sandstones, marls, evaporites, and the tuffs of the Mio-Pliocene Cihanbeyli Formation (Görür, 1981; Görür et al., 1984) (Figure 6).

2.2 Stratigraphy of the Study Area

The stratigraphy of the region is studied by Ünalan et al. (1976), Gençoğlu and İrkeç (1994) and Gözler et al. (1996).

The stratigraphical units in and around of the study area are composed of various metamorphic and ophiolitic rocks, volcanic, sedimentary rock sequences and Quaternary alluvium. The lithostratigraphical units from older to younger are as follows: Pre-Miocene Bedrocks, Early-Mid Eocene Beldede Formation, Early-Mid Eocene sedimentary and volcanic rocks, Late Miocene-Pliocene Porsuk Formation and Quaternary alluvium (Akdağ, 2005; Türkbey, 2005) (Figures 7 and 8).

Pre-Miocene rocks consist of crystalline dolomitic limestones, granitoids, metamorphic-ophiolitic bedrocks and Early-Mid Eocene Beldede Formation. This formation consists of reddish to brownish conglomerate, sandstone, siltstone and clayey, sandy limestone (Ünalan et al., 1976) (Figure 8).

Early-Mid Miocene units unconformably overlie the Pre-Miocene units. These units are claystones, limestones, tuffs and basalts. The age of these units have been identified by K/Ar age determination applied to the basalts intercalating with the sediments (Temel et al., 2001, 2005) (Figure 8).

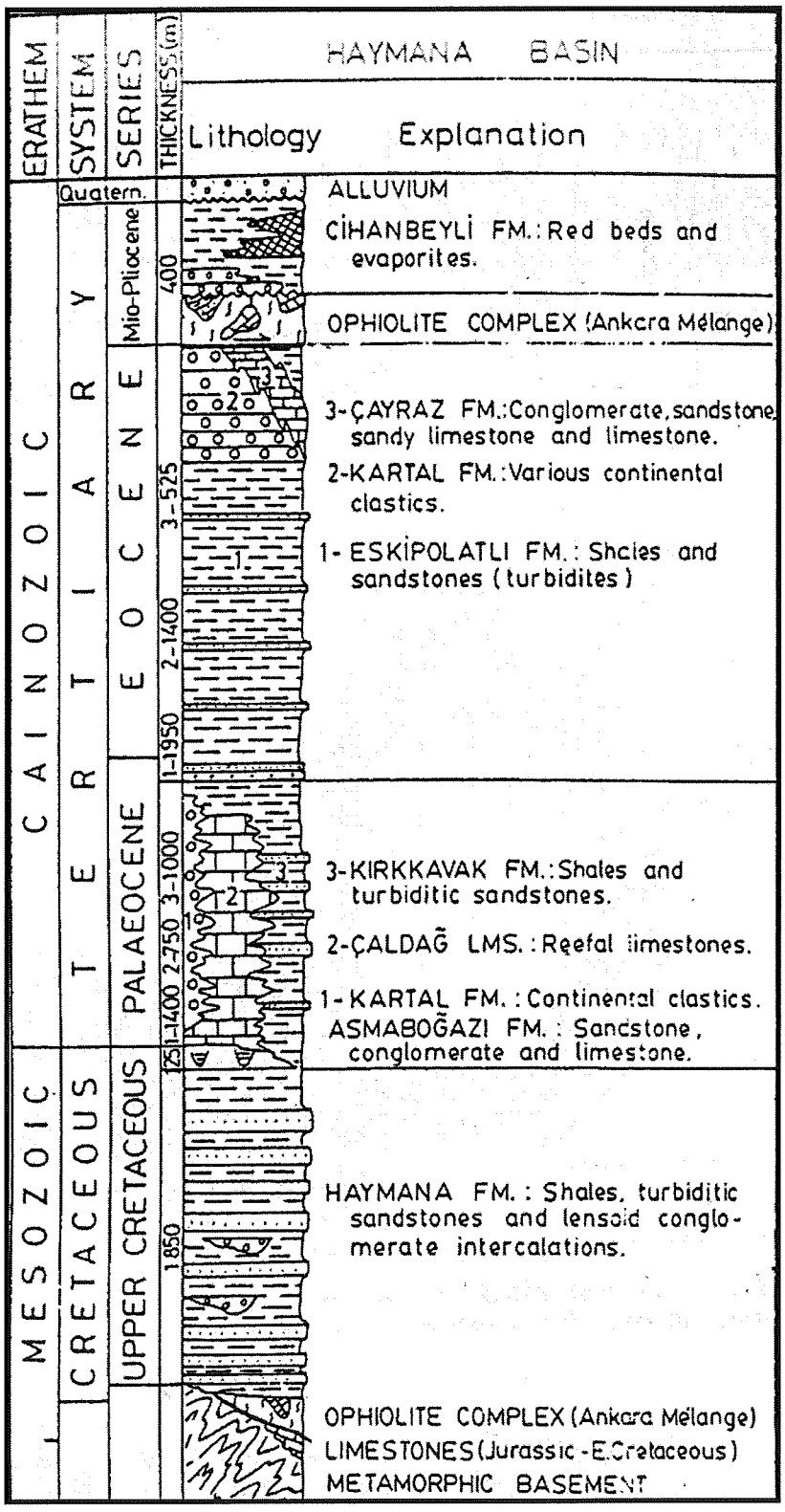

Figure 6. Generalized Stratigraphic Columnar Sections of Haymana Sub-basin (Görür et al., 1984).

Porsuk Formation defined by Gözler et al. (1996) overlies unconformably the Early-Middle Miocene lithostratigraphic units. Porsuk Formation is composed of conglomerate, tuff and tuffite, marl and claystones, gypsiferous marl and claystones, gypsum, limestones and basalts (Gözler et al., 1996). Quaternary alluvium overlies the Porsuk Formation (Figures 7 and 8).

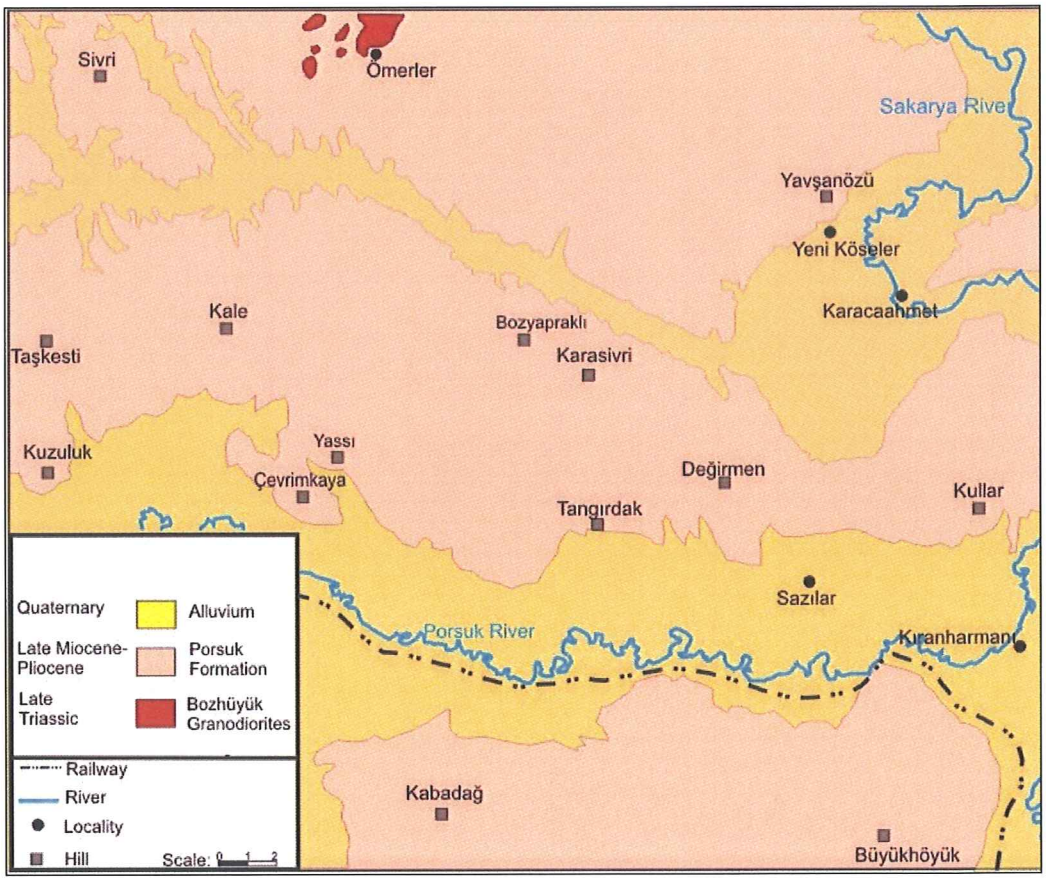

Figure 7. Geological Map of the Polatlı Sazılar Region (modified from Gözler et al., 1996 in Türkbey, 2005)

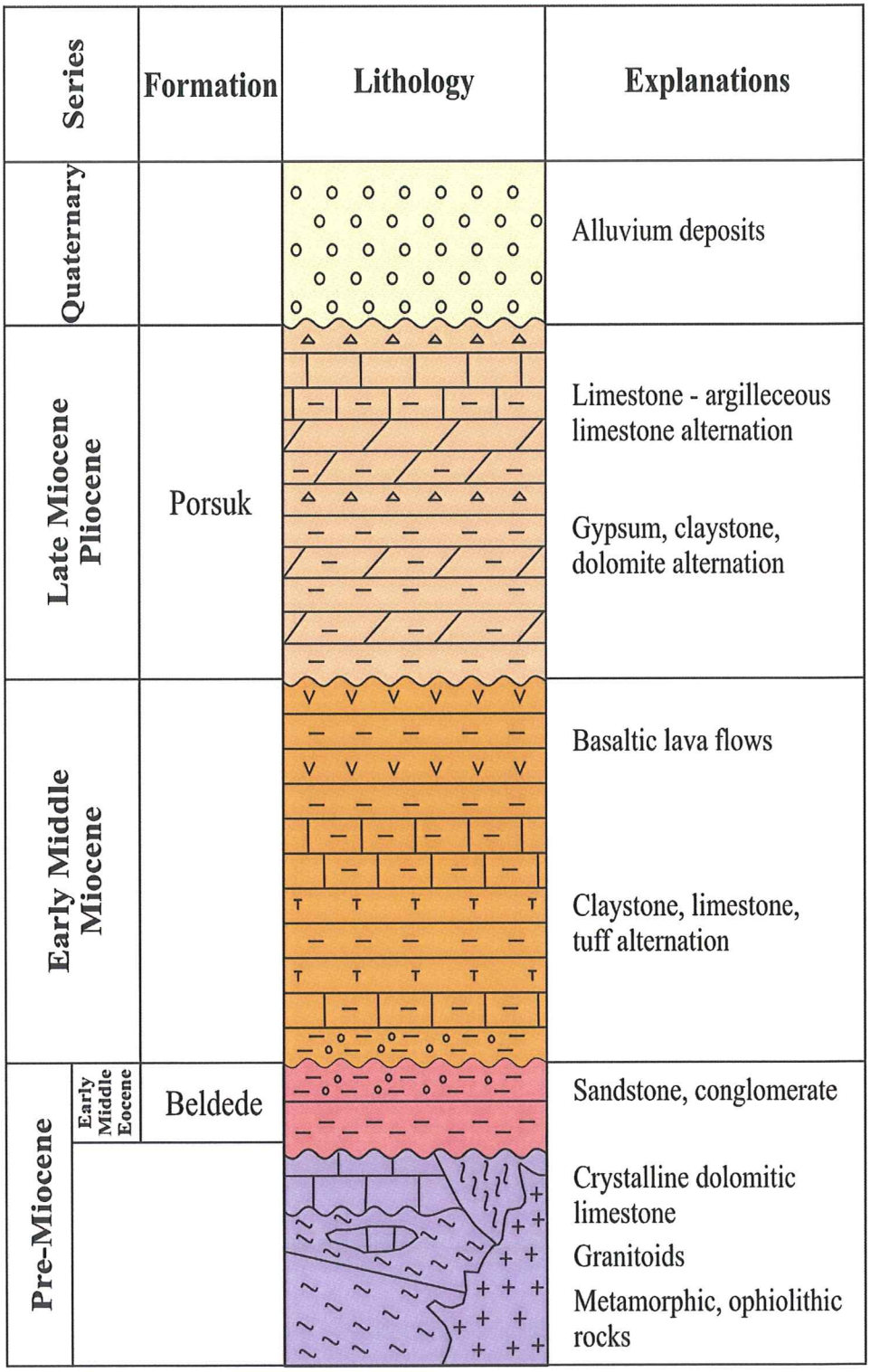

Figure 8. Generalized Stratigraphic Section of the Study Area (Ünalan et al., 1976; Gençoğlu and İrkeç, 1994; Gözler et al., 1996 in Akdağ, 2005; not to scale).

CHAPTER 3

PETROGRAPHY AND MINERALOGY

3.1 Introduction

Petrographical studies were conducted based on the logging of two drillcores and studies with polarized microscobe. 20 samples from drillcore I and 7 samples from drillcore II were handled in thin section studies.

Under the scope of mineralogical studies, scanning electron microscope with energy dispersive X-ray and X-ray diffractometry analyses have been performed aiming to define the impurities in the gypsum rock and to understand the 3-D relationship of these impurities and the rock.

Initially, petrographic studies, then mineralogical studies will be explained.

3.2 Definition of Gypsum Related Terminology

While performing petrographic determination, the terms regarding some physical properties of gypsum varieties have to be identified. In this sense, the following terms are explained to clarify the confusion in the terminology of gypsum and to make clear naming of different gypsum varieties.

Alabaster is the massive variety and is fine grained, compact rock gypsum, generally white in colour, mainly used in sculpture.

The term secondary gypsum which originates from the hydration of precursor anhydrite rock was first used by Murray (1964) and later by Mossop and

Shearman (1973). Secondary gypsum is divided into two main petrographic groups such as coarse porphyroblastic secondary gypsum and fine grained alabastrine secondary gypsum (Holliday, 1970; Warren, 1999).Porphyroblastic gypsum often retains dispersed relics of the precursor anhydrite. Crystal forms are coarse, up to 2 cm across, and can be euhedral or anhedral, thin and acicular or thick and stubby. Porphyroblasts often aggregate into centimeter scale rosettes or blebs with acicular gypsum rinds. This creates a texture that is sometimes described as "daisywheel gypsum". Because of the destructive nature of porphyroblastic overprinting, interpreting original depositional environment from near surface $CaSO_4$ units, composed entirely of diagenetically regenerated gypsum is impossible (Warren, 1999).

The other form of bedded gypsum, generated by anhydrite rehydrated to gypsum in the zone of active phreatic flow, is fine grained alabastrine gypsum. Individual gypsum grains are typically less than 50μm, with grain boundaries that range from poorly defined to equidimensional granuloblastic (Figure 9). It is milk-white coloured, homogeneous and its general appearance resembles the finely crystalline white marble (Gündoğan et al, 2005). Alabastrine and pophyroblastic texture are easily distinguishable with the naked eye and with hand lens, and these two terms have been used for macroscopic identification (Gündoğan et al, 2005). In thin section, alabastrine texture shows erratically migrating extinction shadows when the section is rotated under cross-polarized light (Gündoğan et al., 2008). The other variety of gypsum is selenite or selenitic gypsum. Selenite is frequently used to indicate well-crystalline gypsum, as opposed to the massive gypsum. It is transparent, vitreous. The origin of it could be primary and secondary.

Satin spar is another variety of gypsum. It is fibrous in appearance and contains needle shaped crystals. The fibrous satin spar gypsum may occur as gypsum veins interbedded within the evaporites and as well as the carbonates (Makhlouf,

2006). Many authors consider satin spar gypsum as bi-product of the rehydration process of anhydrite (Shearman et al., 1972; Testa and Lugli, 2000).

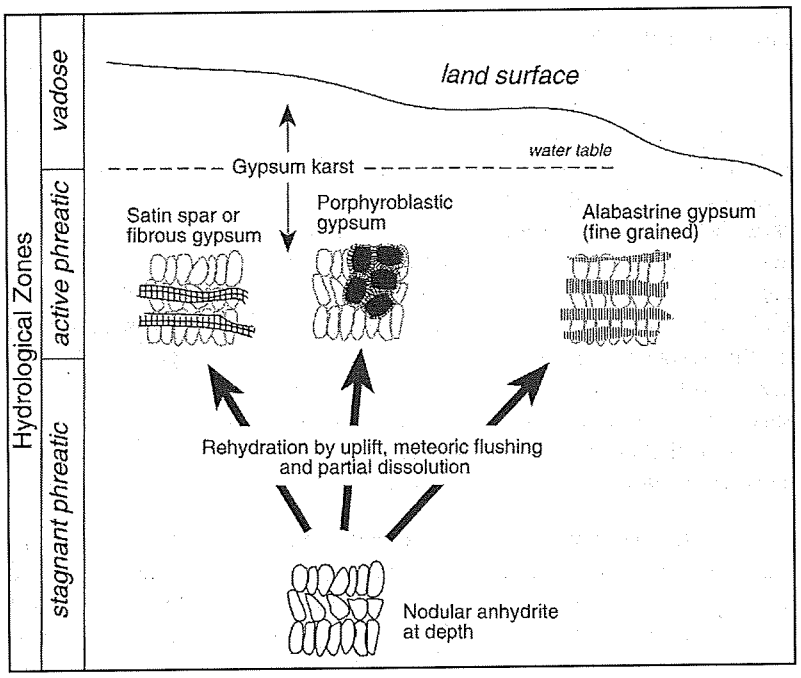

Figure 9. Rehydration fabrics in calcium sulphate from uplift, meteoric flushing and dissolution, Tertiary evaporites (Warren, 1999).

3.3 Logging of Drillcores I and II

Two drillcores representing the gypsum quarry in Polatlı Sazılar region, Ankara with the length of 19.50 m and 21.50 m have been examined petrographically. The distance between these two drill sites is 50 m. Initially, three drillcores were planned to be analyzed; however, due to the weather conditions, it was observed that some of the drillcores were weathered and it was not possible to perform an appropriate study on them. Therefore these two drillcores were selected representing the gypsum quarry concerning the mentioned reasons.

On the other hand, to be able to adopt the nomenclature of the authors mentioned above, the petrographic studies aiming to find out any gypsum variety have been conducted. According to these studies:

Transparent, nearly prismatic selenitic gypsum is identified with various sizes ranging from 0.1 mm –1 cm. The selenite crystals are both in a clayey matrix and in isolated lenses.

A massive, white coloured, nearly pure, finely crystalline gypsum is identified, resembling to alabastrine gypsum. However, to prove that whether this massive gypsum is alabastrine gypsum, corroded anhydrite relics (Gündoğan et al., 2005) must be present in the rock indicating the gypsum has secondary origin.

Both petrographically and with the aid of polarized microscope, anhydrite crystals were searched; however, any crystal of anhydrite is not found. Therefore, this white massive, finely crystalline gypsum is mentioned shortly in the following chapters as "white massive gypsum" instead of alabastrine gypsum.

Another identification in this study is "grayish gypsum". Grayish gypsum is not a variety of gypsum, but just a term to define the gypsum rock which consists of sand sized selenite crystals and gypsum grains present in a gray coloured clayey material.

Below petrographic features of each drillcore are explained based on its macroscopic properties. The described morphologies of gypsum in drillcore I are shown in figures 10-12 and figures 13-14 for drillcore II, respectively. Figure 15 illustrates the logging of two drillcores.

Drillcore I (From surface to bottom)

0.00 – 1.00 m: Gypsiferous soil

1.00 – 1.40 m: First 10 cm is nearly pure, finely crystalline, equigranular, white and massive gypsum (white massive gypsum). The remaining part consists of irregular lenses of this type of massive gypsum in a beige coloured calcite and clay rich matrix. (Figure 10-A)

1.40 – 1.70 m: Sand sized gypsum grains and selenite crystals are observed in a grayey clayey matrix (grayish gypsum). The colour of the calcite and clay rich matrix here darkens and becomes light grayish. Calcite and clay rich material constitutes both the matrix and irregular beds. Sand size to fine gravel sized selenite crystals are present in the calcite and clay rich matrix. In some parts, selenite crystal size increases (1-2mm) and form isolated selenite lenses.

1.70 – 2.10 m: First 30 cm is composed of grayish gypsum and the remaining 10 cm consists of alternation of nearly 1-1.5 cm thick grayish gypsum rich in calcite and clay rich material and the white massive gypsum (Figure 10-B).

2.10 – 3.50 m: Sand sized gypsum grains and selenite crystals are present in the light gray coloured calcite and clay rich matrix, similar to the part 1.40 – 1.70m (Figure 10-C).

3.50 – 3.65 m: Large selenite crystals with the size of 1mm to 1cm are observed. Within the large crystals beige colored calcite and clay rich material is present similar to the material within white massive gypsum.

3.65 – 4.00 m: Sand sized gypsum grains and selenite crystals are present in the light gray coloured calcite and clay rich matrix.

4.00 – 5.20 m: Sand sized gypsum grains, selenite crystals are observed in higher amount of calcite and clay rich material compared to the upper parts of the section. The selenite crystals and translucent gypsum grains are scattered in the matrix.

5.20 – 5.55 m: Sand sized gypsum grains and selenite crystals are present in the light gray coloured calcite and clay rich matrix.

5.55 – 5.80 m: This part seems like the part where sand sized gypsum grains and the selenite crystals are observed in the grayish calcite and clay rich matrix. However, clayey material content is highest than in this part of the drillcore. Calcite and clay rich material both constitutes the matrix and form max. 0.5 cm thick irregular beds (Figure 10-D).

5.80 – 6.00 m: In this part, the main morphology is grayish gypsum. However, in some part of the core, lenses of selenite crystals with the size of 1-5mm and lenses of white massive gypsum are observed.

6.00 – 6.25 m: Alternation of white massive gypsum and grayish gypsum. The 2 cm thick white massive gypsum alternates with clayey gray coloured gypsum.

6.25 – 8.00 m: Petrographically, the highest calcite and clay rich material content of box 2 is detected in this part. Selenite crystals and the gypsum grains with the size of nearly 0.2 cm are present in this higher content of calcite and clay rich material (Figure 11-A).

8.00 – 10.40 m: Sand sized gypsum grains and selenite crystals are present in the light gray coloured calcite and clay rich matrix. However, upper 1m contains 0.5cm beds of calcite and clay rich material (Figure 11-B).

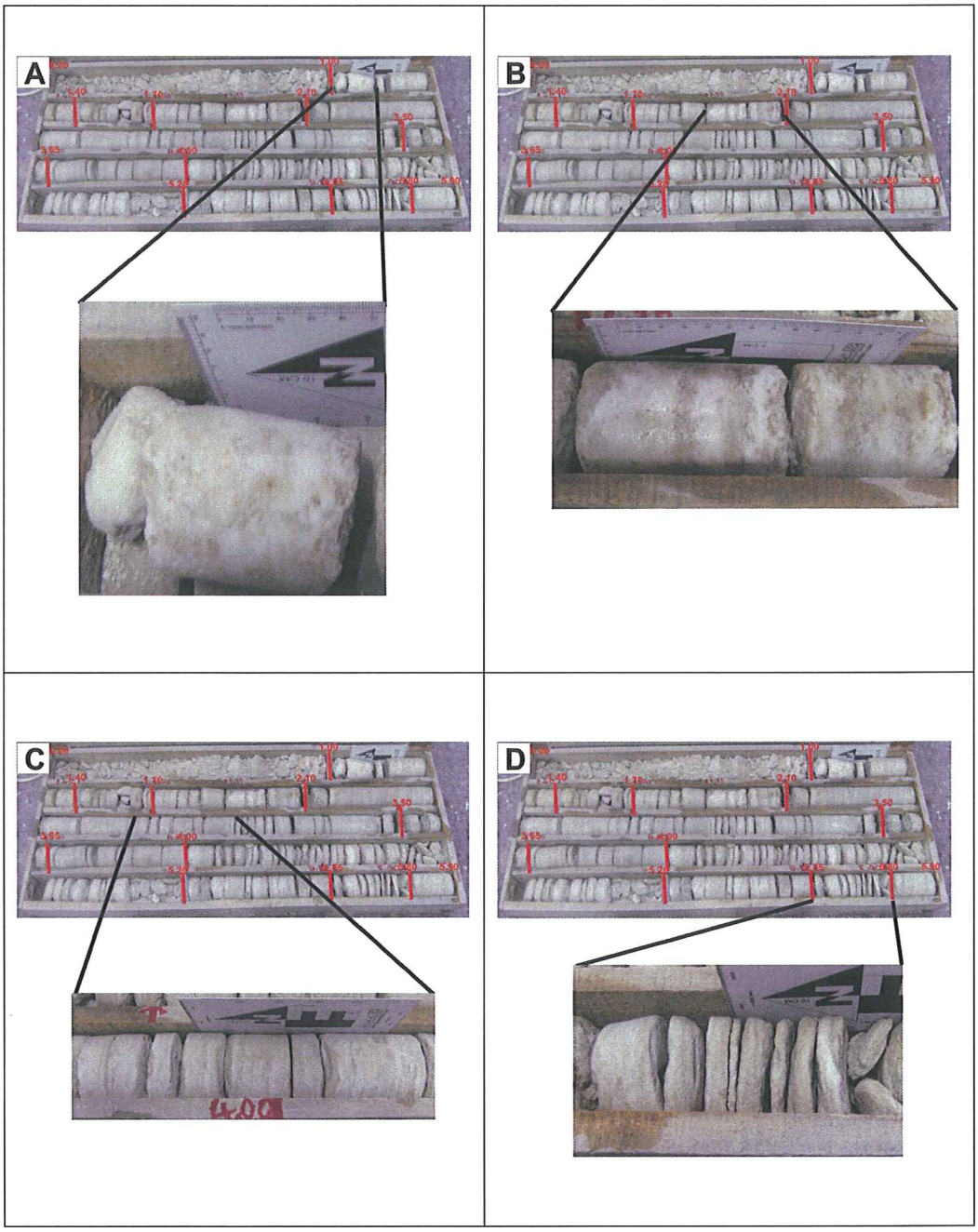

Figure 10. Photographs of some of the described morphology in Box 1 (Drillcore I). A: White massive gypsum present in 1.00-1.10m. B: Alternation of grayish gypsum and white massive gypsum in 1.90-2.10m. C: Gray coloured gypsum with sand size selenite crystals and gypsum grains in 2.10-3.50m. D: Grayish gypsum with highest content of calcite and clay rich material in 5.55-5.80 m.

10.40 – 10.60 m: This part is similar to the part of 3.50-3.65m in box 1 where large selenite crystals with the size of 1mm to 1cm are observed. Within the large crystals beige coloured calcite and clay rich material is seen (Figure 11-C).

10.60 – 12.35 m: Sand sized gypsum grains and selenite crystals are present in the light gray coloured calcite and clay rich matrix. However, the size of the selenite crystals increases (max. 0.3 cm) in different part of this section (Figure 11-D).

12.35 – 13.35 m: This part also resembles to the upper part, but different from that part, crystal size of the selenite increases to 0.5-1 cm in the calcite and clay rich matrix in various parts of this section (Figure 12-A).

13.35 – 14.50 m: Large selenite crystals (max. 3cm) are observed in the calcite and clay rich matrix as irregular lenses and alternate with grayish gypsum. In some parts, white massive gypsum alternates with selenite and grayish gypsum (Figure 12-B).

14.50 – 15.35 m: Sand sized gypsum grains and selenite crystals are present in the light gray coloured clayey matrix. However, the size of the selenite crystals are recorded as max. 0.5 cm in different parts of this section.

15.35 – 15.45 m: Sand sized gypsum grains and selenite crystals are present in the light gray coloured clayey matrix.

15.45 – 15.55 m: Irregular lenses of large selenite crystals (1-2 cm) in calcite and clay rich matrix including sand sized gypsum grains and selenite crystals.

15.55 – 15.80 m: Sand sized gypsum grains and selenite crystals are present in the light gray coloured calcite and clay rich matrix.

15.80 – 15.95 m: Large selenite crystals with the size of 1mm to 1cm are observed where there is nearly any calcite and clay rich material between the crystals.

15.95 – 16.90 m: Alternation of selenite crystals of the size of 1-5mm in irregular lenses with the white massive gypsum in irregular, 1-3 cm thick beds including 1-4 cm isolated selenite crystals in and gray coloured gypsum (Figure 12-C).

16.90 – 17.30 m: Sand sized gypsum grains and selenite crystals are present in the light gray coloured calcite and clay rich matrix.

17.30 – 19.50 m: In this part, irregular beds of white massive gypsum including isolated selenite crystals of max. 1 cm in and calcite and clay rich material containing sand sized selenite crystals and gypsum grains alternate with each other at nearly 1-2 cm intervals (Figure 12-D).

19.50 - ?: Green coloured clay enriched calcite material

Drillcore II (From surface to bottom)

0.00 – 1.00 m: Gypsiferous soil

1.00 – 1.70 m: Sand sized selenite crystals and gypsum grains in a considerable amount of grayish clayey material (grayish gypsum). The max 3mm thick beds of calcite and clay rich material alternates with the gray gypsum (Figure 13-A)

1.70 – 2.95 m: Lenses of selenite crystals with the size of max. 0.5 cm is observed together with grayish gypsum (Figure 13-B).

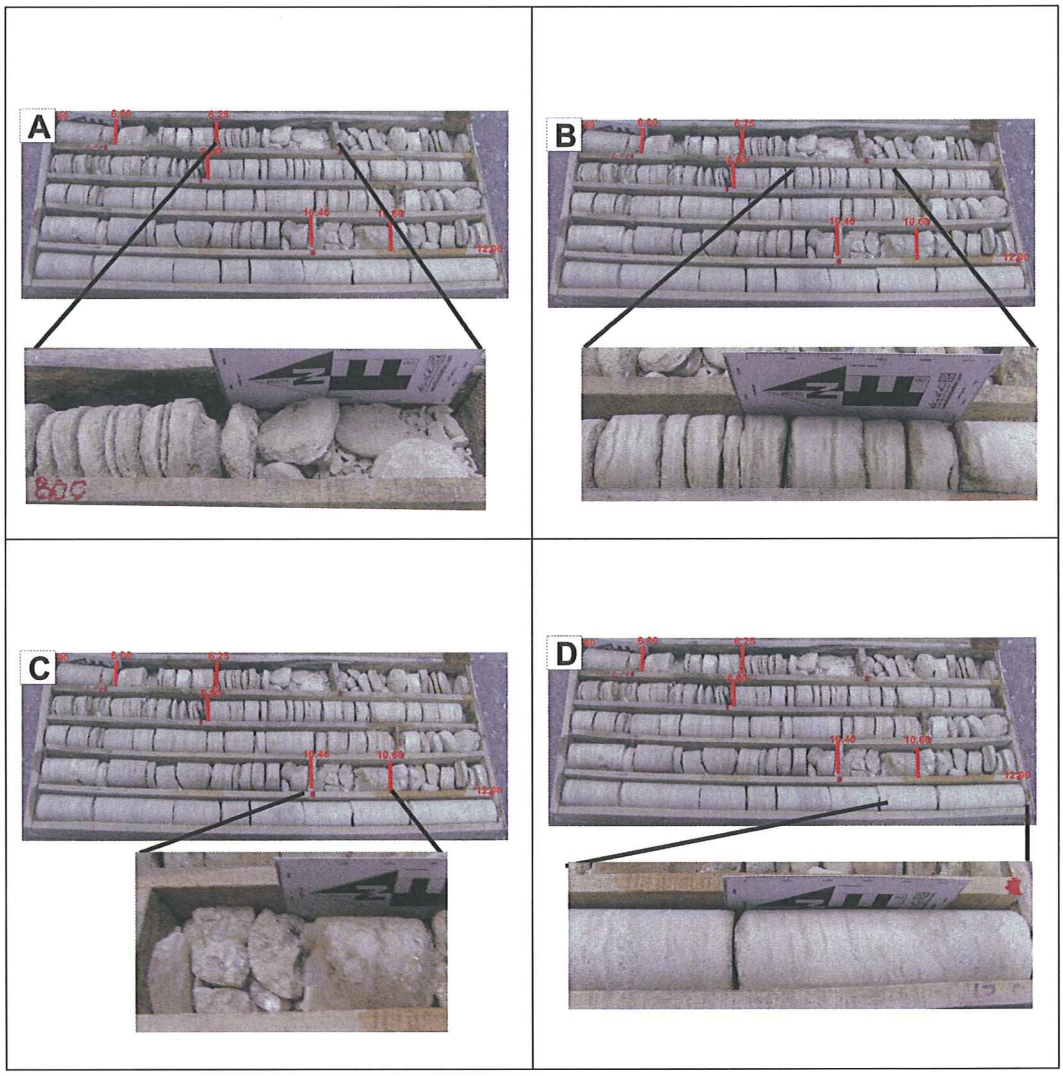

Figure 11. Photographs of some the described morphology in Box 2 (Drillcore I). A: Petrographically, highest amount of calcite and clay rich material in Box 2 in 6.25 – 8.00m. B: Alternation of gray coloured gypsum and max. 0.5 cm thick calcite and clay rich material in 8.00-10.40 m. C: Large selenite crystals in 10.40-10.60 m. D: Grayish gypsum with 0.1-0.2cm selenite crystals in 10.60-12.00 m.

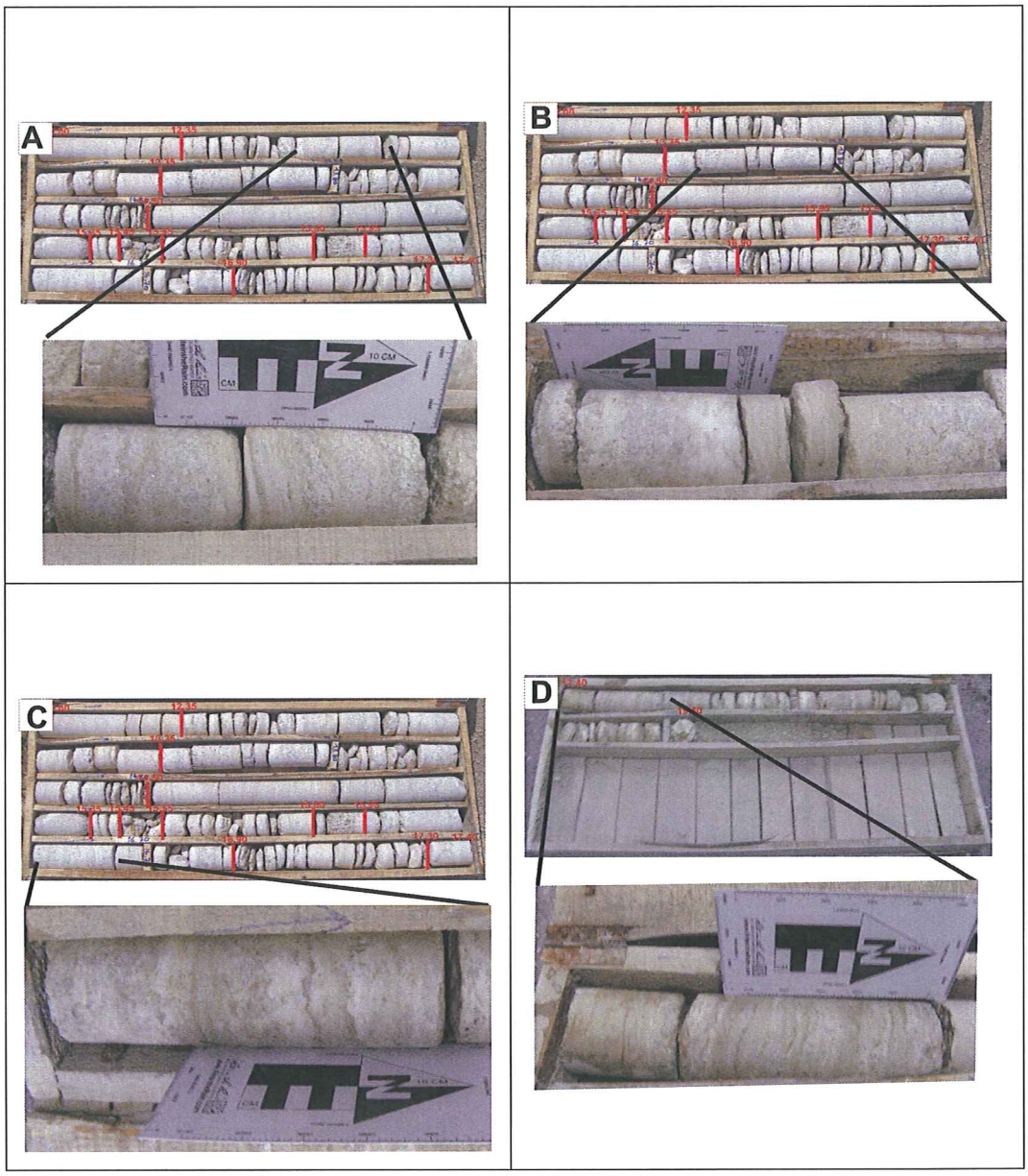

Figure 12. Photographs of some of the described morphology in Box 3 and Box 4 (Drillcore I). A: Gray coloured gypsum where selenite crystals increase up to 0.5-1 cm in 12.35-13.35 m. B-C-D: white massive gypsum alternates with grayish gypsum and selenite in 13.35-14.50m, 15.95-16.90m in Box 3 and 17.30-19.50m in Box 4.

2.95 – 3.80 m: Sand sized gypsum grains and selenite crystals are scattered in the grayish, calcite and clay rich matrix (Figure 13-C).

3.80 – 4.20 m: Selenite crystals with the size of 3-4 mm in the calcite and clay rich matrix (Figure 13-D).

4.20 – 6.50 m: Sand sized gypsum grains and the selenite crystals present in the grayish matrix.

6.50 – 7.60 m: Large selenite crystal (1-1.5 cm) in the light gray coloured calcite and clay rich matrix (Figure 14-A).

7.60 – 7.70 m: White, finely crystalline, equigranular, massive gypsum (Figure 14-B).

7.70 – 8.10 m: Grayish gypsum alternating with 1-2 mm thick calcite and clay rich material. The clay content of the matrix of grayish gypsum is higher than the upper parts (Figure 14-C).

8.10 – 8.20 m: Selenite crystals of 1-2 mm in lenses in the grayish gypsum

8.20 – 13.45 m: Sand sized gypsum grains and selenite crystals are present in the light gray coloured matrix.

13.45 – 14.30 m: Sand sized gypsum grains and selenite crystals are present in the light gray coloured matrix. In different parts of the section, the small selenite crystals (max. 0.5 cm) are observed in lenses.

14.30 – 15.30 m: Calcite and clay rich material enriches here in the matrix of grayish gypsum and also observed as thick beds (max. 2 cm) (Figure 14-D)

15.30 – 16.40 m: Sand sized gypsum grains and the selenite crystals are scattered in a light grayish matrix. In some parts, nearly 0.3 cm sized selenite crystallization is observed in lenses.

16.40 – 16.80 m: Calcite and clay rich material enriches in this part of the drillcore. White massive gypsum is observed in this calcite and clay rich matrix.

16.80 – 18.35 m: Calcite and clay rich material constitutes both the matrix of the grayish gypsum and thin beds (0.2-0.4 cm) alternating with the gypsum.

18.35 – 21.10 m: Irregular beds of white massive gypsum including isolated selenite crystals of max. 1 cm and alternates with grayish gypsum at nearly 1-2 cm intervals.

21.10 – 21.50 m: Green coloured clay enriched calcite material

3.4 Comparison of the Drillcores

The two drillcores has a length of 19.50m and 21.50m, respectively and there is 50 m between each drillcore. Once the drillcore I is considered from top to bottom, white massive gypsum is present at the upper parts of the core; whereas grayish gypsum is the type of the rock in drillcore II. Towards the middle of the core I, grayish gypsum with thin clay bands is observed. On the contrary to drillcore I, grayish gypsum is present in drillcore II. In the middle of the core, selenitic gypsum is observed in drillcore I; whereas, grayish gypsum and alternation of selenite and white massive gypsum are present in drillcore II. Towards the bottom of the cores, grayish gypsum with selenite crystals of 0.5-1 cm are dominant on both of the drillcores. Drillcores end with alternation of selenite, white massive gypsum and grayish gypsum.

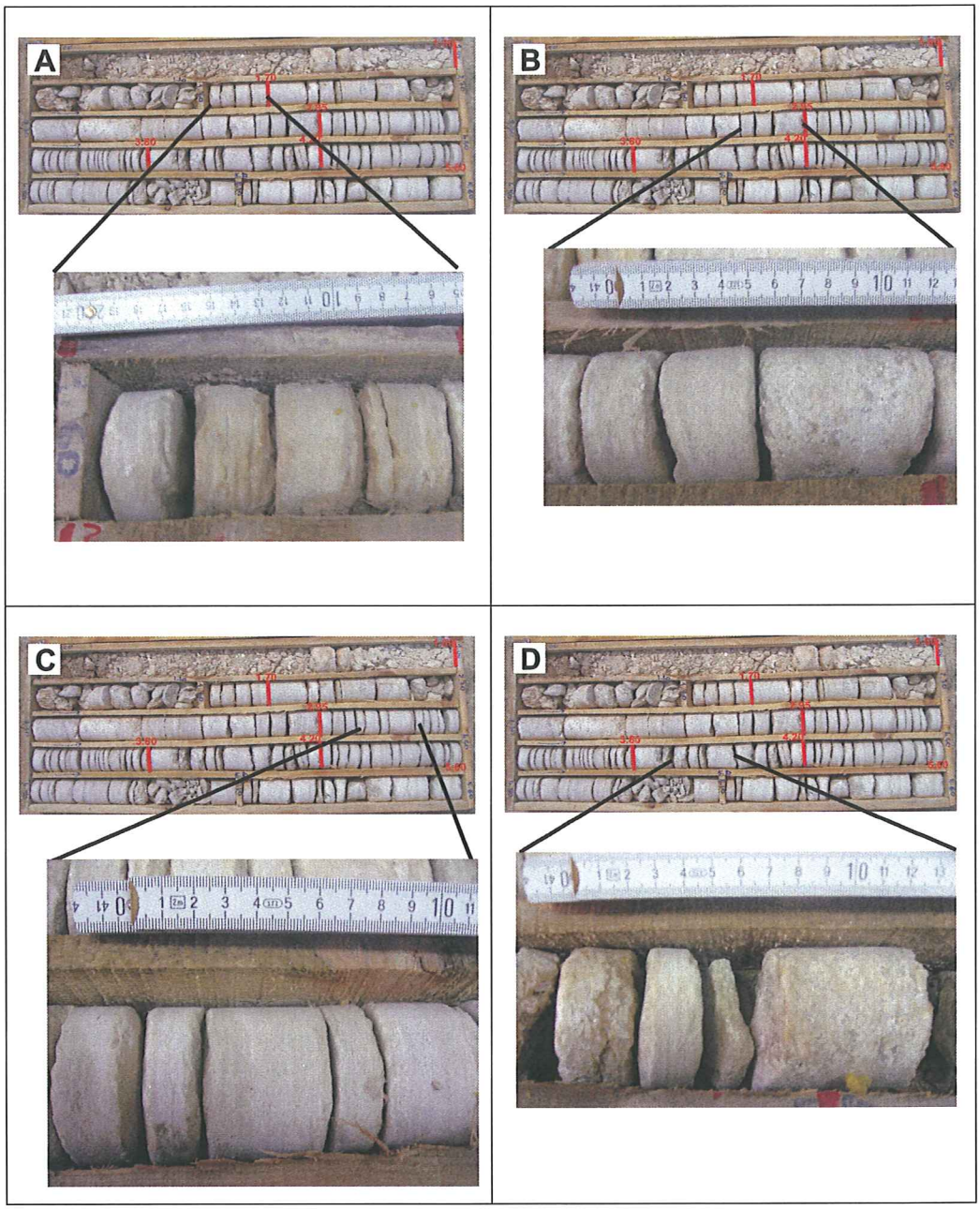

Figure 13. Photographs of some of the described morphology in Box 1(Drillcore II). A: Alternation of grayish gypsum with nearly 3 mm thick calcite and clay rich material in 1.00 – 1.70 m. B: Selenite lenses in grayish gypsum in 1.70-2.95 m. C: Gray coloured gypsum in 2.95-3.80 m. D: Selenite crystals with the size of 3-4 mm in 3.80-4.20 m.

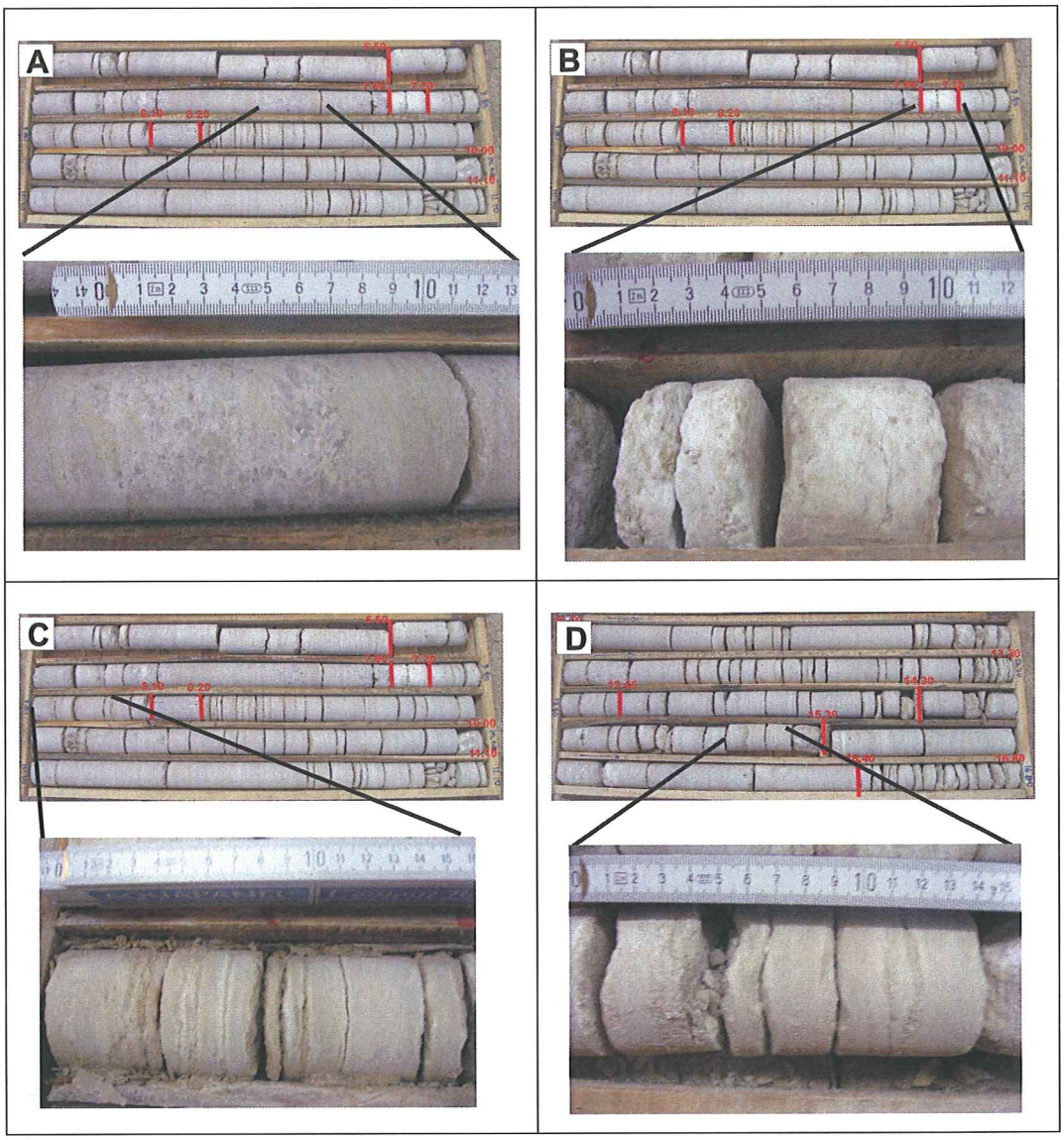

Figure 14. Photographs of some of the described morphology in Box 2 and 3 (Drillcore II). A: Large selenite crystals in the light gray coloured matrix in 6.50 – 7.60 m in Box 2. B: White massive, equigranular gypsum in 7.60 – 7.70 m .in Box 2. C: Gray coloured gypsum alternating with beds of clayey material in 7.70 – 8.10 m. D: Clayey material enriches in the matrix of grayish gypsum and also observed as thick beds up to 2 cm in 14.30 – 15.30 m . in Box 3.

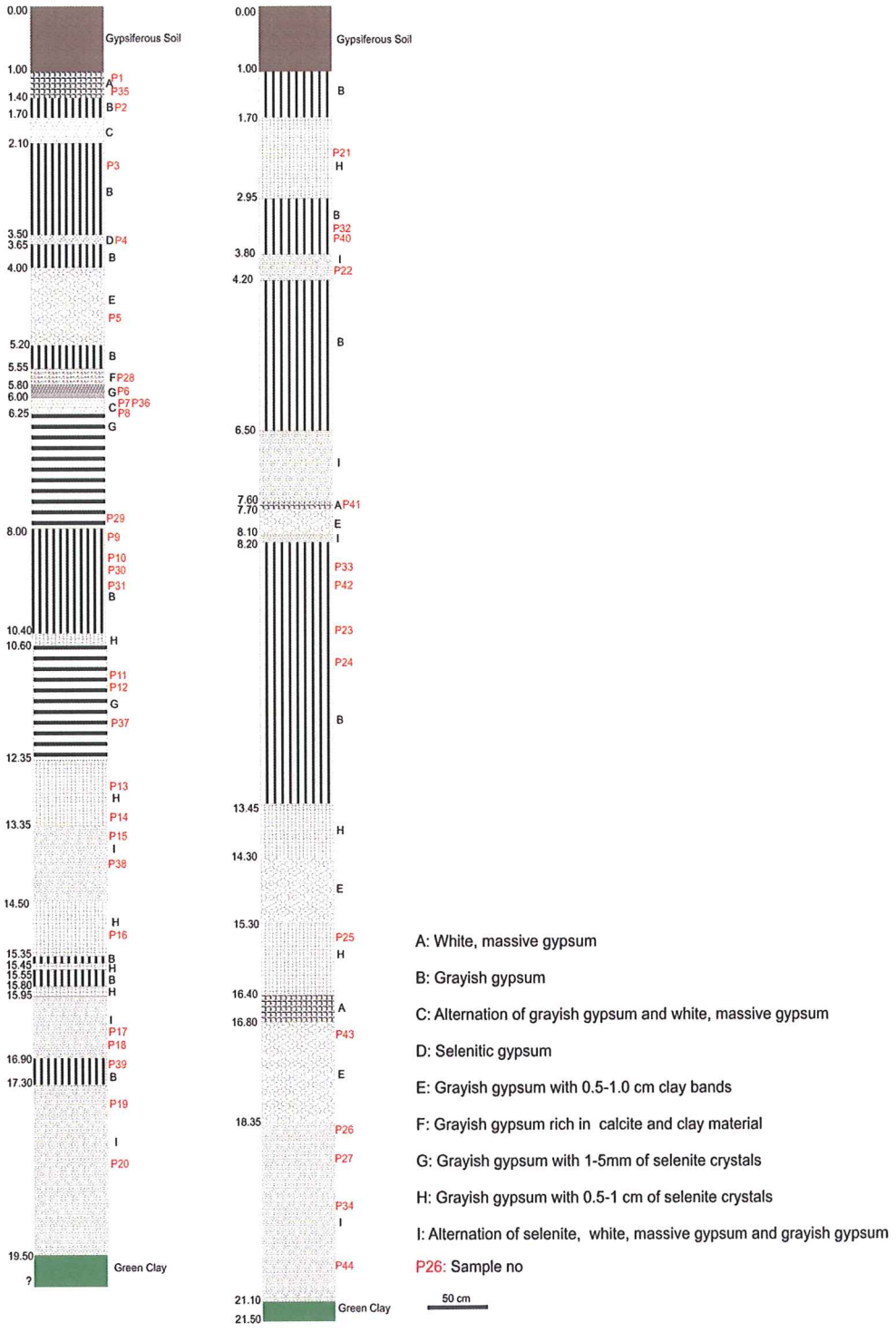

Figure 15. Logging of the Drillcore I and Drillcore II.

3.5 Petrographic Studies

For better understanding of the gypsum rock and its varieties, 20 samples from drillcore I and 7 samples from drillcore II have been selected for petrographic studies by thin section analysis. These samples are the ones that best represent the varieties of gypsum and relationship between the impurity and the gypsum minerals. The sample locations are shown in Figure 15 and Appendix A on the drillcore photos.

Once the white, finely crystalline, nearly pure gypsum is observed under microscope, it is viewed that this type gives few details in plane polarized light (PPL). Nearly nothing is identified, just a brownish surface is observed. In crossed polarized light (XPL), ghost gypsum crystals are identified in white massive gypsum. These ghost gypsum crystals form by replacement of original gypsum crystals by white massive gypsum. In XPL, massive gypsum is isotropic without any crystal margins. Figure 16 illustrates examples of white massive gypsum with ghost crystals. (Here, in these sections, impurities are not present).

The selenite minerals can be identified under polarized microscope. They are generally prismatic and idiomorphic. In Figure 17-A and Figure 17-B, calcite bearing clayey material is observed inside the selenite crystal. In PPL, cleavage planes are recognized as shown in Figure 17-C and Figure 17-D. These cleavage planes are also defined in the XPL. However, calcite bearing clayey material is identified by its shining, orange to brownish colour.

In some parts of the section, finer grains and large grains of gypsum can exist together. The finer grains are generally equigranular (Figure 18).

However, the general appearance of the gypsum rock is different from the types that are mentioned above. Throughout the drillcores, what is observed is the selenite and fine to medium sized gypsum grains present in a clayey matrix.

Figure 19 shows the relationship between the clayey rich material and the gypsum minerals. The clayey material is between the gypsum grains constituting the matrix. The amount of the impurity can increase as in the Figure 20 and decrease as in Figure 21. The impurity in Figure 20 fills the empty spaces of a dissolved gypsum crystal. Indeed, the sharp edges and the outline indicate presence of a former crystal.

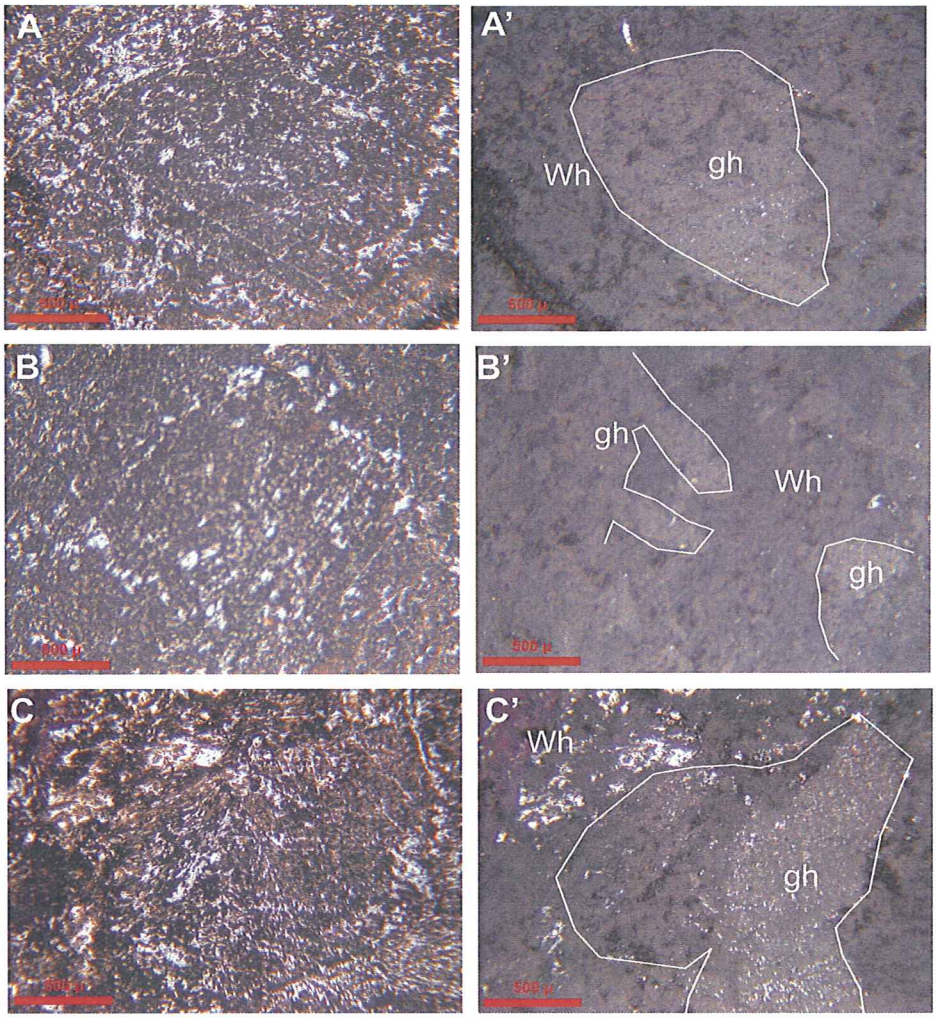

Figure 16. Thin section photomicrograph of white massive gypsum with ghost crystals. A-B-C:PPL and A'-B'-C': XPL. (gh: ghost gypsum crystals; wh: white massive gypsum) (A-A', B-B', C-C': Sample No: P1)

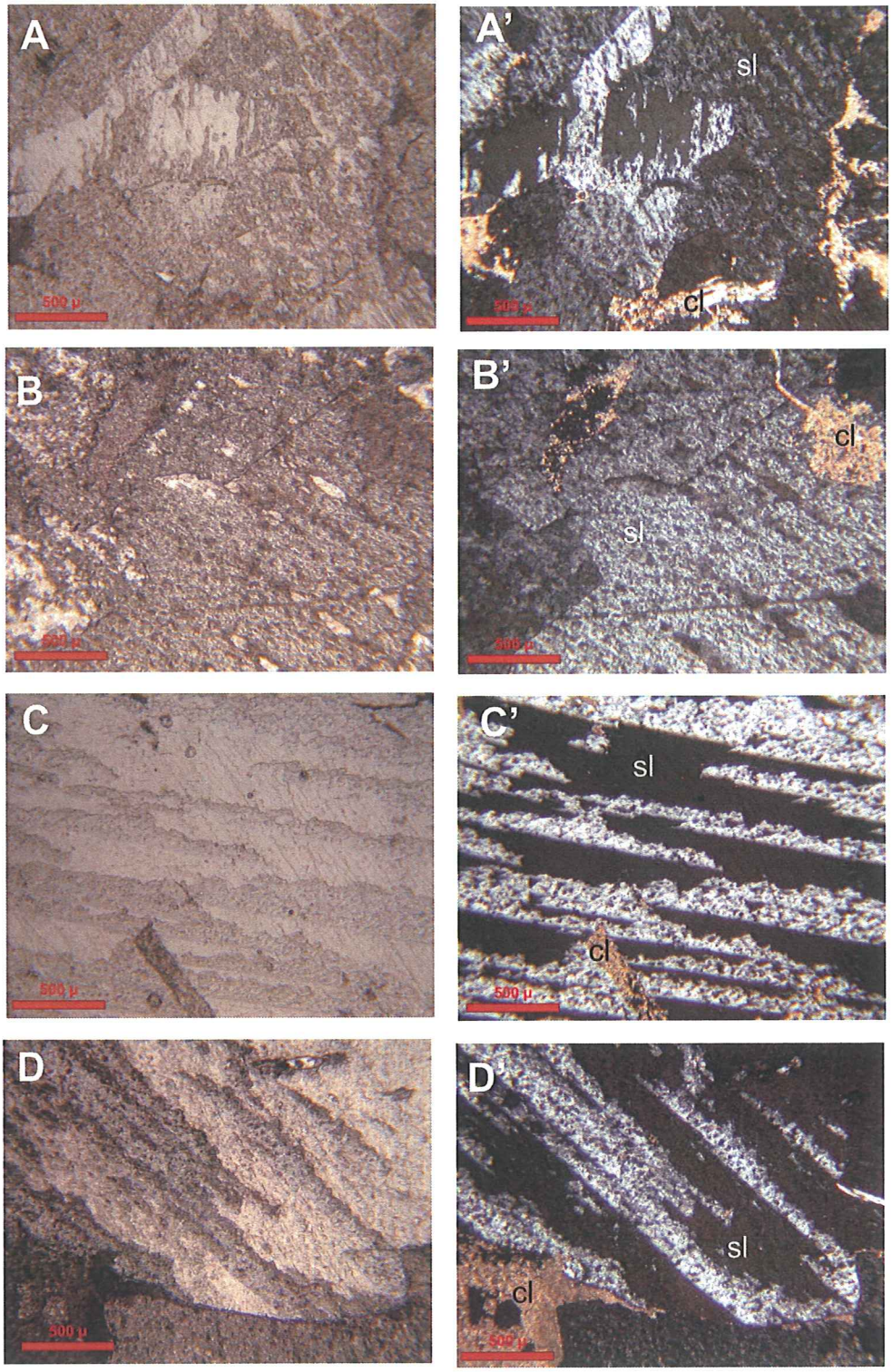

Figure 17. Thin section photomicrograph of selenite crystals with the calcite and rich rich material inside the crystals. A-B-C-D: PPL. and A'-B'-C'-D': XPL (sl: selenite crystals, cl: clayey material) (A-A', B-B': Sample No. P4; C-C', D-D': Sample No. P24)

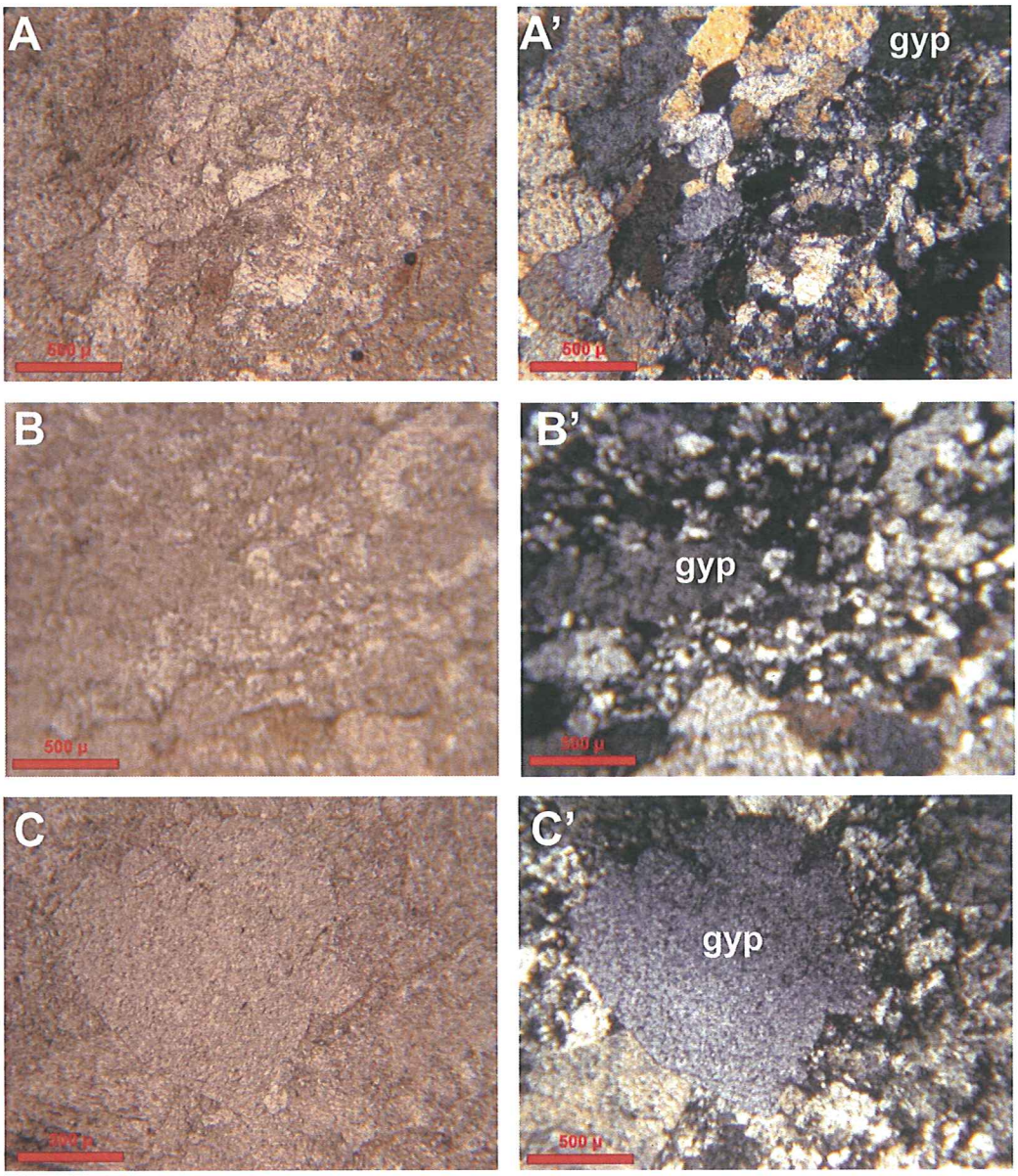

Figure 18. Thin section photomicrograph of finer grains of gypsum and large grains. A-B-C: PPL and A'-B'-C': XPL (gyp: gypsum) (A-A', B-:B', C-C': Sample No: P11)

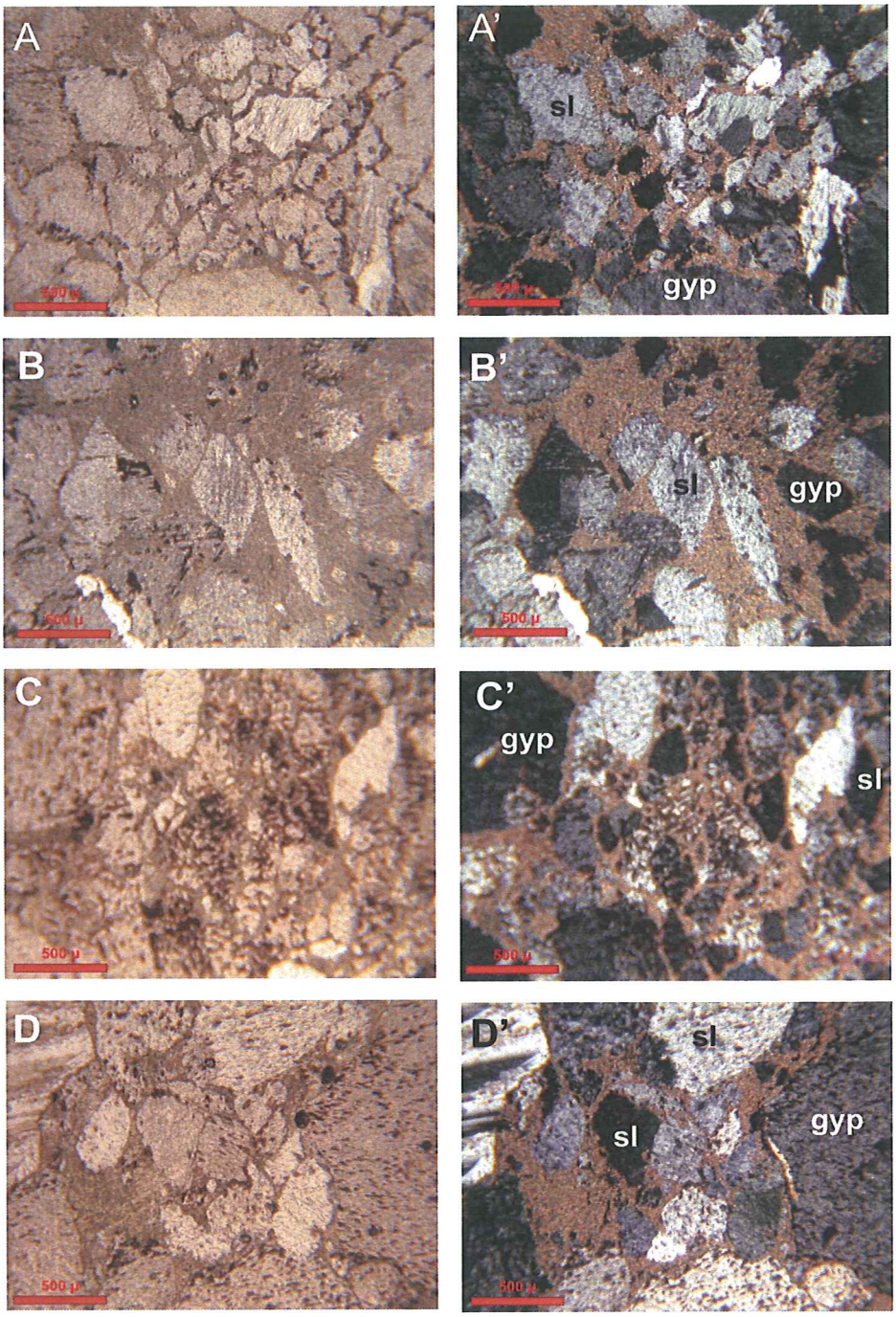

Figure 19. Thin section photomicrograph of prismatic selenite crystals and gypsum grains in the calcite and clay rich matrix. A-B-C: PPL and A'-B'-C': XPL (sl: selenite, gyp: gypsum) (A-A', B-B': Sample No: P10; C-C', D-D': Sample No: P9)

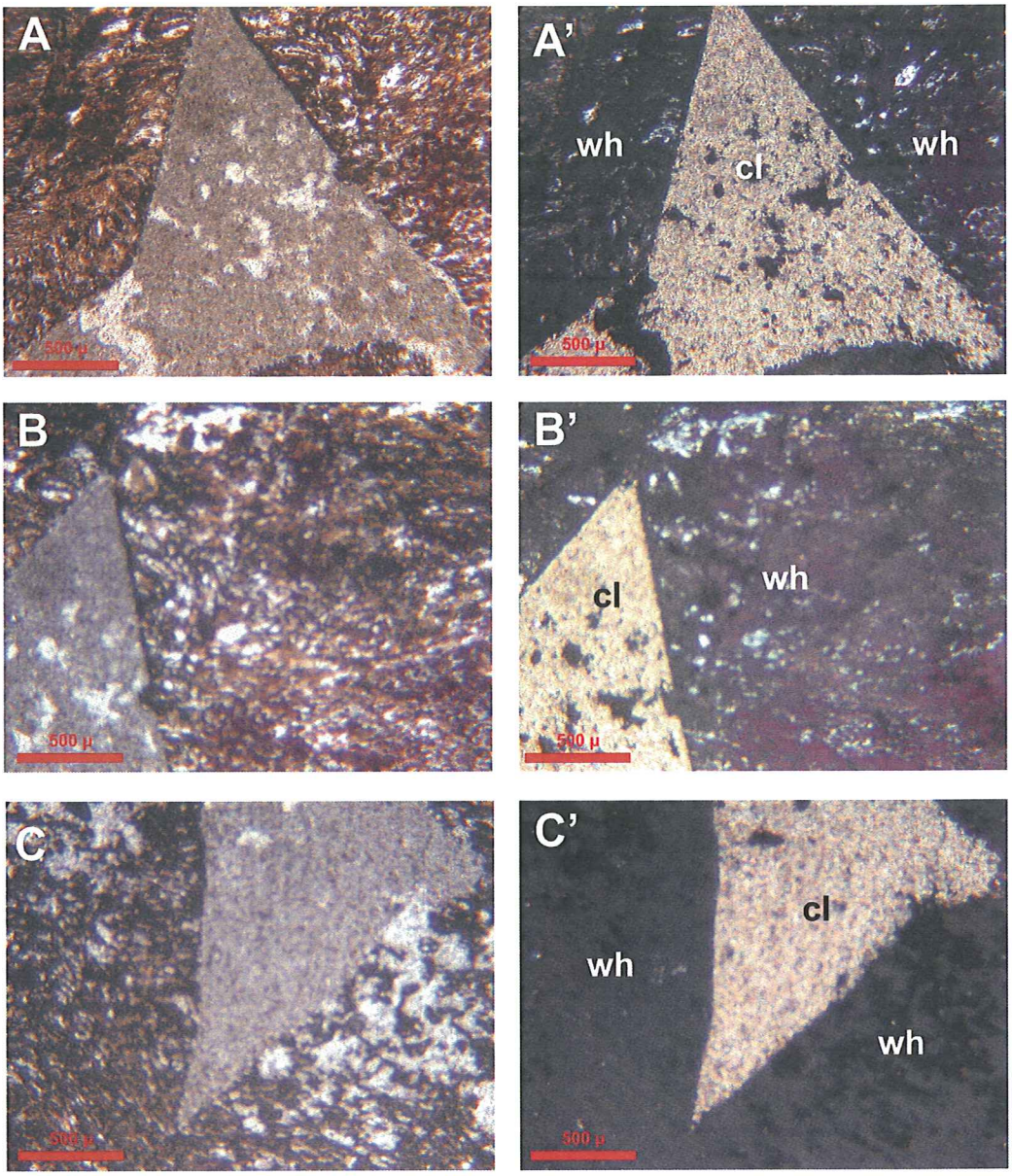

Figure 20. Thin section photomicrograph of calcite and clay rich matrix between white massive gypsum. A-B-C: PPL. and A'-B'-C': XPL (wh: white massive gypsum, cl: clayey material) (A-A', B-B', C-C': Sample No: P1)

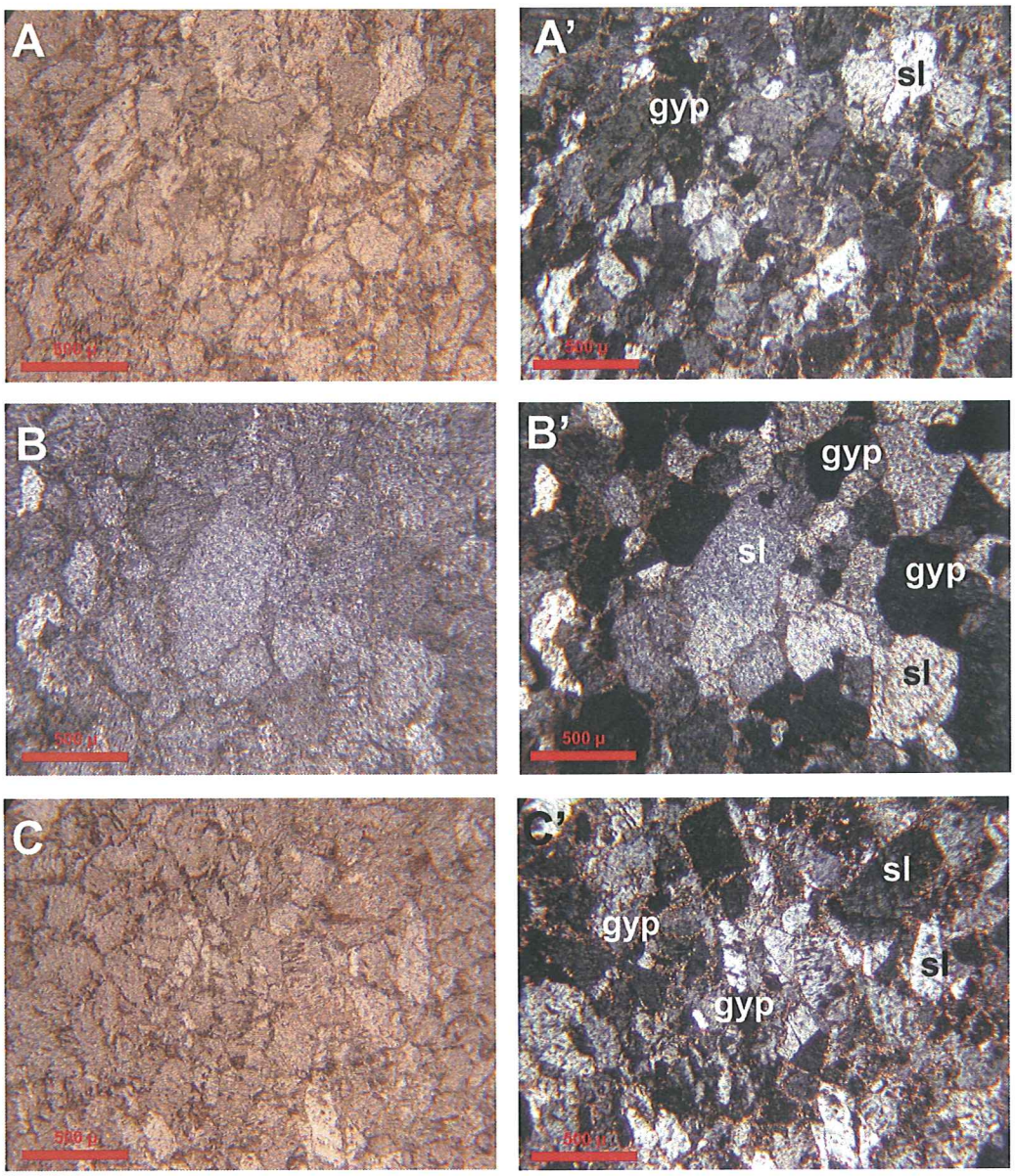

Figure 21. Thin section photomicrograph of calcite and clay rich material between the gypsum crystals forming a network. A-B-C: PPL and A'-B'-C': XPL (sl: selenite, gyp: gypsum) (A-A': Sample No: P21; B-B': Sample No: P7; C-C': P23)

3.6 Scanning Electron Microscope-Energy Dispersive X-Ray Analyses

In order to examine the three–dimensional relationship between the crystals and the impurities, scanning electron microscope (SEM) studies have been performed on 8 samples that were previously petrographically studied. The sample locations are indicated in Figure 15 and Appendix A on drillcore photos. This study focuses on the morphological aspects of certain gypsum varieties and impurities associated with gypsum. Energy dispersive X-ray analysis (EDS) is used to check semi quantitatively the chemical content of the minerals.

One of the varieties of gypsum that is described in previous chapters is white massive, finely crystalline gypsum. The scanning electron microscope photo of this variety is depicted in Figure 22. In this figure, anhedral crystals are observed without any impurity. Any matrix has not been detected in these images since the white massive gypsum does not contain any non-gypsum minerals.

Another variety is selenitic gypsum. Figure 23 illustrates prismatic, idiomorphic selenite crystals in finer gypsum grains and the fine clay material. The selenite crystals are distributed in this fine gypsum and clay matrix. EDS spectrum of selenite crystal in Figure 24 indicates the chemical composition of the crystal, which is calcium sulfate dehydrate.

The impurity, defined as calcite and clay rich material in the previous chapters, has also been detected in the SEM photomicrographs. It is observed that clay material has flaky appearance and sharp edges (Figure 25). This clay material is found in the matrix of the large gypsum crystals together with fine gypsum crystals (Figure 26).

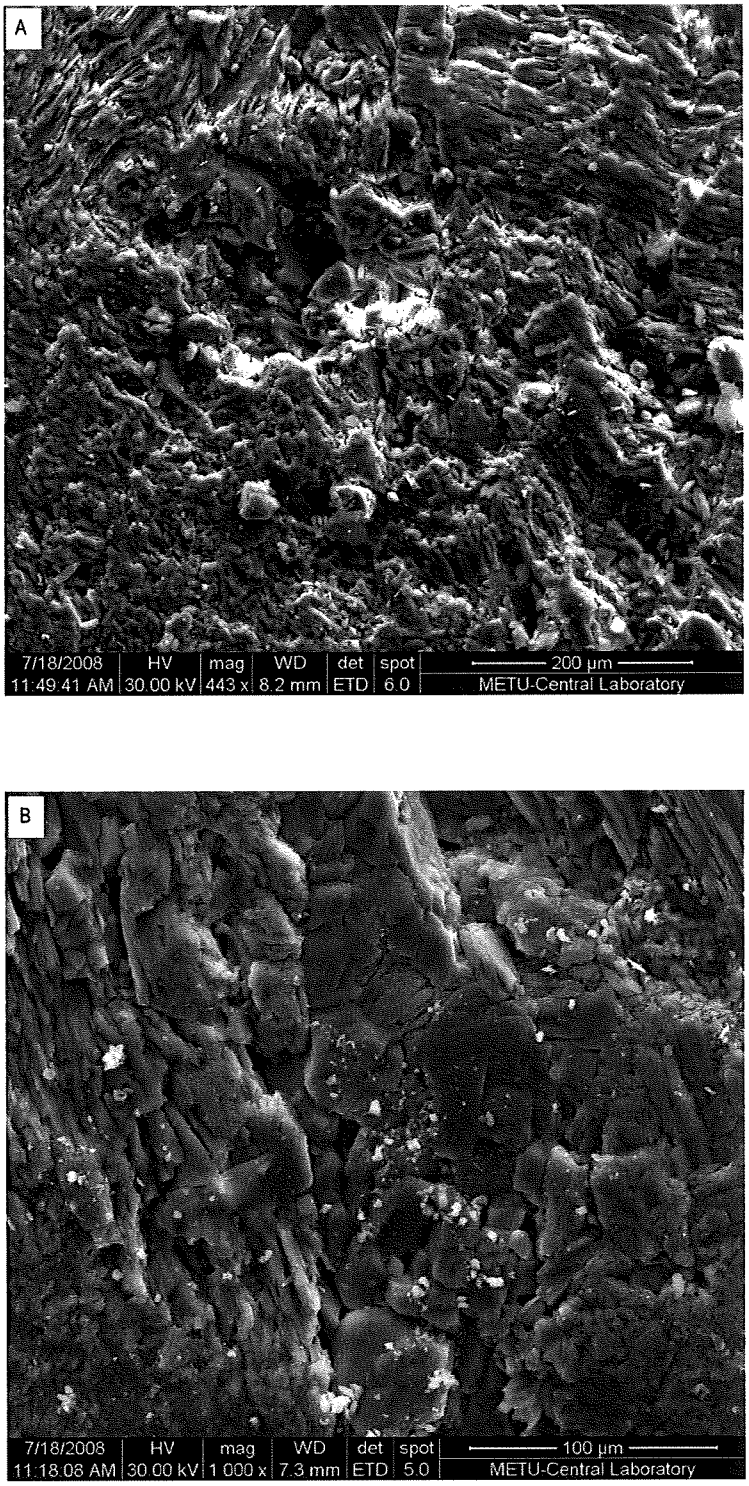

Figure 22. SEM photomicrograph of white massive, finely crystalline gypsum (A: with magnification 443x; B: with magnification 1000x) (A, B: Sample No: P1)

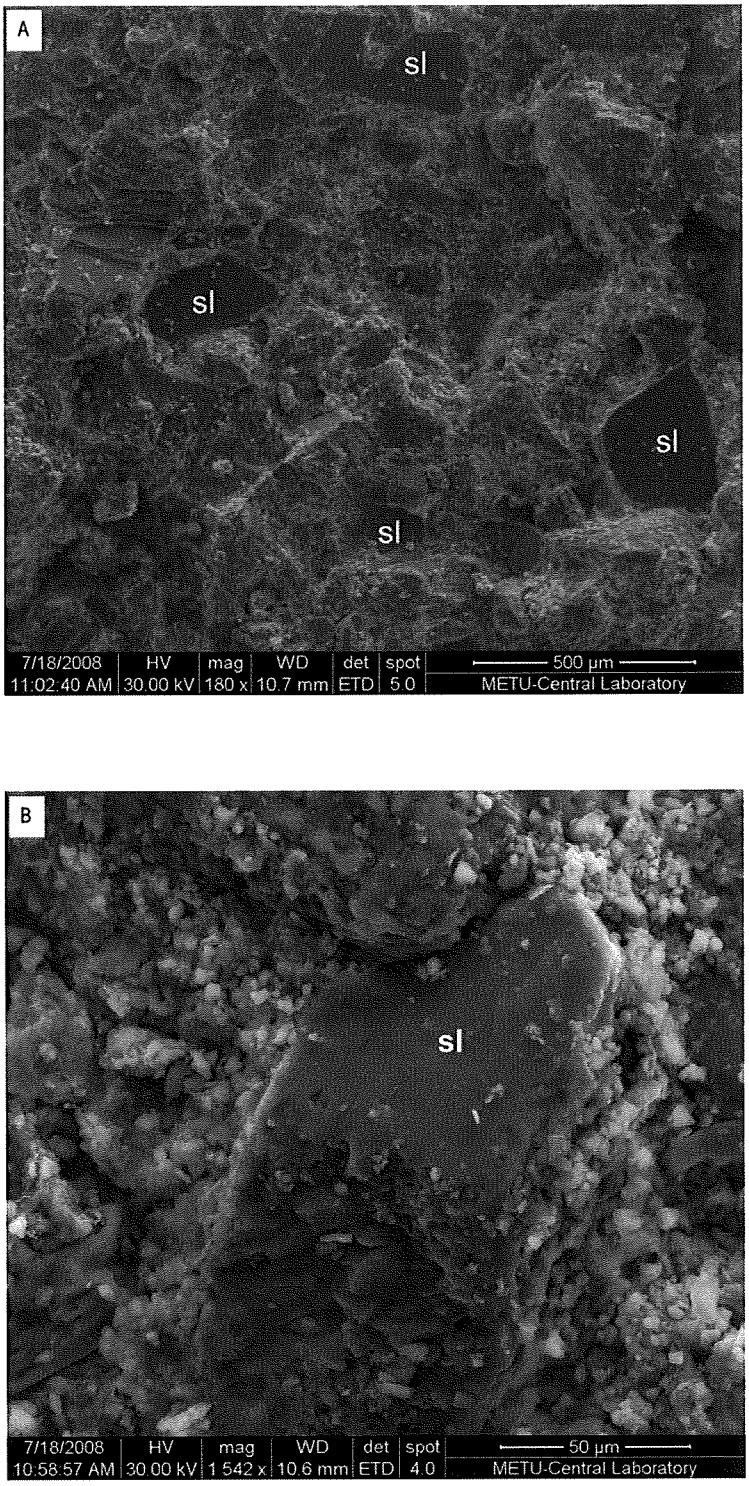

Figure 23. SEM photomicrograph of nearly prismatic selenite crystals (sl: selenite) (A: with magnification 180x; B: with magnification 1542x) (A, B: Sample No: P4)

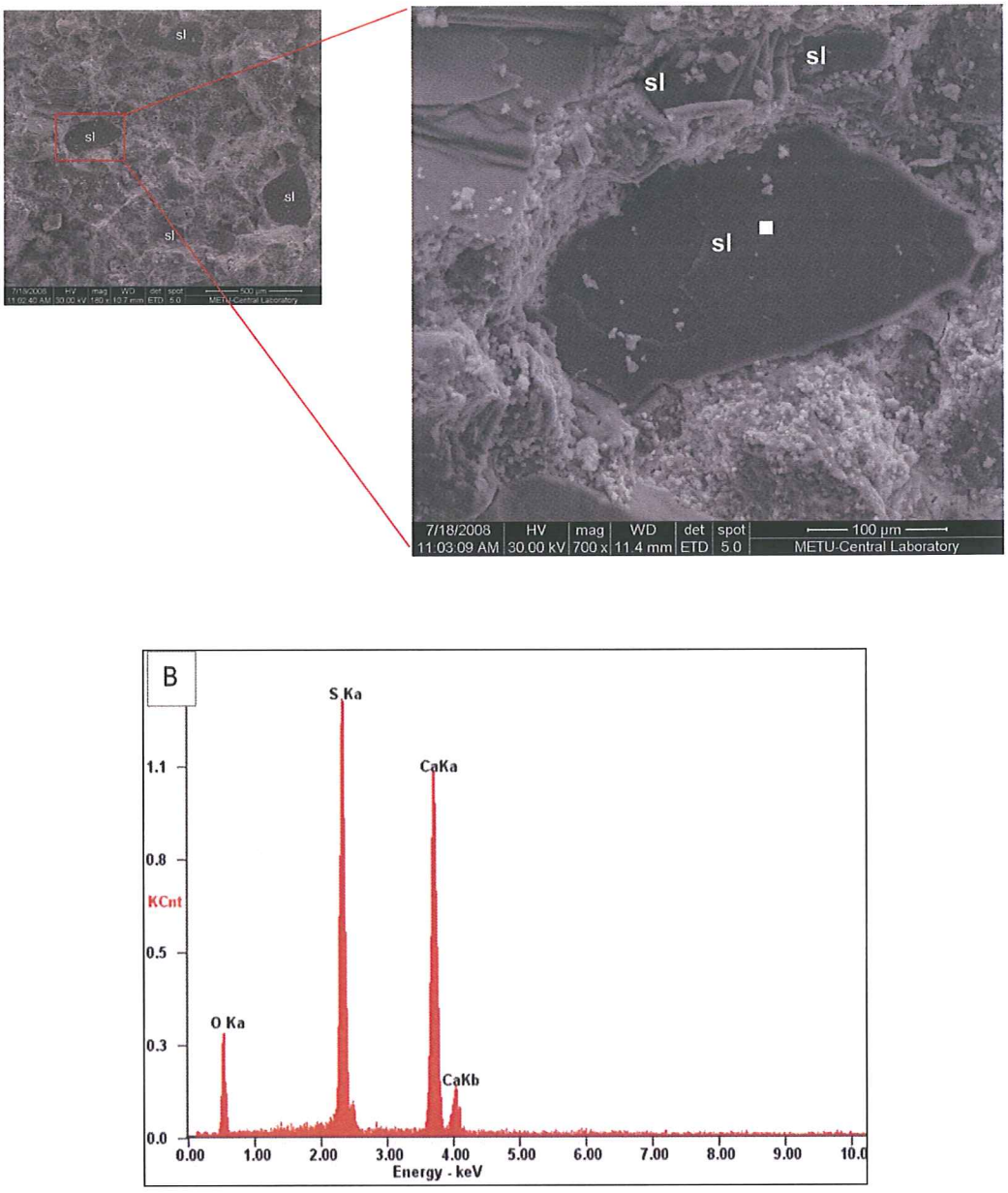

Figure 24. SEM photomicrograph of selenite crystal with EDS spectrum illustrating the chemical composition of the selenite (sl: selenite) (A: selenite crystal with 700x magnification; B: EDS spectrum) (A: Sample No: P24)

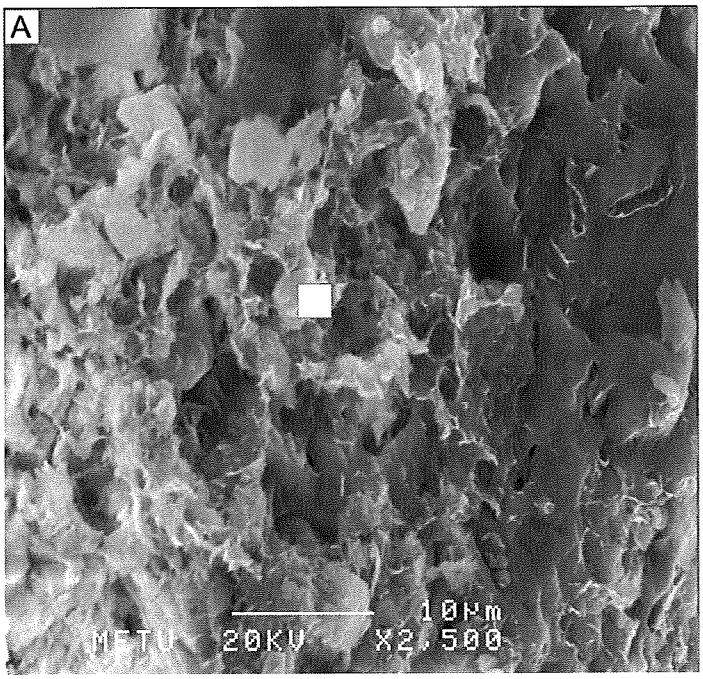

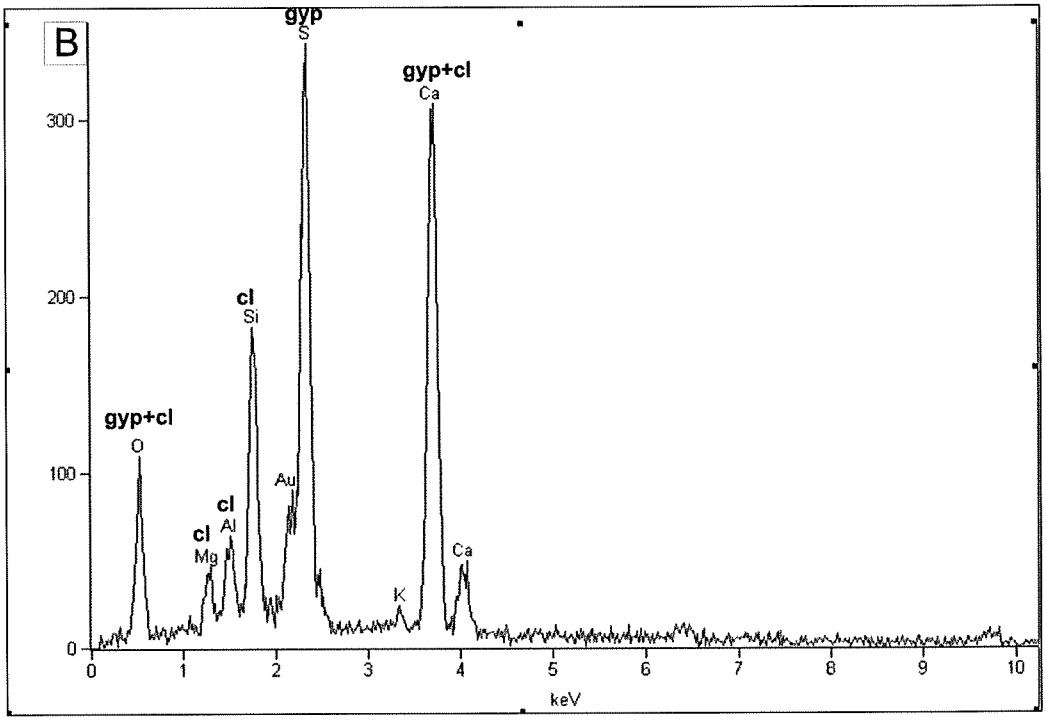

Figure 25. SEM photomicrograph of clay material with EDS spectrum illustrating the chemical composition. (A: clayey material with 2500x magnification; B: EDS spectrum) (A: Sample No: P9) (gyp: gypsum, cl: clay mineral)

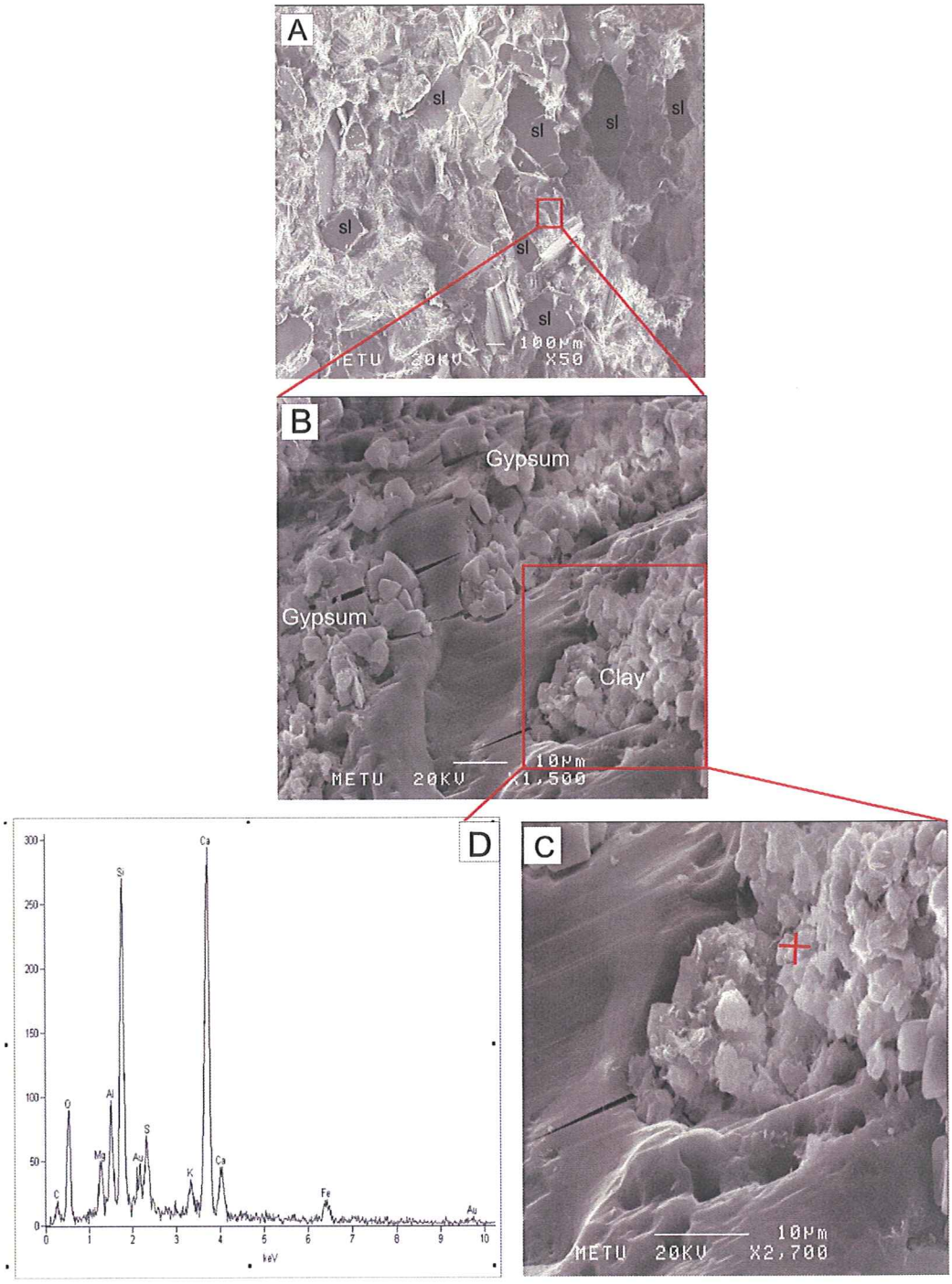

Figure 26. SEM photomicrograph of selenite crystals in the clay matrix. (A: selenite crystals with magnification 50x; B: fine gypsum crystals and clay material, magnification 1500 x; C: clay material with mag. 2700x; EDS spectrum of clay material. (A, B, C: Sample No: P9)

3.7 X-Ray Diffractometry Analyses

X-ray diffractometry (XRD) analyses are aimed to define the type of impurity present in the rock. Petrographically, calcite bearing clayey material is identified as the impurity present both in the matrix of sand sized selenite and gypsum grains and present as alternating thin beds.

X-ray diffractometry analyses have been conducted on 7 samples that are petrographically rich in clayey material and from different parts of the drillcore. 4 samples from drillcore I and 3 samples from drillcore II have been selected for the analysis. The sample locations are indicated on Figure 15 and Appendix A on drillcore photos.

Before X-ray diffractometry analyses, chemical treatment has been performed aiming to remove the sulfate minerals to have enough clayey material for detection the type of the material.

3.7.1 Method of Chemical Treatment

In order enrich the clayey material, sulfate minerals have to be dissolved through some treatments. The separation of clays and other silicates from carbonate and sulfate mineral through acid solution may result in undesirable damage to, or alteration of, some of the silicate minerals.

Water is one of the dissolving agent that does not harm the minerals left. The solubility of gypsum is 0.21 g per 100 g of solution, which is a slight quantity Gypsum is also soluble in sulfuric acid, phosphoric acid and nitric acid (Ullmann's Encyclopedia, 1985). However, these acids might harm the rest of the material while dissolving gypsum. However, the use of complexing or chelating agents has been one means of avoiding problem of deforming clay minerals. Hill and Runnel (1960) and Glover (1961) have described the

effectiveness of one such agent, ethylenedinitrilotetraacetic acid (Versene), hereafter abbreviated as EDTA. However, their studies were limited to the solubility of aragonite and calcite minerals. Bodine and Fernald (1973) have shown that EDTA is an extremely effective agent for dissolving several nonsilicate minerals, i. e., gypsum, anhydrite, dolomite, and magnesite, calcite and aragonite. In addition, they proved that EDTA has no more detectable damage to the clay minerals determined by comparative X-ray diffraction studies. 43 g of gypsum is soluble in 1 liter of EDTA solution in four hours.

Considering the reasons explained above, EDTA was preferred in the dissolution of gypsum. For this procedure, an EDTA stock solution was prepared by dissolving 74.45 g of reagent grade disodium EDTA salt in water to yield 800-900 ml of solution. The pH was then adjusted to about 11 by addition of NaOH pellets. This was diluted to one liter, yielding a 0.2M EDTA solution.

4 samples (P28, P29, P30, P31) petrographically rich in clayey material from drillcore I, and from 3 samples (P32, P33, P34) from drillcore II were ground to 90 mesh and nearly 40 g of samples were added to 1 liter of EDTA. Following explains the result of the experiments.

Sample no. 28 is from drillcore I from 5.50 – 5.80m. 40.62 g of sample was added to the 1 liter of 0.2 M EDTA solution with a pH of 11-12. The solution was stirred with a Clifton hot magnetic stirrer for 8 hours. The temperature was adjusted to 25°C without water loss and the speed was adjusted to 6. After heating of 8 hours period, the solution was put in suspension in order to extract clayey material from suspension. The upper 10 cm of suspended material was siphoned after 8 hours (according to the Stoke's law). The material acquired from suspension was centrifuged two times by distilled water to eliminate the acid content. Then, clayey material left from centrifugation was put onto the glass slides for X-ray diffractometry analyses.

Sample no. 29 is from drillcore I from 6.00 – 6.30 m. 40, 84 g of sample put into 1 liter of EDTA. Solution was stirred for 8 hours with the magnetic stirrer with temperature of 25°C and speed 6. After 8 hours period in suspension and siphoning, it was observed that almost no material was available for further steps. Therefore, the experiment was repeated. Another 8 hours of heating was applied and then put into the suspension. Nevertheless, there was not enough material for X-ray diffractometry (XRD) analyses after second trial.

Sample no. 30 is from drillcore I from 8.65- 8.85 m. 40.80 g was dissolved in 1 liter of 0.2 M EDTA. Solution was heated for 8 hours at temperature 25°C and speed 6. After another 8 hours in suspension, the material was collected from suspension and centrifuged. However, the material obtained was nearly white in colour, indicating that gypsum was still present in the suspended material.

Sample no. 31 is from drillcore I from 9.20 – 9.40 m. 40.64 g of sample was put into 1 liter of solvent. After 8 hours of heating, white coloured material, containing probably gypsum observed here in the suspended material.

Sample no. 32 is from drillcore II from 3.50 – 3.80 m. 40.45 g of sample was dissolved in 1 liter of 0.2 M EDTA. Additional to 8 hours of heating, 24 hours of heating was applied; however, even after this procedure, there was not adequate material for X-ray diffractometry analyses

Sample no. 33 is from drillcore II from 8.40 – 8.70 m. 40.54 g of sample was used. This time, a small quantity of 0.02 N sodium polyphosphate was added to the solution to aid dispersion. After 24 hours of boiling and 8 hours of suspension duration, the obtained material was not enough for further analyses.

Sample no. 34 is from drillcore II from 19.00 – 19.30 m. 10.00 g of sample was dissolved in 1 liter of 0.2 M EDTA in order to prevent flocculation of the clay minerals. A small quantity of 0.02 N sodium polyphosphate was added. This

sample was heated again 24 hours and left to suspension for 8 hours. After, this trial, there was not adequate material present for further steps.

At the end of these trials to obtain clay material, sample no. 28, sample no. 30, and sample no.31 were the ones used in the X-ray diffraction analysis.

3.7.2 X-Ray Diffraction Studies

After chemical treatment of the samples, 3 samples (sample no.28, sample no. 30 and sample no. 31) from drillcore I were available for preparation of oriented specimens. Air-dried specimens, the specimens saturated with ethylene glycol, and the specimens heated to 300 °C and 550 °C were examined together with random specimens of 7 samples.

4 random samples (sample no. 28, sample no. 29, sample no. 30 and sample no. 31) from drillcore I were evaluated and it is seen that 4 of the random specimens gives the same peaks. Therefore, only one diagram for 4 samples is illustrated in Figure 27. According to this diagram, d values of 7.596 A°, 4.279 A°, 2.870 A°

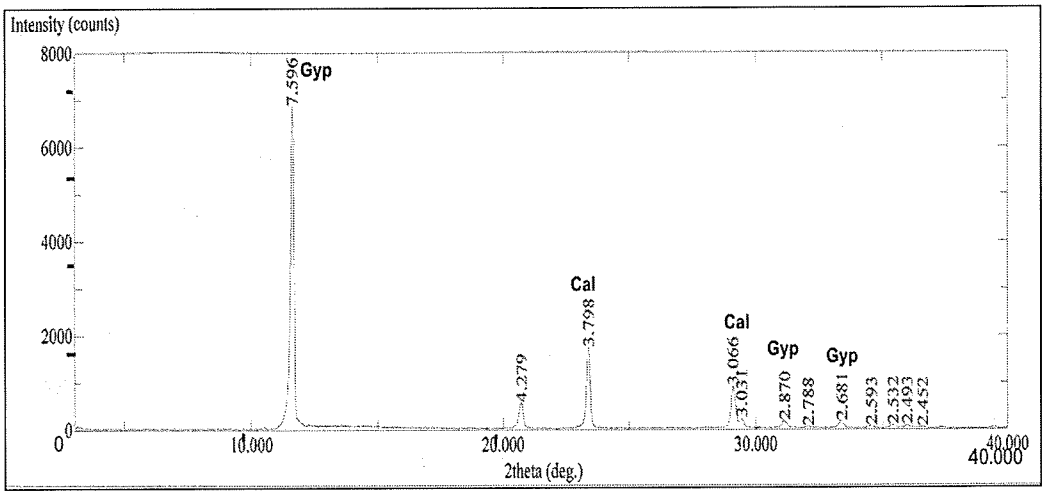

Figure 27. X-ray diffraction patterns of random specimens of sample P28 from drillcore I (Gyp: gypsum; cal: calcite)

and 2.681 A° indicate the presence of gypsum in the specimen. In addition, d values of 3.798 A° and 3.066 A° indicate calcite. The random analyses of 3 samples (sample no.32, sample no. 33 and sample no.34) from drillcore II are similar to the diagram above with slight differences in d values. Gypsum and calcite identified from the diagram shown in Figure 28. Similarly, d values of 7.5703 A°, 4.279 A°, 3.033 A° indicate gypsum, d values of 3.795 A° and 3.064 A° corresponds to calcite peaks.

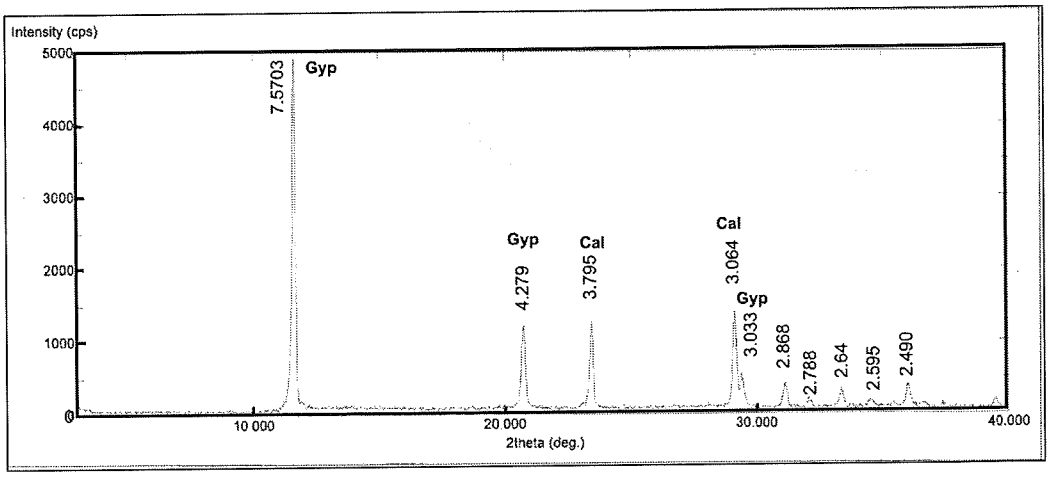

Figure 28. X-ray diffraction patterns of random specimens of sample no. P32 (Gyp: gypsum; cal: calcite)

Concerning the oriented specimens, 3 samples of sample no. 1, sample no. 3 and sample no. 4 are examined. However, the X-ray diffraction diagrams of these samples show that upon heating, intensity and the number of the peaks increases at 300°C and 550°C., while air dried and ethylene glycolated samples have few peaks with certain d-values. Such an XRD pattern does not indicate clay fraction (Figure 29, 30 and 31). The reason of having this kind of diagram where peaks get stronger upon heating could result from the EDTA present in the specimen. X-ray pattern of EDTA has been checked as a blank sample in order to evaluate its effect onto the specimens. However, XRD diagram of EDTA (Figure 32) do not show similar peaks with the 3 specimens that have been analyzed. The

reason of these peaks might due to result of the interaction of the EDTA with gypsum specimen.

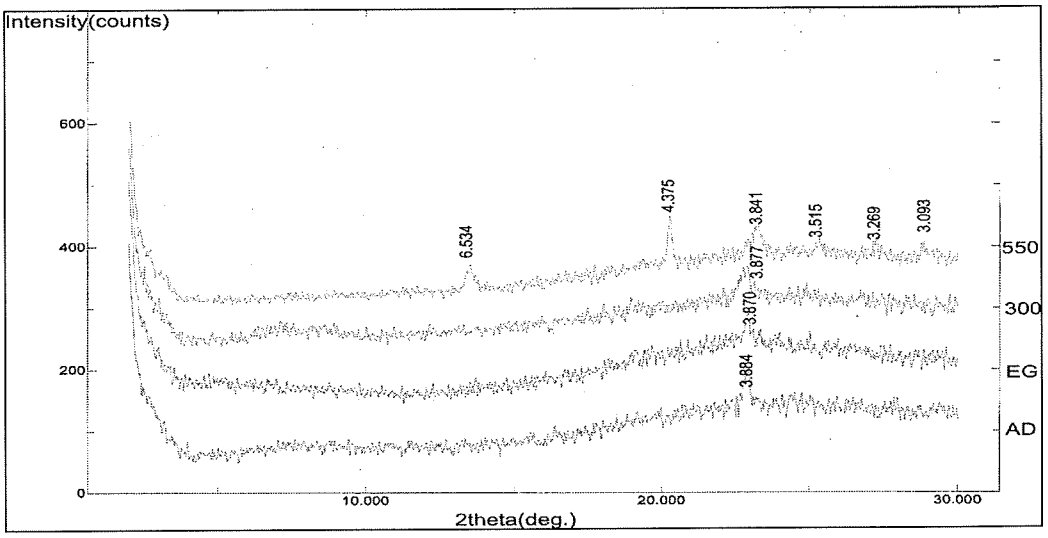

Figure 29. X-ray diffraction patterns of oriented sample no. P28 (AD: Air dried, EG: Ethylene glycol, heated 300 °C and heated 550°C)

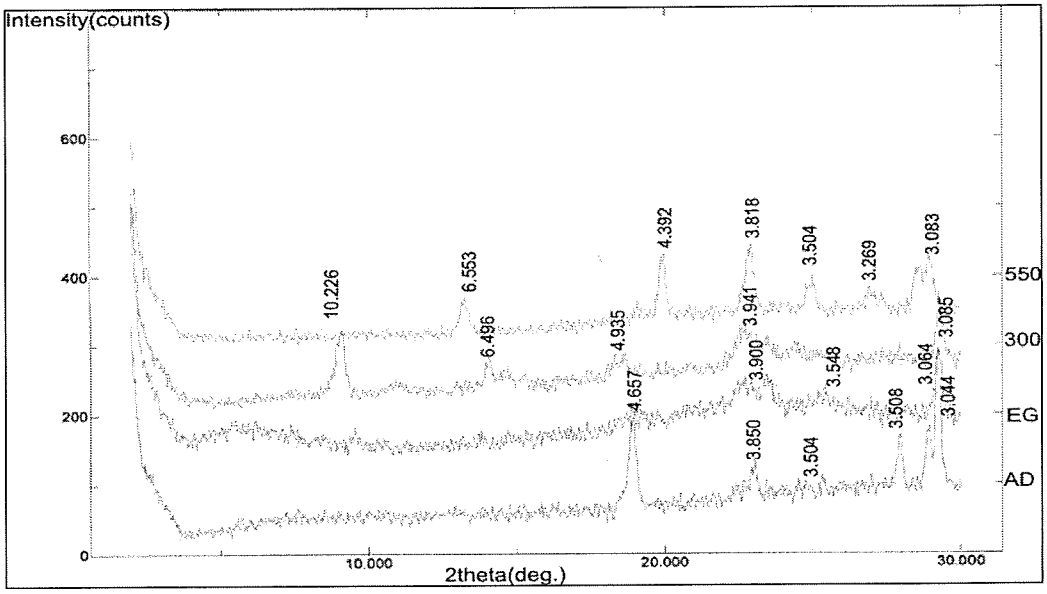

Figure 30. X-ray diffraction pattern of oriented sample no. P30 (AD: Air dried, EG: Ethylene glycol, heated 300°C and heated 550°C)

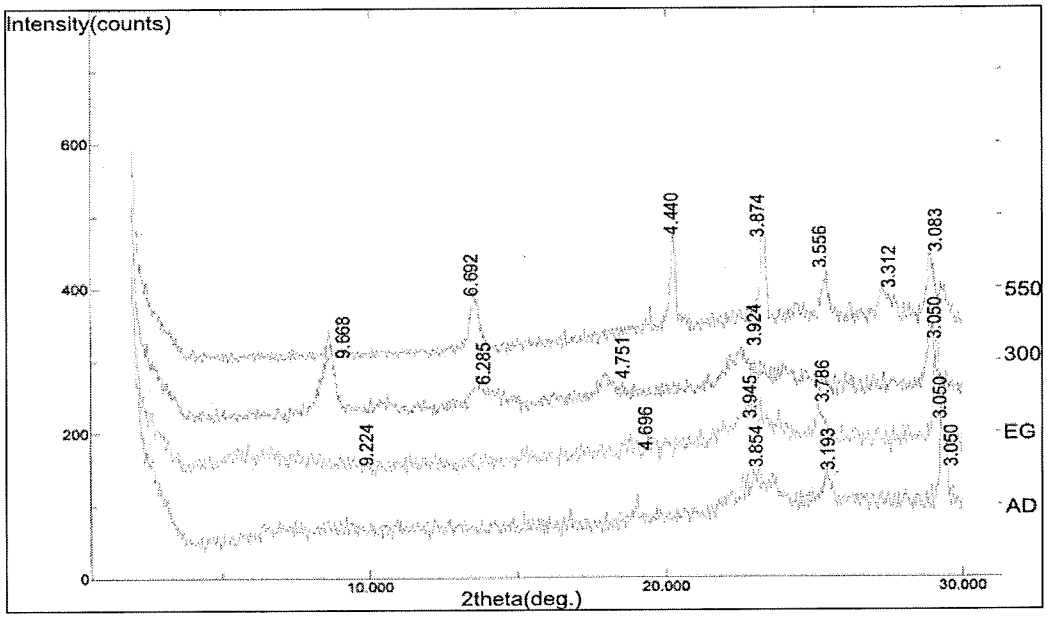

Figure 31. X-ray diffraction pattern of oriented sample no. P31 (AD: Air dried, EG: Ethylene glycol, heated 300°C and heated 550°C)

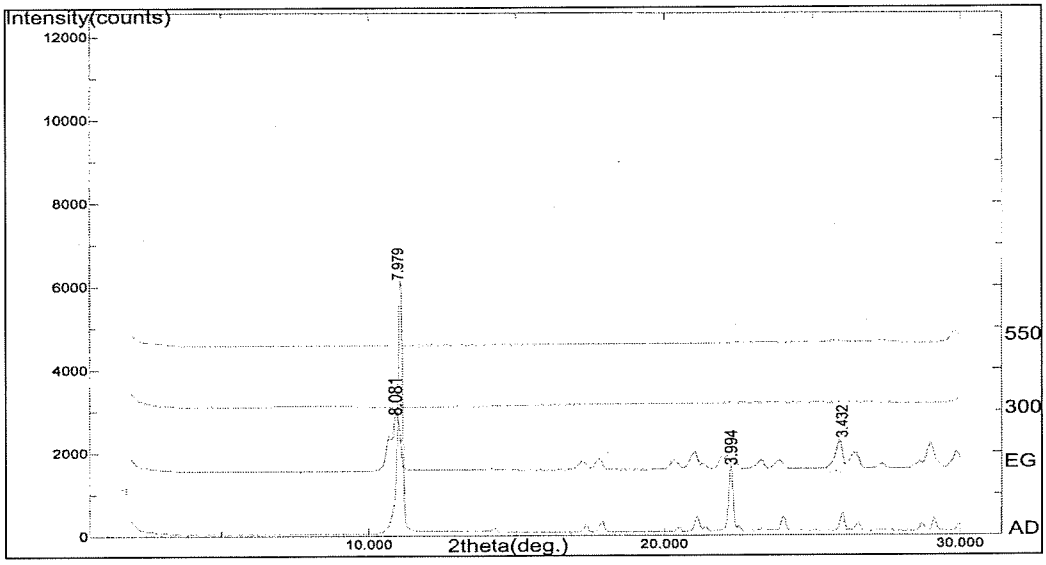

Figure 32. X-ray diffraction pattern of EDTA (AD: Air dried, EG: Ehtylene glycol, heated 300 °C and heated 550 °C)

After these experiments, the aim of which is to detect the clayey material in the rock, different clay samples have been gathered from the quarry. Beige coloured clay and gray coloured clay are the samples collected from the blasted rock in the quarry. These samples are primary clays present between the gypsum crystals. The X-ray diffractometry diagrams of random specimens (Figure 33) of beige clay illustrates that gypsum and calcite are present in the clay sample and the oriented specimens (Figure 34) indicate the type of the clay is Calcium (Ca) smectite. The EDS pattern of the SEM samples also indicates that the impurity contains Ca.

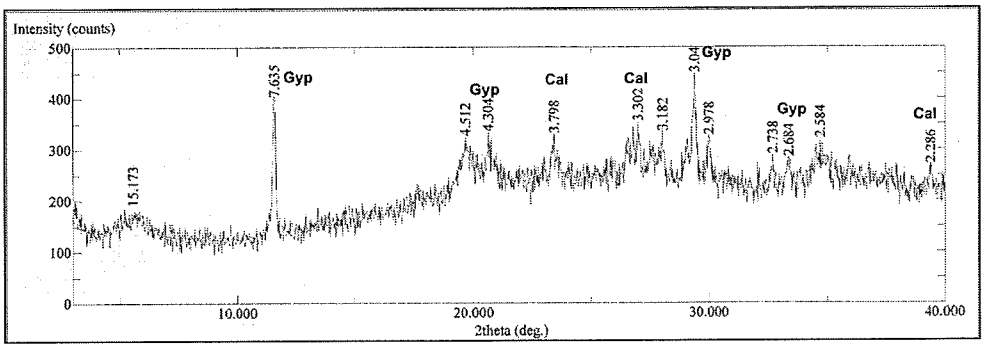

Figure 33. X-ray diffraction pattern of random specimen of beige clay (Sample no. P52) (Gyp: gypsum; cal: calcite)

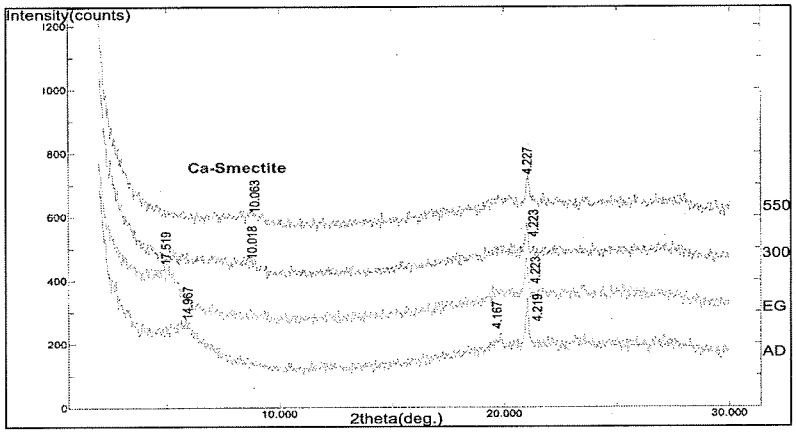

Figure 34. X-ray diffraction pattern of oriented specimen of beige clay (Sample no. P52) (AD: air-dried; EG: ethylene glycol; heated 300; heated 550)

X-ray diffractometry analysis of gray clay shows that gypsum and calcite present in the clay sample and Ca-smectite is the type of the clay. Figure 35 and 36 illustrates the pattern of random and oriented specimens.

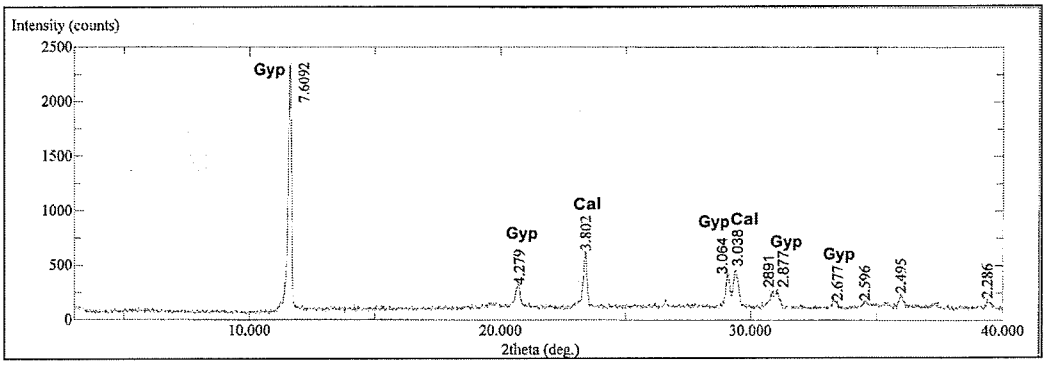

Figure 35. X-ray diffraction pattern of random specimen of gray clay (Sample no. P49) (Gyp: gypsum; cal: calcite)

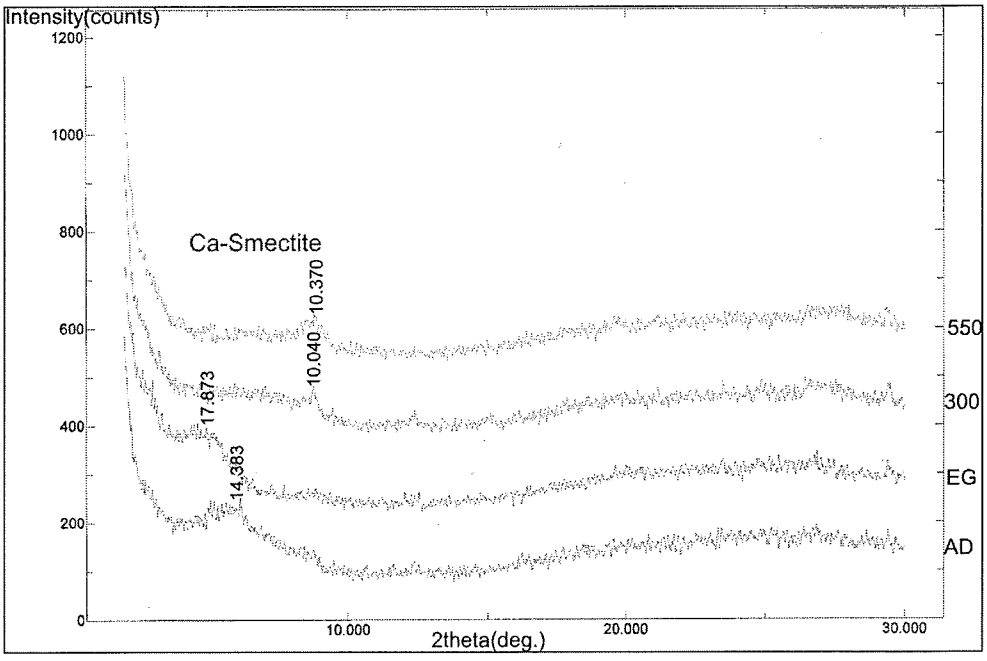

Figure 36. X-ray diffraction pattern of oriented specimen of gray clay (Sample no. P49) (AD: air-dried; EG: ethylene glycol; heated 300 ; heated 550)

Another X-ray diffractometry analysis has been applied to the green clay that is at the bottom of the gypsum bed (Figure 15) in order to identify the type of clay present inside the rock. Assuming that the type of clay inside the rock will be same as the clay at the bottom, this green clay has been analyzed. Green clay contains calcite and the illite – Ca-smectite mixed layer clay mineral is the type of clay mineral (Figure 37 and 38).

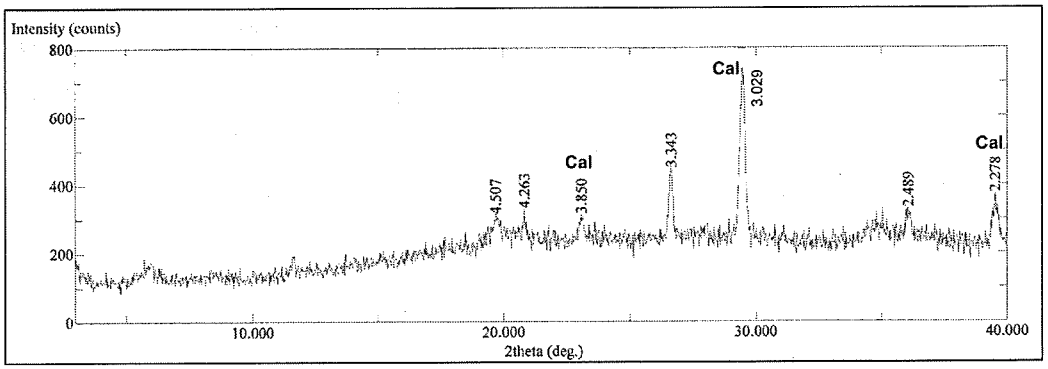

Figure 37. X-ray diffraction pattern of random specimen of green clay (Sample no. P47) (Gyp: gypsum; cal: calcite)

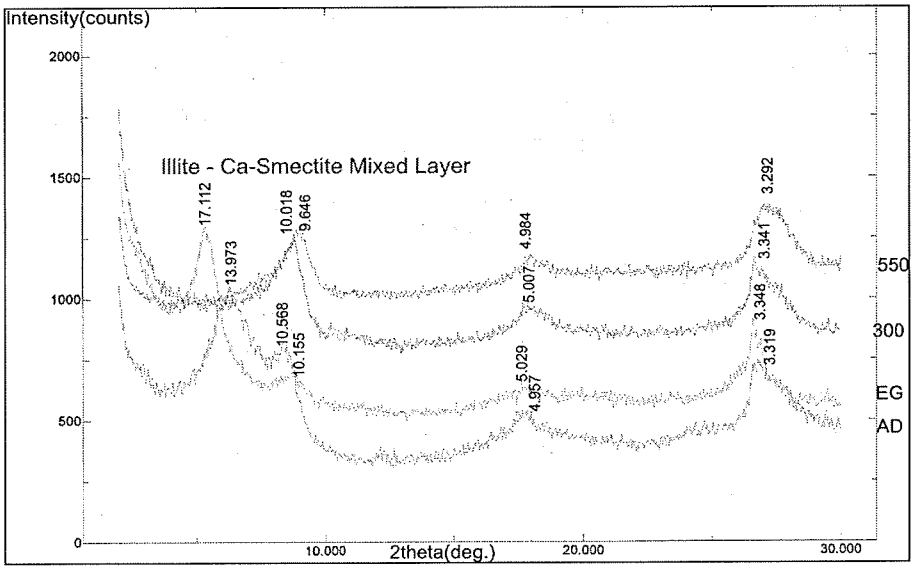

Figure 38. X-ray diffraction pattern of oriented specimen of green clay (Sample no. P47) (AD: air-dried; EG: ethylene glycol; heated 300 ; heated 550)

Gypsiferous soil at the top of the gypsum has been also under consideration in order to help identify the clay type in the rock. Two samples from drillcore I and drillcore II are analyzed. Based on these analyses, gypsum and calcite are present in the gypsiferous soil (Figure 39 and 40).

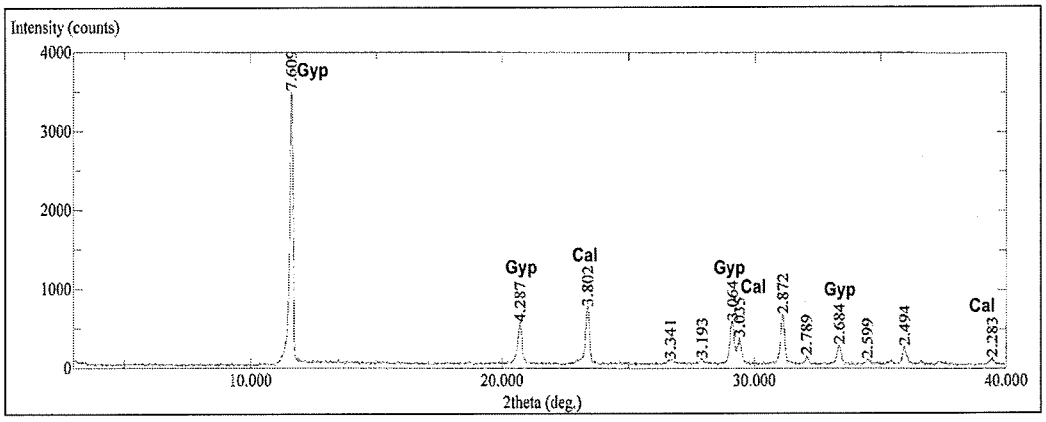

Figure 39. X-ray diffraction pattern of random specimen of gypsiferous soil from drillcore I (Sample no. P45) (Gyp: gypsum; cal: calcite)

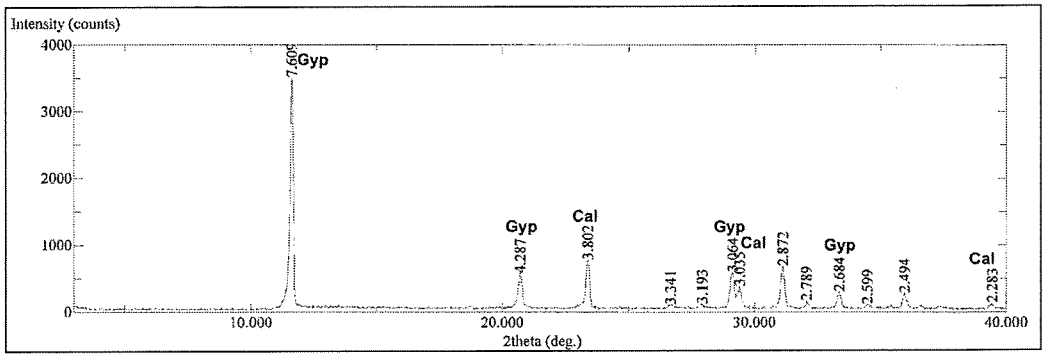

Figure 40. X-ray diffraction pattern of random specimen of gypsiferous soil from drillcore II (Sample no. P46) (Gyp: gypsum; cal: calcite)

CHAPTER 4

GEOCHEMICAL STUDIES

4.1 Introduction

The analysis of 10 gypsum rich samples and 8 clay rich samples have been performed in the Research and Development Laboratory of Knauf Gips KG in Germany. Based on these analysis, depending on the standards of the elements available and the methods applied, CaO, SO_3, MgO, Al_2O_3, Fe_2O_3, Na_2O, K_2O and SrO are determined for gypsum rich samples. Addition to these major elements, the trace elements Ti, V, Cr, Ni, Mo, Cu are determined for the clay rich samples. Moreover, crystal water content is determined for gypsum. The HCI insolubles are regarded as quartz and some clay minerals, which are not dissolved by HCI (Table 3). The sample locations are indicated in Figure 15 and Appendix A on the drillcore photos.

4.2 Method of Calculation

According to mineralogical and petrographical studies, presences of the three minerals which are gypsum, calcite and Ca-smectite are interpreted. All of these three minerals are the source of CaO in the given analysis list (Table 3). By using weight percentage of anionic groups (SO_3^{-2}, CO_2^{-2}) and relative amount of CaO used by these anionic groups, the volume percentage of each mineral can be determined. The calculation is started with gypsum composition. The proportion of CaO used by SO_3 is known. By multiplying the SO_3 of the analyzed sample with a factor obtained from proportion of CaO to SO_3 in pure gypsum, the CaO of the sample provided by gypsum can be obtained. Then, by subtracting the CaO used by gypsum, the remaining CaO is either calcite and/or Ca- smectite.

Although it is possible to calculate percentage of each mineral in a bulk sample using geochemical data, geochemical data of the studied samples are not appropriate to calculate the chemical formula and the percentage of the minerals. The data set of the samples (Table 3) in this study, are incomplete. For instance, the data does not sum up to 100 since there are undetected oxides such as CO_2 and SiO_2. Moreover, there are some minerals reported as insolubles. These HCl insolubles are quartz and some clay minerals, which are not dissolved by HCl. Therefore, these limitations are taken into consideration during the calculations.

Since the CO_2 contents are unknown, percentages of calcite and Ca-montmorillonite and thus how much amount of CaO is provided by these minerals could not be calculated.

The calculated amount of the gypsum in each sample is given in Table 4. In this table, CaO-Std is weight percentage of CaO in a pure gypsum sample, which is 36.5 % and the SO_3 content in a pure gypsum sample (SO_3-Std) is 46.6 %. Based on this calculation, it can be expressed in the clay rich samples, calcite and/or Ca-montmorillonite content ranges from 4 % to 20 %.

The gypsum content in the gypsum rich samples are calculated by first by determination of the crystal water content in the samples. Then, the crystal water content is multiplied by the factor 4.7785, which the proportion of H_2O content (36 %) to $CaSO_4.2H_2O$ (136.15 %) in pure gypsum. Table 3 illustrates the gypsum contents, in other words, purity of gypsum. The samples high amount of gypsum in their content, ranging from 88 % to 95 %.

Table 3. Chemical analysis of the gypsum rich and clay rich samples

Gypsum-rich Samples											
Sample	**CaO**	**SO_3**	**MgO**	**Al_2O_3**	**Fe_2O_3**	**Na_2O**	**K_2O**	**HCl**	**SrO**	**Crystal**	**$CaSO_4$**
No								**insol.**		**Water**	***$2H_2O$**
	(%)	**(%)**	**(%)**	**(%)**	**(%)**	**(%)**	**(%)**	**(%)**	**(%)**	**(%)**	**(%)**
P35	34,0	41,5	0,20	0,15	0,09	0,01	0,04	0,70	0.07	18,5	88,4
P36	32,7	45,8	0,17	0,18	0,11	0,04	0,05	0,60	0.03	19,9	95,1
P37	32,4	44,4	0,37	0,30	0,19	0,03	0,06	1,10	0.14	19,4	92,7
P38	32,6	44,9	0,31	0,20	0,12	0,03	0,04	0,80	0.06	19,7	94,1
P39	32,5	43,3	0,40	0,28	0,18	0,03	0,06	1,10	0.17	19,2	91,7
P40	32,2	44,6	0,23	0,28	0,02	0,04	0,07	1,00	0.05	19,7	94,1
P41	32,8	45,6	0,09	0,08	0,04	0,02	0,02	0,50	0.36	19,7	94,1
P42	32,3	44,7	0,27	0,34	0,18	0,05	0,06	0,80	0.03	19,7	94,1
P43	30,9	41,6	0,76	0,70	0,41	0,02	0,12	1,80	0.19	18,8	89,8
P44	31,9	44,1	0,32	0,31	0,19	0,05	0,06	0,90	0.06	19,7	94,1

Clay-rich Samples															
Sample	**CaO**	**SO_3**	**MgO**	**Al_2O_3**	**Fe_2O_3**	**Na_2O**	**K_2O**	**HCl**	**SrO**	**Ti**	**V**	**Cr**	**Ni**	**Mo**	**Cu**
No								**insol.**							
	(%)	(%)	(%)	(%)	(%)	(%)	(%)	(%)	(%)	ppm	ppm	ppm	ppm	ppm	ppm
P45	32,9	34,1	0,5	1,0	0,6	0,02	0,19	3,8	0,04	<1	6	13	20	<1	5
P46	29,7	21,5	1,0	2,4	1,6	0,03	0,37	12,4	0,04	<1	15	32	49	<1	10
P47	13,7	0,8	4,2	5,8	5,6	0,05	1,25	46,2	<0,01	<1	84	157	237	<1	38
P48	20,1	0,9	3,6	4,9	4,5	0,04	1,05	37,6	<0,01	<1	74	121	187	<1	24
P49	6,3	2,8	14,7	6,3	3,4	0,06	0,97	41,9	<0,01	<1	87	75	100	<1	14
P50	25,7	26,9	4,2	2,2	1,3	0,04	0,37	8,7	0,0	<1	35	26	36	<1	6
P51	8,1	5,7	6,4	6,2	3,9	0,04	0,96	44,7	1,9	<1	66	73	89	<1	28
P52	10,1	8,9	9,1	5,3	3,0	0,03	0,82	35,4	4,9	<1	62	61	70	<1	24

Table 4. Gypsum content in clay rich samples

Sample No	CaO	SO_4^{-2}	CaO in Gypsum	Calcite/Ca-Montmo.
			F= (CaO-std/SO_4-std)x(SO_4)	CaO-F
	(%)	(%)	(%)	(%)
P45	32,9	34,1	23,78	9,12
P46	29,7	21,5	14,99	14,71
P47	13,7	0,8	0,56	13,14
P48	20,1	0,9	0,63	19,47
P49	6,3	2,8	1,95	4,35
P50	25,7	26,9	18,76	6,94
P51	8,1	5,7	3,98	4,12
P52	10,1	8,9	6,21	3,89

4.3 Interpretation of Chemical Data

Assuming that all the Al2O3 are from the clay minerals, binary diagrams are prepared. In these diagrams, major oxides are plotted against Al2O3 (Figure 41). Initially, CaO is plotted against Al_2O_3 (Figure 41-A). In this diagram, a negative correlation between CaO and AI_2O_3 is observed. As the CaO content increases, the Al_2O_3 content decreases. The lowest value of CaO which is 6% corresponds with highest Al_2O_3. The diagram of MgO vs. Al_2O_3 (Figure 41-B) shows that up to 6 % of MgO is used by clay minerals since there is almost a positive correlation. Above the 6% of MgO, the Al_2O_3 content is constant, which means that, MgO content is independent from Al_2O_3.This might indicate the presence of other minerals containing MgO or an enrichment of MgO in these samples. In the diagram of Fe_2O_3 vs. Al_2O_3 (Figure 41-C), it is seen that there is a positive correlation between them up to 4% Fe_2O_3. The two samples with higher iron content are independent from Al_2O_3, which is an indication of presence of iron minerals or an enrichment of Fe_2O_3. The diagram of SO_3 vs. Al_2O_3 is very similar to the diagram of CaO vs. Al_2O_3 and it points out that there is a negative

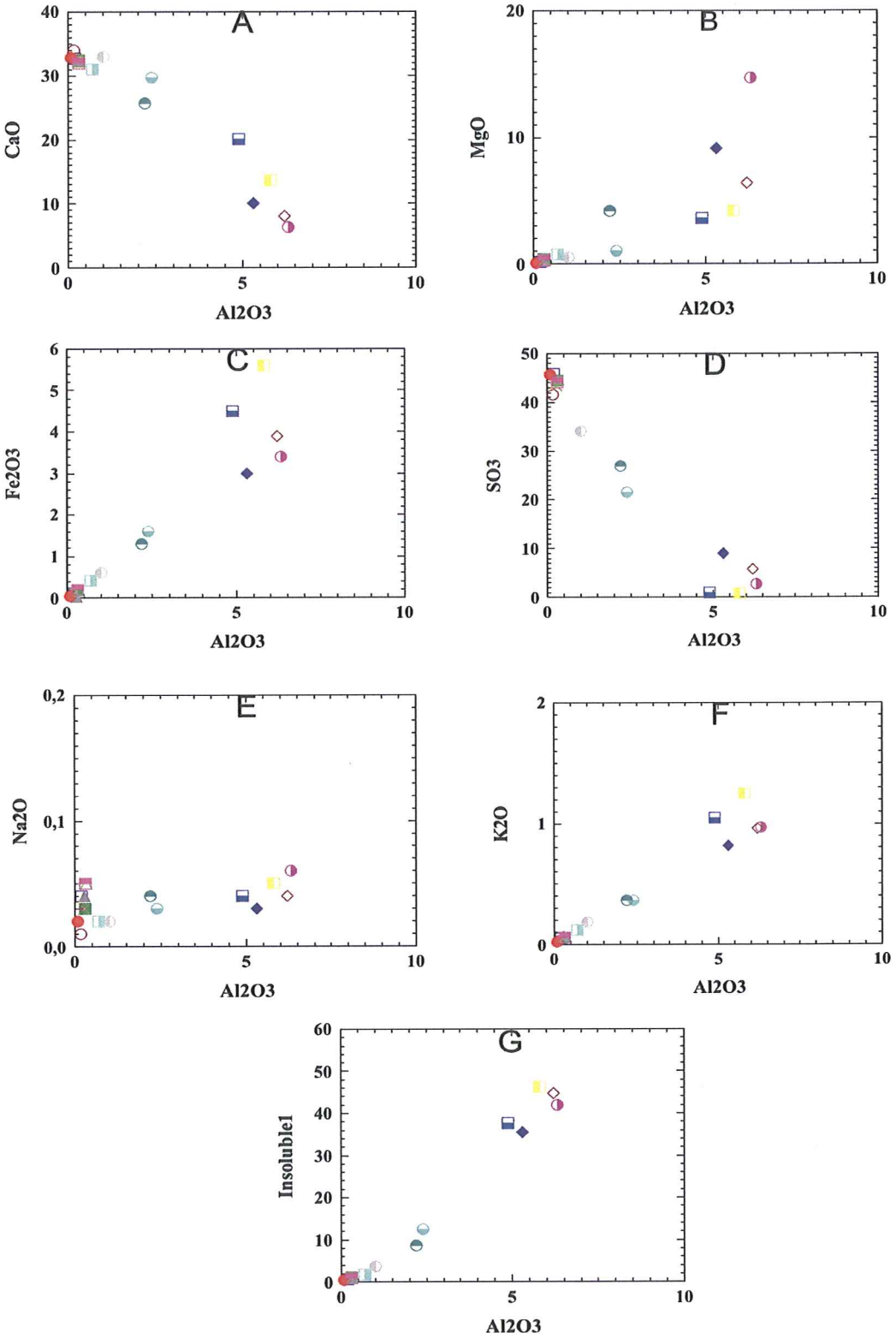

Figure 41. Binary diagrams of major oxides vs. Al_2O_3

Table 5. List of the symbols used in binary diagrams

Symbol	Sample No	Explanation
○	P35	Gypsum
□	P36	Gypsum
■	P37	Gypsum
+	P38	Gypsum
×	P39	Gypsum
▲	P40	Gypsum
●	P41	Gypsum
△	P42	Gypsum
◧	P43	Gypsum
▣	P44	Gypsum
◑	P45	Gypsiferous Soil-01
◓	P46	Gypsiferous Soil-02
◨	P47	Green Clay-01
▬	P48	Green Clay-02
◐	P49	Gray Clay-01
◒	P50	Gray Clay-02
◇	P51	Beige Clay-01
◆	P52	Beige Clay-02
▽	Stn-gyp	Standard Gypsum
▼	Stn-cal	Standard Calcite
◁	Stn-clay	Standard Montmori.

correlation between SO_3 values and Al_2O_3 (Figure 41-D). Since the SO_3 is assumed to be used by gypsum, one can conclude that as the clay content increases, the gypsum content decreases. Concerning the diagram of Na_2O vs. Al_2O_3, some of the samples tend to be independent from Al_2O_3. (Figure 41-E) Low to zero values of Al_2O_3 corresponds to high Na_2O values. Therefore, the excess of Na_2O is used by non-clay minerals. Binary diagram of K_2O vs. Al_2O_3 shows a strong correlation, which indicates that K_2O is part of the clay minerals. (Figure 41-F). Finally, the insolubles are plotted against Al_2O_3. It is observed that there is a strong correlation (Figure 41-G). Since the HCI insolubles can be quartz and some insoluble clay minerals and quartz, it is understood from the strong correlation that the insolubles are clay minerals.

The trace element analyses were performed for the clay minerals. Among the trace elements, Chromium (Cr), Vanadium (V), and Copper (Cu) are plotted against Al_2O_3 since they can be accumulated in the interlayer of clay minerals (Figure 42). Cr vs. Al_2O_3 diagram indicates that there is positive correlation and two clay samples enriched in Cr (Figure 42-A). V vs. Al_2O_3 shows that nearly a positive correlation is observed (Figure 42-B). Slight correlation is seen in Cu vs. Al_2O_3 diagram, three of the samples are independent from Al_2O_3 (Figure 42-C).

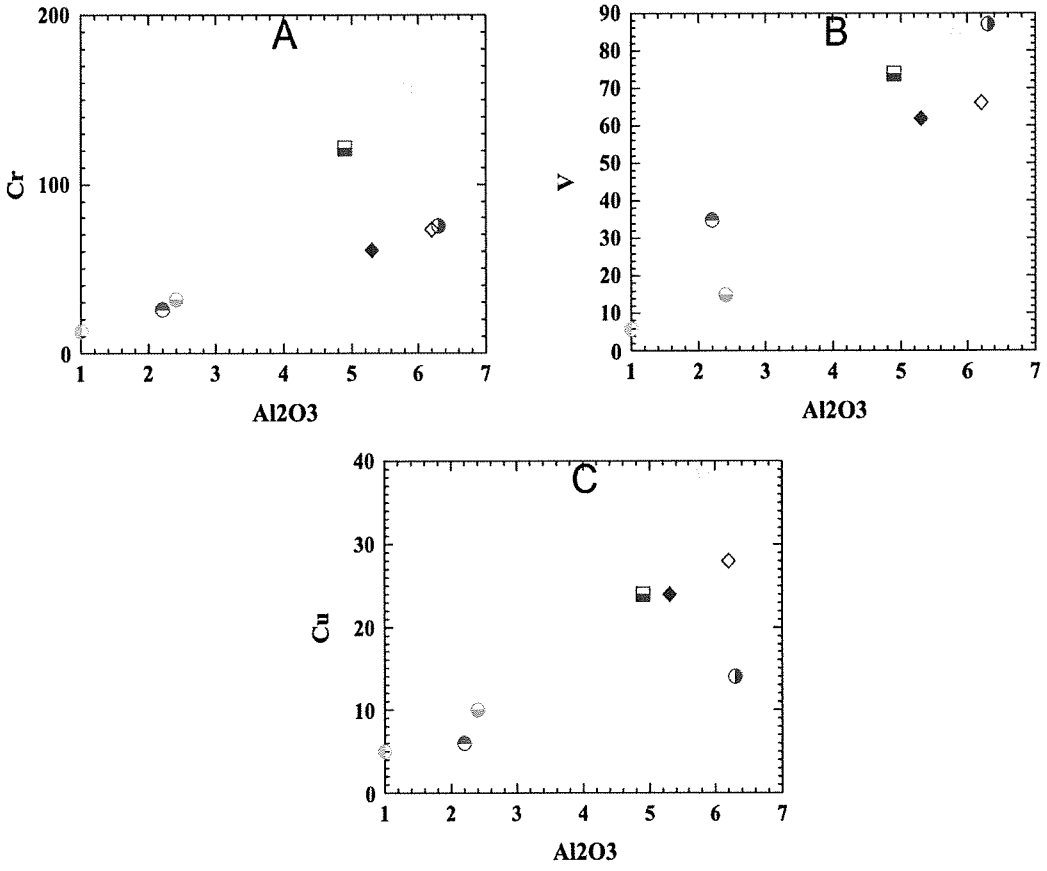

Figure 42. Binary diagrams of trace elements against Al_2O_3

Assuming all SO_3 is from gypsum, to able to make assumption about relative abundances of gypsum and impurity minerals, the SO_3 values of the samples are normalized to SO_3 of standard gypsum. Moreover, the other compounds (i.e. $Al2O_3$, MgO, Na_2O, K_2O) are normalized to those compounds in the standard sample (standard montmorillonite, Deer, Howie and Zussman, 1980). Table 6 illustrates values of standard clay used in the diagrams. The normalized values are plotted against normalized SO_3 values. Essentially, 5 different chemical groups are obtained (Figure 43). Table 5 lists the used symbols in the binary diagrams.

Table 6. Standard clay (montmorillonite) values utilized in the diagrams (Deer, Howie and Zussman, 1980)

Compound	(%)
SiO_2	51,14
Al_2O_3	19,76
Fe_2O_3	0,83
MgO	3,22
CaO	1,62
Na_2O	0,11
K_2O	0,04

Initially, normalized CaO (CaO-N) value and normalized SO_3 (SO_3-N) value are plotted (Figure 43-A). The group 1 samples are characterized by very low SO_3 values, which may indicate these samples are does not contain gypsum in their content. In addition, their CaO contents are enriched compared to the standard clay hence this enrichment may indicate that CaO is mainly supplied by calcite. Group 2 samples, on the other hand, are relatively enriched than normalized SO_3 and depleted in CaO compared to group 1 samples. This may indicate these samples are still rich in clay minerals since the samples plot close to the standard clay sample. Group 3 samples contain both higher content of CaO and SO_3 compared to group 1 and group 2 samples. There is nearly positive correlation between CaO and SO_3 indicating presence of gypsum. Group 4 also contains

gypsum, but CaO content is slightly higher than Group 5. A positive correlation can be seen for Group 5, which indicates that CaO is used by gypsum.

Considering the diagram MgO-N against SO_3-N (Figure 43-B), group 1 samples have MgO value same as the standard clay (montmorillonite) and have very low SO_3 values, which indicates that these samples are almost gypsum free. Group 2 samples contains highest amount of MgO and with low values of SO_3. The samples are enriched by MgO and they have higher values than the standard clay. Group 3 samples contain lower MgO values and higher SO_3 values. Group 4 and group 5 have the highest SO_3 values with the lowest MgO values. The enrichment of SO_3 indicates presence of gypsum in the samples with absence of MgO. The enrichment of MgO in the group 2 samples indicates that not only the clay but also the other minerals having MgO in their content might be the reason of this enrichment. However, it is not possible to detect these minerals based on this data.

Binary diagram of Al_2O_3-N against SO_3-N is given in Figure 43-C and the diagram of Fe2O3 against SO3 are indicated in Figure 43-D. Based on these diagrams, it can be expressed that group 1 samples have lower Al_2O_3 content than the standard clay samples and have higher content of Fe_2O_3 content than the standard clay sample. Group 2 samples have lower Al_2O_3 as group 1 samples but Fe_2O_3 content is higher then the rest of the sample groups. Group 3 samples have low Al_2O_3 and Fe_2O_3 content. Group 4 and group 5-gypsum rich samples- have the lowest Al_2O_3 and Fe_2O_3 content.

The Na_2O-N value and K_2O-N value are considered against normalized SO_3 (Figure 43-E and Figure 43-F). All the values of Na_2O are lower that the standard clay and all the values of K_2O are higher than the standard except group 5 and group 4 samples which are rich in gypsum. Concerning Na_2O values of Group 5, the content of the Na_2O is high in these gypsum rich samples.

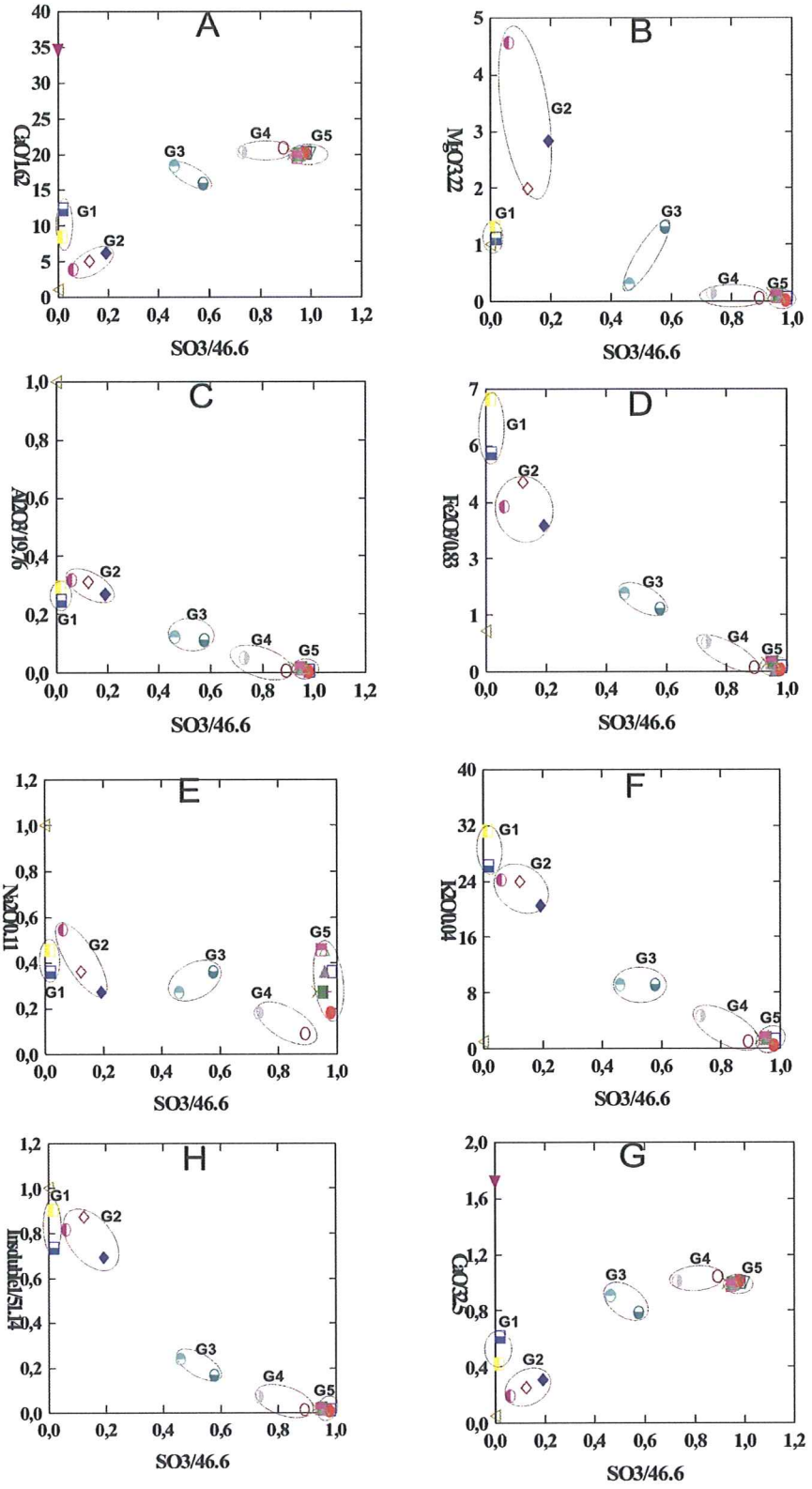

Figure 43. Binary diagrams of normalized oxides vs. normalized SO_3

Figure 43-G illustrates the diagram of the normalized insoluble value vs. SO_3. Based on this, the group 1 and group 2 samples have highest content of insolubles, close to the standard clay. On the other hand, group 5 does not contain any insolubles. Group 3 and group 4 have slightly higher insolubles than the group 5.

The last diagram belongs to normalized CaO based on gypsum and normalized SO_3 (Figure 43-H). According to this diagram, group 1 samples have highest content of CaO and lowest SO_3 content. The excess of CaO could be presence of calcite. Group 2 samples have lower CaO value and higher SO_3 than group 1. Group 3, group 3 and group 5 have considerable SO_3 and CaO, indicating presence of gypsum.

Based on these analyses, one can conclude that group 1 samples which are defined petrographically as green clays are nearly gypsum free and contain calcite. The Al_2O_3 is lower than compared standard clay (montmorillonite). There is excess of Fe_2O_3, K_2O and MgO in the clay samples, which indicates an enrichment .of these oxides in these clays or presence of other minerals. Group 2 group has low amount of gypsum in their content and high amounts of MgO and Fe_2O_3. Al_2O_3 content for these samples are close to group 1 samples. The interpretation and the petrographic determination also indicate the group 2 samples are clay rich samples. Group 3 samples are defined previously as gray clay and gypsiferous soil. This group has intermediate values of the oxides under consideration. This group can be categorized as gypsiferous clay or clayey gypsum. Group 4 and group 5 have highest SO_3 content with lowest Al_2O_3 content. There is only increase in Na_2O content. These groups are defined as gypsum rich petrographically and geochemically.

The trace elements vanadium (V), chromium (Cr), nickel (Ni), copper (Cu), molybdenum (Mo), titanium (Ti) are determined for clay rich samples. Strontium (Sr) content is determined for both clay rich samples and gypsum rich samples.

The binary diagrams of these trace elements against normalized SO_3 is given in Figure 44.

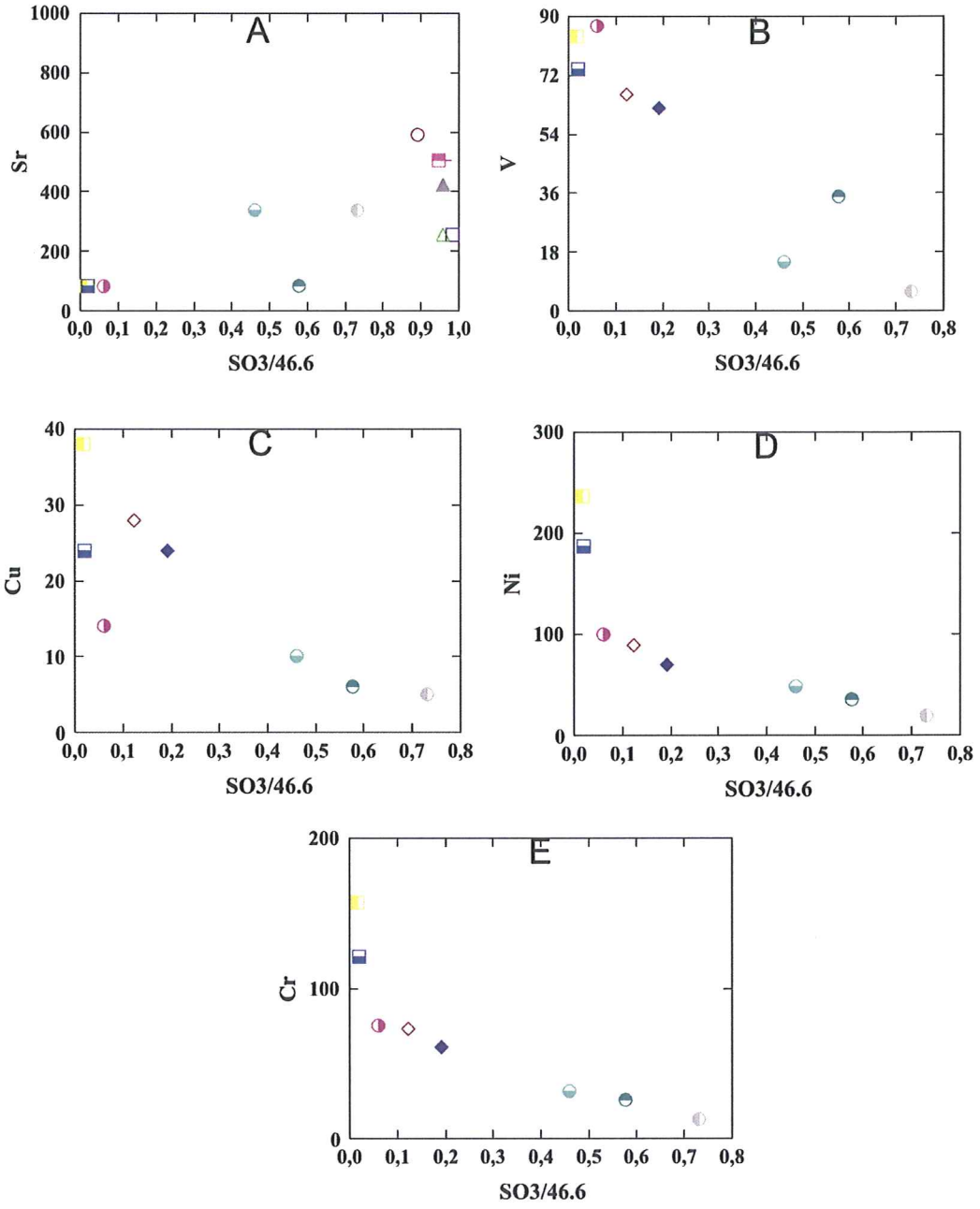

Figure 44. Binary diagrams of trace elements vs. normalized SO_3

Clay rich samples depletes in Sr; whereas gypsum samples are enriched in Sr (Figure 52-A). Among the clay rich samples, except gypsiferous and gray clay, the remaining clays are enriched in V (Figure 44-B). There is negative correlation between Cu and SO_3. Only green clay and gray clay deplete in Cu (Figure 52-C). Concerning the diagrams of Ni vs. SO_3 and Cr vs. SO_3, there is negative correlation but two samples of green clay are enriched in Cr (Figure 44-D and 44-E).

CHAPTER 5

ROLE OF IMPURITY IN INDUSTRIAL PRODUCT

Raw gypsum character plays a significant role in the industrial applications. To determine the impurities and its affects is crucial. Below, tests and specifications of raw gypsum and effect of the impurities are explained.

5.1 Tests and Specifications of Raw Gypsum

The tests of the raw gypsum material are a significant step before utilizing the material in the production. Among these tests, chemical analysis is the major and indispensable stage of the tests. Knauf Standards (2002) indicate the necessary determinations for the raw gypsum below.

1. Crystal Water Content
2. Gypsum Purity
3. $CaSO_4$
4. $CaCO_3/MgCO_3$
5. Al_2O_3
6. Fe_2O_3
7. K2O
8. Loss of Ignition

Crystal water is determined in order to calculate the gypsum purity. In the specifications, the minimum crystal water value is 16% and the gypsum purity 80%. If the gypsum purity is between 80-90%, then the quality is good; if the quality between 90-100%, the quality is very good.

$CaSO_4$ (anhydrite) content should be less than 5 %. $CaCO_3$ (calcite)/$MgCO_3$ content should be less than 10 %. Al_2O_3 should be less than 0.3% and Fe_2O_3 should be less than 0.15 %. K_2O value should be less than 0.06 %. Residual loss of ignition (LOI) should be less than 0.1 % (Knauf Standards, 2002).

Out of 10 samples collected from different parts of the drillcore I and drillcore II, chemical analysis has been performed. Table 7 illustrates the results of this chemical analysis.

Table 7. Chemical analysis of gypsum samples from drillcore I and II

Sample No	Crystal Water	$CaSO_4$ *$2H_2O$	$CaSO_4$	$CaCO_3$	$MgCO_3$	K_2O	Fe_2O_3	Al_2O_3
	(%)	(%)	(%)	(%)	(%)	(%)	(%)	(%)
P35	18,5	88,4	0,8	9,5	0,4	0,04	0,09	0,15
P36	19,9	95,1	0,3	3,4	0,4	0,05	0,11	0,18
P37	19,4	92,7	0,3	4,3	0,8	0,06	0,19	0,30
P38	19,7	94,1	0,2	3,8	0,6	0,04	0,12	0,20
P39	19,2	91,7	0,2	5,6	0,8	0,06	0,18	0,28
P40	19,7	94,1	<0,1	4,0	0,5	0,07	0,02	0,28
P41	19,7	94,1	0,4	4,1	0,2	0,02	0,04	0,08
P42	19,7	94,1	0,4	3,7	0,6	0,06	0,18	0,34
P43	18,8	89,8	0,4	4,7	1,6	0,12	0,41	0,70
P44	19,7	94,1	0,4	3,3	0,6	0,06	0,19	0,31

Based on the specifications above, it can be expressed that the gypsum purity is high; the quality of the rock is very good. The $CaSO_4$ content is very low and not critical. Calcite is present but it is less than 10 %, obeying the specifications. $MgCO_3$ is nearly less than 1.6 %, compatible with the specifications. K_2O content is less than 0.06 % with exception of two samples. Al_2O_3 content is more than 0.3 % in five samples, but they are slightly higher than the specification. Fe_2O_3 content is slightly higher than 0.15 %. The LOI and swelling clay content are not detected in these experiments.

5.2 The Principles of Hemihydrate (Plaster of Paris) and Effect of Impurity on Industrial Product

Before explaining the effects of impurity on the product, it is better to identify the properties and uses of gypsum in industrial application.

Though some gypsum is used in the raw state, the greater part of it is first calcined or heated off water. The chief use of gypsum depends on a unique property. When heated to a moderate temperature, about 175 °C, gypsum loses three-fourths of its chemically held water. On cooling, the resulting "hemihydrate" (calcined gypsum-plaster of Paris) may be mixed with water and spread, cast or molded; then sets to a dense rocklike mass of intergrown needle like crystals (Bates, 1969). Calcium sulfate dihydrate, $CaSO_4.2H_2O$, is both the starting material before dehydration and the final product after rehydration (Ullmann's Encyclopedia, 1985).

Dehydration: $CaSO_4.2\ H_2O = CaSO_4.\ 1/2\ H_2O + 3/2\ H_2O$

Rehydration: $CaSO_4.\ 1/2\ H_2O + 3/2\ H_2O = CaSO_4.2\ H_2O$

The product of the calcination to the hemihydrate stage is known in the industry as "stucco", not to be confused with exterior stucco, which is largely portland cement and sand. Gypsum stucco manufactured to many different in-processes specifications, depending upon its use in various types of plasters, wallboard and block.

Concerning the impurities, main impurities present in the gypsum rock are mentioned in the previous chapters. According to this, major impurities are (Carr, 1994):

1) Insoluble or relatively insoluble minerals such as calcite, dolomite, anhydrite, anhydrous clays (brucite, illite), silica minerals (quartz, chalcedony).

2) Soluble evaporite minerals including chlorides: halite, slyvite, etc., and sulfate : mirabilite, epsomite, galuberite, etc.

3) Hydrous but insoluble minerals, e.g., the smectite group clays (montmorillonite)

The first category, to the extent that minerals replace gypsum, reduce the strength of rehydrated stucco and increase the weights of the final finished plaster or wallboard, i.e., more kilograms an impure stucco are required to obtain a given strength. These minerals occasionally act as hydration accelerators.

The presence of second category affects the calcining temperature and stucco slurry fluidity, set or rehydration time and paper core bonding. These minerals are usually limited to no more than 0.02 to 0.03% .

The principle impact of the third category is in moisture pickup of the finished product and on bonding characteristics of the gypsum stucco core of the wallboard to its paper covering. Hydrous clays up to 1.0 to 2.0 % may be tolerated (Carr, 1994).

CHAPTER 6

DISCUSSIONS

In these thesis, petrography, mineralogy and geochemistry of gypsum occurrence in Polatlı Sazılar region, Ankara has been studied. For this purpose, samples from two drillcores were examined.

The studies from the drillcores show that gypsum rocks are deposited on top of the green clay bed. In the overlying gypsum deposit, clay rich beds alternating with gypsum are present. The clay rich beds also constitute the matrix of the gypsum rocks. This interpretation indicates a change in environmental conditions resulting in decrease of clastic supply with increase of evaporitic occurrence. According to Akdağ (2005), gypsum deposits are formed in a lacustrine environment. If this is the case, the clay rich beds interpreted in this study may indicate a fluvial action transporting the clay material into the lacustrine environment. Depending on the degree of supply of clay material, different amounts of clay rich thin beds alternating with gypsum beds are observed. In addition to this, presence of clay in the matrix of gypsum rock imply continuous intake of clay.

The observations on drillcores show that the major type of gypsum rock is the gray coloured gypsum. This gypsum consists of sand sized selenite crystals and gypsum grains in a calcite and clay rich matrix. Moreover, white massive gypsum and selenitic gypsum, in minor amounts, occur due to change in physico-chemical conditions. White massive gypsum might have been resulted from numerous nuclei and slow growth rate due to the oversaturation in solution. On the other hand, selenite identified in lenses might have been crystallized from

few nuclei and rapid growth rate. This might be due to lower saturation degree. Nonetheless, another alternative explanation for large selenite

White massive gypsum might occur by crystallization of numerous nuclei in a saturated solution yielding finely crystalline gypsum. On the other hand, large selenite crystals in lenses might occur by crystallization of few nuclei yielding larger selenite crystals. Nonetheless, another approach is that the selenite crystals might have secondary origin and they become larger by recrystallizaton process.

It is important to determine whether the origin of gypsum is primary or secondary. Since the secondary gypsum is derived from hydration of anhydrite (Murray, 1964; Mossop and Shearman, 1973; Holliday, 1970; Warren, 1990), anhydrite may be present as relics in gypsum, which may cause problems in industrial usage. Therefore, the origin of gypsum in the studied samples is examined to see whether the anhydrite crystals are present or not. The study shows that there are not any anhydrite crystals. In addition, the textural relations (alabastrine, megacrystalline and porphyroblastic: Shearman et al., 1972; Orti, 1977) indicating secondary origin of gypsum are not observed in this study. Therefore, the origin of gypsum is assumed to be primary. The studied gypsum rocks are part of the Beypazarı basin and there is an argument about the origin of gypsum. According to E. Bingöl (oral communication), this Messinian Polatlı gypsum, a part of Beypazarı basin, is syngenetically deposited with anhydrite and dolomite and they are primary in origin. On the other hand, Orti et al. (2002) stated that the presence of secondary gypsum is widespread, and no facies composed of primary gypsum were identified in Beypazarı basin.

The abundance and the type of clay minerals in thin beds and in the matrix of the gypsum are also identified since the clays are important impurities that may affect the quality of plaster and plasterboard production (Carr,1994).To able to perform XRD studies on clays, clay enrichment processes are applied. Gypsum samples were dissolved to enrich the clay material. EDTA solution is chosen for

dissolvement of gypsum since EDTA is an effective agent for dissolving several nonsilicate minerals like gypsum, calcite, anhydrite, dolomite and magnesite and does not damage clay minerals (Hill and Runnel, 1960; Glover, 1961; Bodine and Fernald, 1973). Even though several experiments adjusting different conditions (time, amount of sample, etc.) are applied, clay material was not obtained from most of the samples. Therefore, the abundance and the type of clay material could not be determined quantitatively. The reason of not acquiring enough clay material is that gypsum prevents clay material to disperse and make it flocculate and sink to the bottom. Because of this reason, the studies about how the clay minerals affect the quality of the plaster and plasterboard product could not be performed.

CHAPTER 7

CONCLUSIONS AND RECOMMENDATIONS

The major gypsum rock is not a pure gypsum rock, rather than this, it is composed of scattered sand sized crystals and gypsum grains in a calcite and clay rich matrix. White massive, microcrystalline gypsum is one variety of gypsum which might occur in a saturated solution from crystallization of abundant nuclei. Another variety is large selenitic gypsum which might occur either by growth of few nuclei or recrystallization of primary crystals.

Petrographic studies showed that the calcite and clay rich material is observed both in the matrix of the rock and as alternating thin beds with gypsum. Moreover, it was also observed in the individual selenite crystals.

SEM studies were carried out on gypsum samples both to determine the different gypsum varieties and the impurity. Based on this study, it is observed that white massive gypsum does not contain any impurity, whereas prismatic, large selenite crystals are scattered in the fine clay matrix. The clay material has flaky appearance with sharp edges.

Clay minerals present inside the gypsum rock could not be acquired through dissolution processes. Assuming that the bottom green clay and the gray and beige clay samples gathered from the blasted rock have the same composition with the clay inside the rock, X-ray diffractometry analyses were carried out in order to determine the type of impurity. Based on these analyses, Ca-smectite is determined as the type of the clay, containing gypsum and calcite in it. Rarely, illite-smectite type clay mineral is also identified.

Geochemical studies have been performed on gypsum rich samples and clay rich samples to determine the content and amount of impurities and the gypsum samples. According to chemical analyses, the remaining amount of CaO after used by gypsum can be the related to calcite, which is present both in the gypsum rich samples and in the clay rich sample and to Ca-smectite in the clay samples. The gypsum samples also have slightly higher Na_2O (wt%) values, which indicates the presence of other non-gypsum mineral or a kind of enrichment. Concerning the clay samples, green clay is enriched in Fe_2O_3 (wt%) and K_2O (wt%), and beige and gray clay are enriched in MgO (wt%). Similar to the green clay, these results might be an indication of other minerals present in the sample or enrichment in these oxides. Concerning the trace elements in the clay rich samples, as the samples becomes gypsum free, the percentage of trace elements Cu, Cr, V and Ni also increases.

Once the standards of the raw material are concerned, the purity of the gypsum rock is rather high, ranging between 88% and 95%. The calcite mineral is present, but under the limits of utilization in industrial processes. The clay type in the rock is a swelling clay, Ca-smectite, which causes problems in the wallboard production.

REFERENCES

Akdağ, N., 2005, Polatlı Yöresindeki Neojen Yaşlı Sedimanter Birimlerin Mineralojik ve Jeokimyasal İncelenmesi: Yüksek Lisans Tezi, Hacettepe Üniversitesi, 67s.

Altay, T, Karakaya, M. Ç., and Yavuz E., 2006, Mineralogical and Chemical Properties of the Various Types of Gypsum Occurences at Sivrihisar (Eskişehir, Turkey): 30th Anniversary Fikret Kurtman Geology Symposium, Selçuk Univ., Jeoloji Müh. Böl.

Akarsu, İ., (1956), Ankara Bölgesi Polatlı – Haymana Civarının Detay Petrol Jeolojisi Etüdü, Rapor no: 2502, MTA Derleme, Ankara

Akarsu, İ, 1971, II. Bölge AR/TFO/747 No.lu Sahanın Tek Raporu: Pet. İş. Gen. Md., Ankara (unpublished)

Appleyard, F.C., 1983, "Gypsum and Anhydrite" in Industrial Minerals and Rocks, 5th Ed., S.J. Lefond, Ed., AIME, New York, p.775-792.

Bailey, E., B., McCallien, W. J., 1953, Ankara Mélange and the Anatolian Thrust: Royal Society of London Philosophical Transactions, vol. 62, p. 403-442.

Bates, R.L., 1969, Gypsum in Geology of the Industrial Rocks and Minerals, Dover Pub. Inc., New York, p. 201-212.

Bingöl, E., 2004, Türkiye' nin Çeşitli Bölgelerinde Yer Alan İşletilebilir Alçıtaşı Oluşumları: Evaporitler Tuz Semineri, TMMOB Jeoloji Mühendisleri Odası Yayınları, 81, p.348-365.

Branson, E. B., 1915,"Origin of Thick Gypsum and Salt Deposits: Geological society of America Bulletin, Vol. 26, p. 231-242.

Bodine, M. W. and Fernalld T. H., 1973, EDTA Dissolution of Gypsum, Anhydrite, and Ca-Mg Carbonates: Journal of Sedimentary Petrology, vol.43, no. 4, p. 1152-1156.

Boggs, S., 2001, Priciples of Sedimentology and Stratigraphy, 3rd ed.: Prentice Hall, 726p.

Butler, G.P., 1970, "Holocene Gypsum and Anhydrite of the Abu Dhabi Sabkha, Trucial Coast: An Alternative Explanation of Origin," Proceedings, 3rd Symposium on Salt, Northern Ohio Geological Society, Cleveland, OH, Vol. 1, p. 120-152.

Carr, D.D., 1994, "Industrial Minerals and Rocks", Society for Mining, Metallurgy and Exploration, Inc., Littleton, Colorado, 6th Edition, 1196 p.

Çiner, A., 1992, Sedimentologie et stratigraphie sequentiell du bassin d'Haymana a I'Eocene moyen, Turquie.Theseb d'Universite Louis Pasteur, Strasbourg, 190 p.

Çiner, A., 1993, Geology of Hayman Basin (U. Cretaceous-M. Eocene), Central Anatolia, Turkey: 6th International Meeting and Training School on IGCP Project No: 269, Middle East Technical University.

Clark, F. W., 1924, The Data of Geochemistry, 5th ed.: U.S. Geological Survey Bull., v. 770, 841 p.

Deer, W.A., Howie, R.A. and Zussman, J., 1980, The Introduction to Rock-forming Minerals: Longman Group Ltd., 528p.

Ece, Ö. I, Suner, F., and Çoban, F., 2003, Varying Depositional Environments of Gypsum Successions in the Upper Miocene Eskişehir-Sivrihisar Lacustrine Basin, NW Türkiye: Neues Jahrbuch für Mineralogie Montashefte, vol. 11, p. 481-502.

Erol, O. 1955, [Weingart 56/2, 56/4 ve 57/1, 57/3 Paftalarının Jeolojik Haritası Hakkında Rapor] una Ait Korelasyon Revizyonu Raporu, Rapor No. 2473, MTA Derleme, Ankara.

Fourquin, C., 1975. L'anatolie du Nord-Ouest, marge méridionale du continent europeén, histoire paléogéographique, tectonique et magmatique durant le Secondaire et Tertiare : Bull. Soc. Géol. France, vol.7, p.1058-1070.

Gençoğlu, H., and İrkeç, T., 1994, Eskişehir-Sivrihisar Civarındaki Sedimanter Sepiyolit Oluşumlarının Ortamsal Yorumu: Türkiye Jeoloji Kurultayı Bülteni, no. 9, 281-296 p.

Glover, E. D., 1961, Method of Solution of Calcerous Materials Using The Complexing Agent, EDTA: Jour. Sed. Petrology, v. 31, p.622-626.

Görür, N and Derman, A.S., 1978, Tuzgölü-Haymana Havzasının Stratigrafik ve Tektonik Analiz: T.P.A.O. Arşivi 1514, Ankara.

Görür, N., 1981, Tuzgölü-Haymana havzasının stratigrafik analizi: TJK, İç Anadolunun Jeolojisi Simpozyumu, Ankara, 60-66.

Görür, N., Oktay, F.Y., Seymen, I. and Şengör, A.M.C., 1984, Paleotectonic Evolution of the Tuzgölü Basin Complex, Central Turkey: Sedimentary Record of a Neo-Tethyan Closure. In: J. E. Dixon and A. H. F. Robertson (Eds.), The Geological Evolution of the Eastern Mediterranean Spec. Pub. 17, Geol. Soc. London, 467-481.

Görür, N., Şengör, A.M.C. and Oktay, F.Y., 1989, Sedimentological Evolution of Central Anatolian Basins and the Assembly of the Alpine Tectonic Collage in Turkey. In: Tethyan Tectonostratigraphic Terrane-Models Tested, EUG V, Terra Abstracts, p.55.

Gözler, M. Z., Cevher, F., Ergül, E. and Asutay, H.J., 1996, Orta Sakarya ve Güneyinin Jeolojisi: Maden Tetkik ve Arama Genel Müdürlüğü, Jeoloji Etütleri Dairesi, Ankara, Rapor No: 9973, 87p.

Gündoğan, İ, Önal, M. and Tolga, D., 2005, Sedimentology, Petrography and Diagenesis of Eocene-Oligocene Evaporites: the Tuzhisar Formation, SW Sivas Basin, Turkey: Journal of Asian Earth Sciences, v.25, p. 791-803.

Gündoğan, İ., Helvacı., C. and Hasan S., 2008, Gypsiferous Carbonates at Honaz Dağı (Denizli): First Documentation of Triassic Gypsum in Western Turkey and Its Tectonic Significance: Journal of Asian Earth Sciences, v. 32, p.46-65.

Harben, P.W. and Bates, R.L., 1990, Industrial Minerals: Geology and World Deposits, Industrial Minerals Division, Metal Bulletin Plc., London, p. 130-137.

Hardie, L. A., 1991, On the Significance of Evaporites: Ann. Rev. Earth and Planetary Sciences, vol. 19, p. 131-168.

Hill, W.R., Jr., and Runnels, R.T., 1960, Versene, A New Tool for Study of Carbonate Rocks: Am. Assoc. Petroleum Geologist Bull., v. 44, p. 631-632.

Holliday, D. W., 1970, The Petrology of Secondary Gypsum Rocks: A Review: Journal of Sedimentary Research, v. 40.

Jorgensen, D. B., 1994, Gypsum and Anhydrite: Industrial Rocks and Minerals, Society for Mining, Metallurgy and Exploration, Inc, 580 p.

Karakaş, Z., and Varol, B., 1994, Sivrihisar Neoljan Basenindeki Gölsel Dolomitlerin Petrografisi ve Oluşum Koşullarının Duraylı İzotoplar (δ^{18} O; δ^{13} C) Yardımıyla Yorumlanması: Maden Tetkik Arama Dergisi, vol. 116, p.81-95.

King, R.H., 1971, "Sedimentation in Permian Castle Sea", Origin of Evaporites, American Association of Petroleum Geologists, Reprint Series, no. 2, Tulas, OK, p. 90-97.

Kinsman, D.J.J., 1966, "Gypsum and Anhydrite of Recent Age, Trucial Coast, Persian Gulf," 2nd Symposium on Salt Northern Ohio Geological Society, vol. 1, Cleveland, OH, p. 302-326.

Knauf Standards, 2002, Standards and Specifications, Research and Development Laboratory, Germany.

Koçyiğit, A. and Lünel, T., 1987, Geology and Tectonic Setting of Alcı Region, Ankara, Middle East Technical University: Journal of Pure and Applied Sciences, vol. 20, p. 35-57.

Koçyiğit, A., 1991, An example of an accretionary fore-arc basin from northern Central Anatolia and its implications for the history of subduction of Neo-Tethys in Turkey: Geological Society America Bull., vol. 103, p.22-36.

Leeder, M. R., 1982, Sedimentology, Process and Product, George Allen and Unwin Pub., 343 p.

Lugli, S., Testa, G., 1993, The Origin of the Gypsum and Alabaster spheroids in the Messinian Evaporites from Castellina Marttima (Pisa, Italy), Preliminary Observations, Geology 55, 51-68.

Lüttig, G.W., 1980, "General geology of the Federal Pebublic of Germany" in Proceedings, 26th Int. Geol. Congress, Paris, E. Schweizerbart'sche Verlagsbuchhandlung, Stuttgart, p. 41-42.

Miloskii, A. V., 1985, Mineralogy: Mir Publishers, 450 p.

Mossop G. D., Shearman, D. J., 1973, Origins of Secondary Gypsum Rocks: Institute of Mining and Metallurgy Transactions (Section B), v. 82, p.147-154.

Murray, R. C., 1964, Origin and Diagenesis of Gypsum and Anhydrite: Journal of Sedimentary Petrology, v. 34, p.512-523.

Newland, D. H., 1929, The Gypsum Resources and Gypsum Industry of New York: New york State Mus. Bull., 283, 188pp.

Nesse, W.D., 2000, Introduction to Mineralogy: Oxford University Press, 452p.

Norman, T., 1975, Paleocurrents and Submarine Mass Movements in the Lower Tertiary Sediments of Çankırı-Çorum-Yozgat Basin: TJK, vol. 18, p. 103-10.

Norman, T., Gökçen, S. L., Şenalp, M., 1980, Sedimentation Pattern in Central Anatolia at the Cretaceous-Tertiary boundary: Cretaceous Research, vol. 1, p. 61-84.

Orti, F., 1977, Aproximacion al studio petrografico de las microstructuras del yeso secundario ya su origin: Rev. Inst. Inv. Geol. Dip. Prov. Barcelona, vol. 32, 87-152p.

Orti, F., Gündoğan, İ., and Helvacı, C., 2001, Sodium Sulphate Deposits of Neogene Age: the Kirmir Formation, Beypazarı Basin, Turkey: Sedimentary Geology, vol. 146, p305-333.

Önenç, D. İ., 2004, "MTA Genel Müdürlüğünün Türkiye Potaş Tuz Aramalarına Yönelik Çalışmaları", Evaporitler Tuzlar Semineri, s. 19- 23.

Prentice, J.E., 1990, "Geology of Construction Materials", Chapman and Hall,1st Edition, 202 p.

Reckamp, J.U. and Özbey, S., 1960, Petroleum Geology of Temelli and Kugtepe Structures, Polatlı Area: Pet. İş. Gen. Md., Ankara (yayımlanmamış)

Ries, H., 1985, Economic Geology: John Wiley & Sons, Inc, New York, p. 281-299.

Rigo de Righi, M., Cortesini, A., 1959, Regional Studies in Central Anatolian Basin: Progress Report 1, Turkish Gulf Oil Co., Pet. İş. Gen. Md., Ankara.

Schimidt, G., C., 1960, AR/MEM/365-366-367 Sahalarının Nihai Terk Raporu: Pet. İş. Gen. Md., Ankara (unpublished)

Schroeder, H.J., 1970, "Gypsum," Mineral Facts and Problems, Bulletin 650, US Bureau of Mines, p. 1039-1048

Sirel, E., 1975, Polatlı (GB Ankara) Güneyinin Stratigrafisi: Türkiye Jeoloji Kurumu Bülteni, vol. 18, p.181- 192.

Shearman, D. J., 1985, Syndepositional and Later Diagenetic Alteration of Primary Gypsum to Anhydrite: The Sixth Symposium Salt, the Salt Institute, vol. 1, p.44-55.

Shearman, D. J., Mossop, G., Dunsmore, H., Martin, M., 1972, Origin of Gypsum Veins by Hydraulic Fracture: Institution of Mining and Metallurgy, Transactions, Sect. B 81, p149-155.

Sirel, E., 1975. Polatlı (GB Ankara) Güneyinin Stratigrafisi: TJK Bülteni, 18/2, 181-192.

Stewart, F. H, 1963, Marine Evaporites, in Fleisher M. (ed.), Data of Geochemistry: U.S. Geol. Survey Prof Paper 440-Y, 54p.

Şengör, A.M.C. and Y., Yılmaz, 1981, Tethyan Evolution of Turkey: A Plate Tectonic Approach: Tectonophysics, vol. 75, p. 181-241.

Temel, A., Gourgaud, A., Alıcı P. and Bellon, H., 2000, The Role of Asthenospheric Mantle in the Generation of Tertiary Volcanism in the Polatlı-Ankara Region, Central Anatolia, Turkey: Constraints from Major-element, Trace-element and Sr-Nd Isotopes: Journal of Conference Abstracts, vol. 5(2), 989p.

Temel.,A., Varol, E., Yürür T., Alıcı, P. and Gourgaud, A., 2001, Ankara' nın Güneybatısında Yer Alan Volkaniklerin Kökeni ve Teknonikle İlişkisi, Hacettepe Üniversitesi Araştırma Fonu Projesi, Proje No: 9901602007

Temel A., Yürür T., Alıcı, P., Gourgaud, a., Bellon, H., Varol, E., and Demirbağ, H., 2005, Alkaline Series Related to Early-Middle Miocene Intra-continental rifting in a Collision Zone: An Example from Polatlı, Central Anatolia, Turkey: Geological Magazine (in review).

Türkbey, S. P., 2005, Sazılar (Polatlı) Yöresindeki Neojen Yaşlı Sedimanter Birimlerin Mineralojik ve Jeokimyasal İncelenmesi: Yüksek Lisans Tezi, Hacettepe Üniversitesi, 86 s.

Ullmann's Encyclopedia of Industrial Chemistry, 1985, Verlagsgesellschaft GmBH, D-6940, Weinheim.

United States Geological Survey, 2005, "Mineral Commodity Summaries, 2005," U.S. Government Printing Office, Washington.

Ünalan, G., Yüksel, V., Tekeli, T., Gönenç, O., Seyirt, Z. and Hüseyin, S., 1976, The Stratigraphy and Paleogeographical Evolution of the Upper Creataceous-Lower Tertiary Sediments in the Haymana-Polatlı Region (SW of Ankara): Bulletin of the Geological Society of Turkey, vol. 19, p. 159-176.

Warren, J.K., 1999, Evaporites. Their Evolution and Economics, Blackwell, Oxford, 438p.

Weingart, W., 1954, [56/2, 56/4 (Sivrihisar) ve 57/1, 57/3 (Ankara)] Paftalarının Jeolojik Haritası Hakkında Rapor: MTA Derleme, Rapor No: 2248.

Yağmurlu F., and Helvacı, C., 1994, Sedimentological Ckaracteristics and Facies of the Evaporite Bearing Kirmir Formation (Neogene), Beypazarı Basin, Central Anatolia, Turkey: Sedimentology, vol. 41, p. 847-860.

Yüksel, S., 1970, Etude Geologique de la region d'Haymana (Turquie centrale): these, Fac. Sci. Univ. Nancy, Fransa (unpublished).

Yurteri, E., 1989, Geology, Petrology and Geochemistry of the Kanarakaya Basalts, Polatlı, Ankara: Master Thesis, METU, Ankara (Unpublished).

Zoltai, T., and Stout, J. H., 1996, Mineralogy, Concepts and Principles: Burgess Publishing Company.

APPENDIX A

DRILLCORE PHOTOS

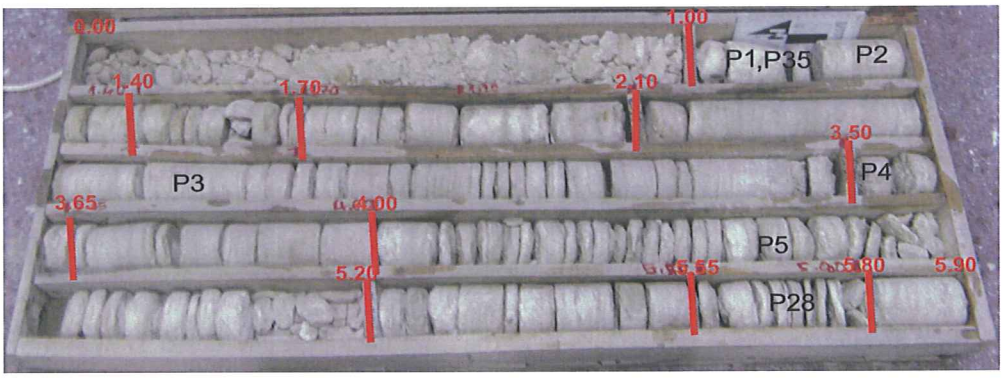

Figure 45. Photograph of Drillcore I - Box 1 from 0.00 to 5.90 m

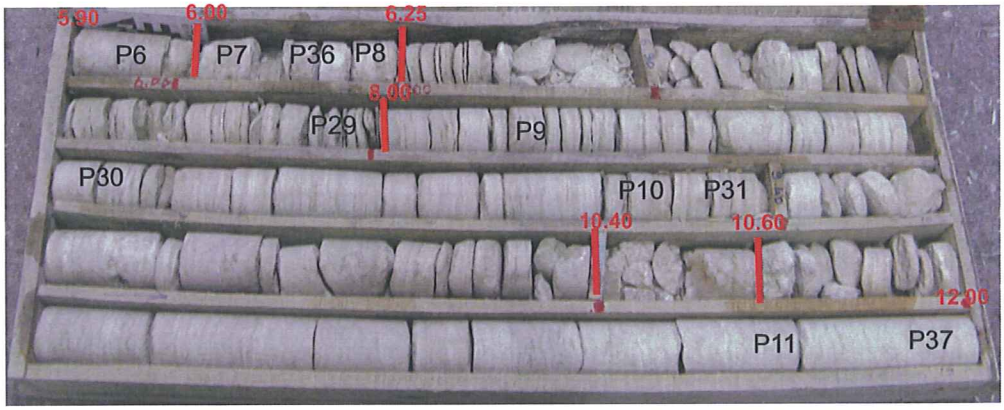

Figure 46. Photograph of Drillcore I-Box 2 from 5.90-12.00 m

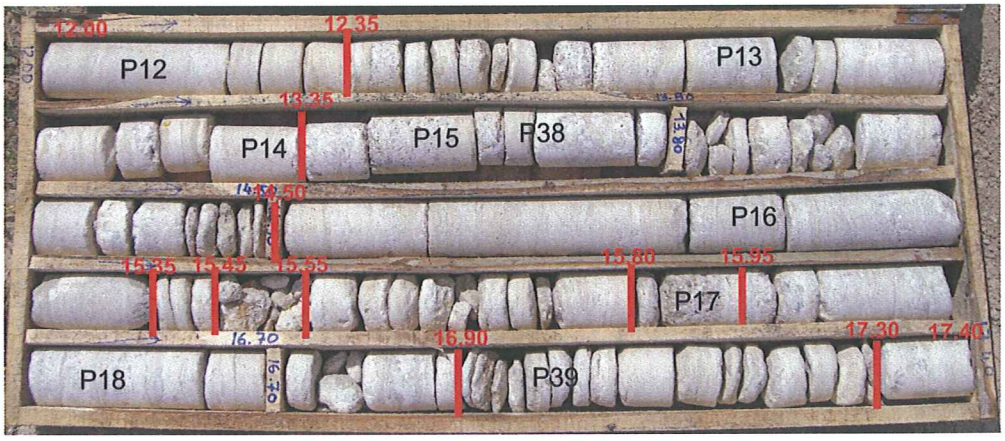

Figure 47. Photograph of Drillcore I –Box 3 from 12.00 to 17.40 m.

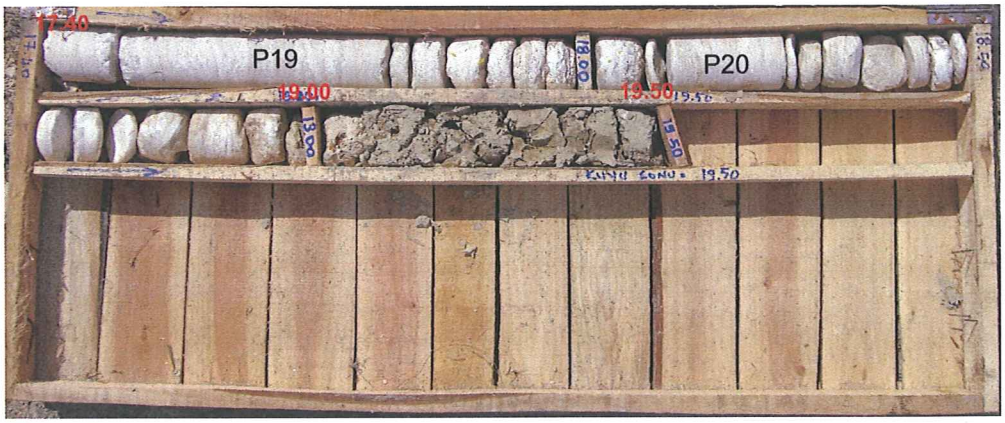

Figure 48. Photograph of Drillcore I-Box 4 from 17.40 to 19.50 m

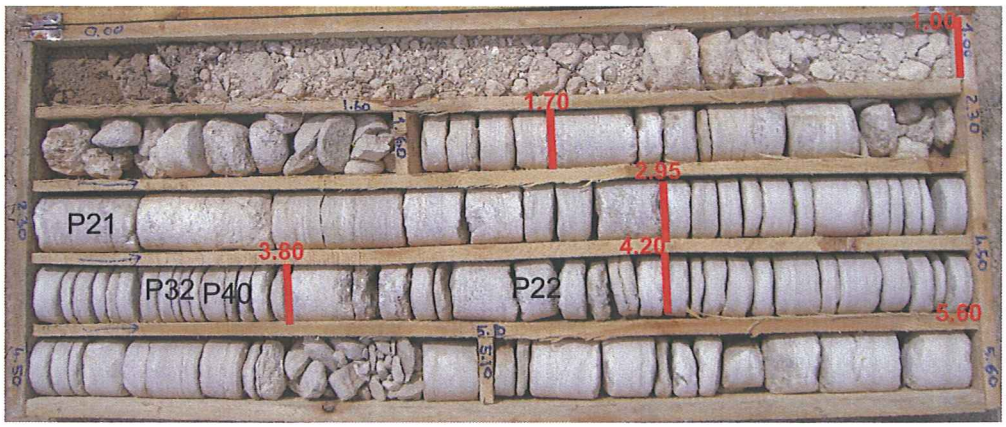

Figure 49. Photograph of Drillcore II-Box 1 from 0.00 to 5.00 m

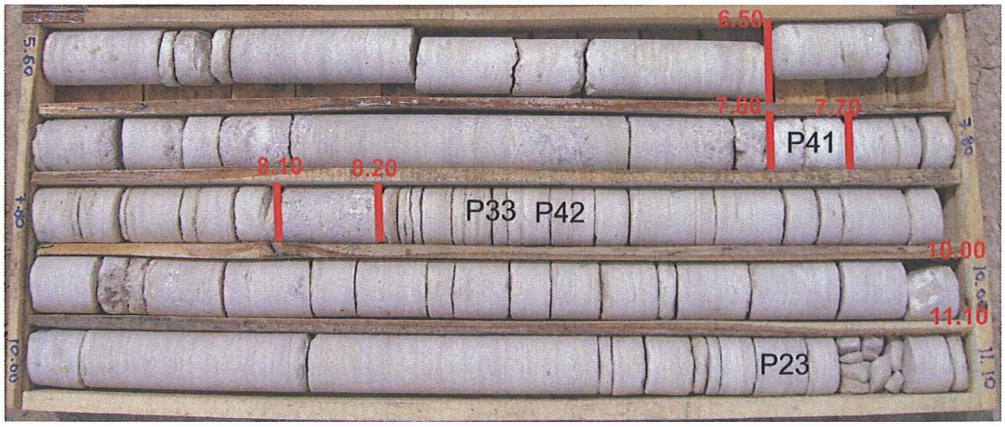

Figure 50. Photograph of Drillcore II – Box 2 from 5.60 to 11.10 m

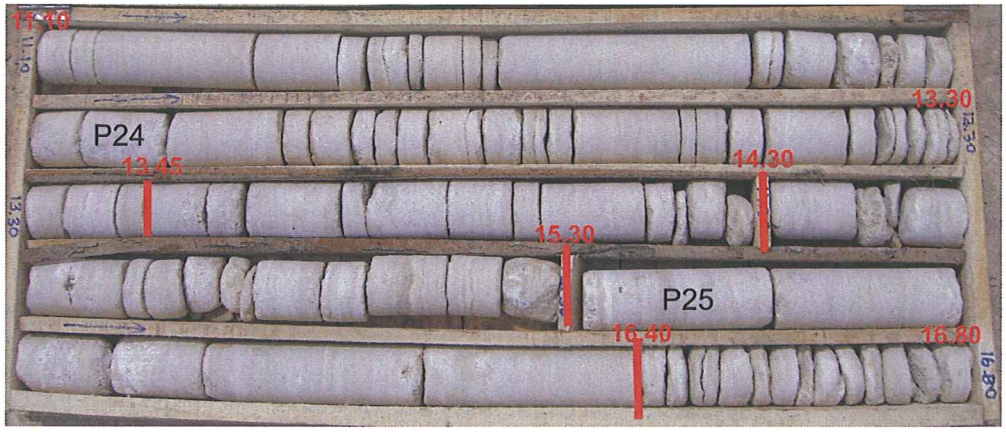

Figure 51. Photograph of Drillcore II – Box 3 from 11.10 to 16.80 m

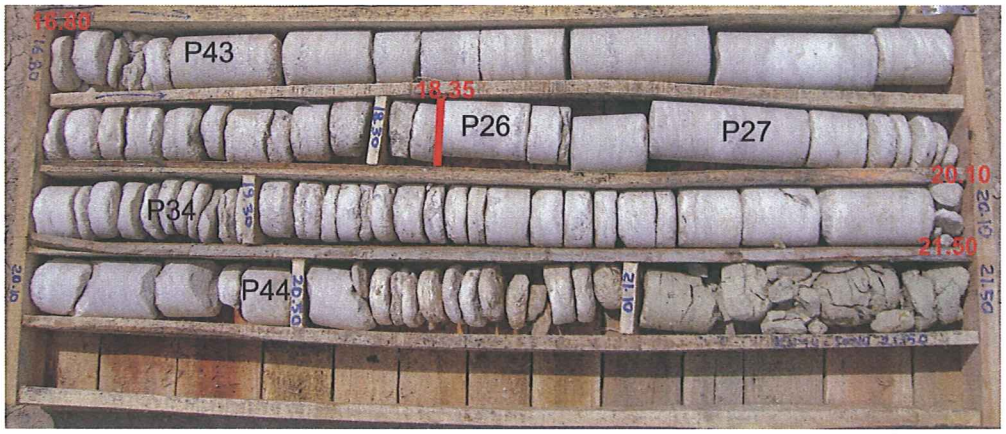

Figure 52. Photograph drillcore II – Box 4 from 16.80 to 21.50 m